
GAMING AND COOPERATION IN FEDERATED LEARNING: WHAT CAN HAPPEN AND HOW TO MONITOR IT

Dongseok Kim, Wonjun Jeong, Gisung Oh
 Department of Computer Engineering
 Gachon University
 Seongnam-si, Gyeonggi-do, South Korea
 {jkds5920, tp04045, eustia}@gachon.ac.kr

ABSTRACT

The success of Federated Learning depends on the actions that participants take out of sight. We model Federated Learning not as a mere optimization task but as a strategic system entangled with rules and incentives. From this perspective, we present an analytical framework that makes it possible to clearly identify where behaviors that genuinely improve performance diverge from those that merely target metrics. We introduce two indices that respectively quantify behavioral incentives and collective performance loss, and we use them as the basis for consistently interpreting the impact of operational choices such as rule design, the level of information disclosure, evaluation methods, and aggregator switching. We further summarize thresholds, auto-switch rules, and early warning signals into a checklist that can be applied directly in practice, and we provide both a practical algorithm for allocating limited audit resources and a performance guarantee. Simulations conducted across diverse environments consistently validate the patterns predicted by our framework, and we release all procedures for full reproducibility. While our approach operates most strongly under several assumptions, combining periodic recalibration, randomization, and connectivity-based alarms enables robust application under the variability of real-world operations. We present both design principles and operational guidelines that lower the incentives for metric gaming while sustaining and expanding stable cooperation.

Keywords Approximation · Federated Learning · Game Theory · Simulation · Submodularity

1 Introduction

1.1 Motivation

Federated Learning enables multiple organizations to train a shared model without moving data, and adoption has been rapidly growing in recent years, particularly through consortia and platforms. Major consulting reports also diagnose that, as the demand for data collaboration expands, the approach of holding data individually while jointly training models has emerged as a leading alternative across industries. For example, BCG [1] evaluates that strategic data collaboration has become safer with technological progress and highlights the pharmaceutical consortium MELLODDY, where Federated Learning improved joint model performance even in low-trust environments. Accenture [2] likewise proposes combining Federated Learning with MPC and homomorphic encryption as an approach to enable secure inter-firm data collaboration.

Concurrently, models for the commercialization of data and AI are becoming increasingly concrete. McKinsey [3, 4] reports that nearly 40% of executives plan to establish new businesses based on data analytics and AI within the next five years, and it summarizes how monetization is diversifying beyond direct data sales into intelligence products, subscriptions, usage-based, and performance-based contracts. Its latest report analyzes that as generative AI productizes vast amounts of unstructured data and embeds actionable intelligence into decision-making flows, the center of data monetization is shifting from raw data to decision-embedded intelligence.

However, the contracts and governance of AI businesses have not yet reached maturity. According to McKinsey’s 2025 Global AI Survey [5], only 1% of organizations report having achieved a mature rollout, with most firms still at an early stage in governance, workflow redesign, and risk mitigation. PwC’s 2025 Global Digital Trust Insights [6] similarly diagnoses that only about 2% of organizations have implemented enterprise-wide cyber resilience. This suggests that across B2B, B2C, and C2C domains, standardized and entrenched practices around SLAs, audit rights, accountability, information disclosure, and consent mechanisms are still a long way off.

In particular, contractual and audit frameworks with third-party ecosystems are pivotal to the trust foundations of Federated Learning. PwC [7, 8] recommends enhancing third-party risk management (TPRM) for the AI context and embedding AI-oriented controls into supplier contracts and vendor governance. Moreover, control assurance reports such as SOC 2 are highlighted as means to validate and communicate internal controls of service providers in a standardized format. These frameworks provide a foundation for concretizing contractual terms and supervisory procedures in subscription-based federated models, data and model marketplaces, and community-driven participatory services.

Meanwhile, reducing privacy and regulatory risks while ensuring collaborative efficiency requires integrating the design of evaluation, information, and incentives. PwC [9] recommends Federated Learning, differential privacy, and secure computation in parallel as privacy-enhancing technologies, and McKinsey [10] proposes using Federated Learning and differential privacy during training to prevent unintentional memorization of sensitive information. Combining such technical and governance safeguards with information design that minimizes publicly observable signals can help align reward criteria with genuine outcomes and secure accountability paths for audits and sanctions.

In sum, Federated Learning is establishing itself as a prominent form of collaboration in industry, but operational design—including reward alignment with true outcomes, evaluation disclosure rules, audits, contracts, and especially third-party ecosystems—remains incomplete. This paper aims to fill this gap by presenting guidelines that realign incentives so that best responses under self-interest also maximize collective performance, through the integration of reward alignment, audit and sanction strength and modality, private evaluation, and randomized challenges. In addition, we contextualize the data monetization models and governance principles proposed in industry reports for the Federated Learning setting.

1.2 Contributions

We redefine Federated Learning (FL) as a strategic system that simultaneously accommodates manipulation and cooperation within a unified framework. We provide metrics and design principles that allow one to determine where incentives for gaming arise, how much they erode collective performance, and which design choices can redirect the same self-interest toward cooperation. We further analyze the dynamics of participation and exit to establish criteria for stable cooperation and validate these insights through simulations under diverse settings. Finally, we compile a practical checklist—including thresholds and auto-switch rules—that organizations can apply immediately.

- **Game-theoretic formalization across observation, reward, audit, and participation:** We provide a unified framework that captures how behaviors that improve performance compete and interact with those that merely target metrics, encompassing both manipulation and cooperation.
- **Core indices for gauging gaming incentives and social loss:** We introduce two indices—Manipulability Index \mathcal{M} and Price of Gaming PoG—that quantify the private gains from manipulation and the degradation of collective performance. We systematically interpret how these indices vary with aggregation methods, reward criteria, audit mechanisms, and evaluation information design.
- **Principles and priorities of alignment, audit, and information design:** We articulate how aligning reward criteria with genuine outcomes, adjusting the strength and modality of audits and sanctions, and mixing private evaluations with randomized challenges can reduce gaming incentives and amplify cooperation incentives. We highlight priority levers to strengthen under different environments.
- **Dynamic participation stability analysis:** We analyze how, even under identical rules, participation and exit diverge depending on initial conditions and reward expectations, and we identify the mechanisms of cooperation retention versus domino exit through thresholds and resilience indicators.
- **Incentive design principles for fostering cooperation:** Beyond the limits of stronger punishments, we propose ways to reallocate incentives so that participants’ best responses naturally align with collective welfare. We demonstrate that when criteria are properly aligned, self-interest directly leads to cooperation.
- **Checklist and auto-switch rules for policy application:** We provide practical guidance by systematizing thresholds, switching rules, and reporting items for design levers such as aggregator choice, audit strength, and evaluation information mix.

- **Algorithms and approximation guarantees from a computational perspective:** We formalize audit resource allocation as a budget-constrained maximization problem and propose procedures with approximation guarantees, combining greedy, delayed greedy, continuous relaxation–rounding, and local search within a monotone submodular structure.
- **Reproducible simulation evidence:** We validate that the proposed indices and design principles consistently predict observed phenomena across noise levels, aggregation, reward, and audit settings, and we release all procedures for reproducibility.

2 Related Work

2.1 FL Attacks, Defenses, and Robust Aggregation

Research on robust aggregation in Federated Learning began with the question of whether a small number of malicious updates can disrupt the majority, and whether convergence and performance can still be preserved. Blanchard et al. [11] set a milestone with Krum, which selects only the updates closest to the majority. Yin et al. [12] proposed statistically robust yet simple alternatives through coordinate-wise median and trimmed mean. El Mhamdi et al. [13] further narrowed the attack surface in high dimensions with Bulyan, which combines candidate filtering and coordinate-wise refinement. Pillutla et al. [14] systematized the family of geometric-median approaches under Robust Federated Aggregation (RFA), summarizing implementation aspects and performance characteristics across diverse settings. From a distributed optimization perspective, Alistarh et al. [15] analyzed convergence conditions of stochastic gradient descent under Byzantine noise, while Bernstein et al. [16] showed that majority-vote–based signSGD updates can withstand certain adversarial fractions. Another important line comes from Chen et al. [17], who leveraged redundant computation to cancel out malicious contributions.

Framework- and system-level efforts have proceeded in parallel. Damaskinos et al. [18] implemented multiple robust aggregation rules within a single stack, illustrating their operational trade-offs. Xie et al. [19] proposed suspicion-score–based filtering of malicious updates in asynchronous environments. Such approaches test the applicability of robust aggregation under real-world constraints such as partial participation, communication delays, and heterogeneous distributions.

Research from the attack perspective has driven progress by exposing assumptions and vulnerabilities in defenses. Baruch et al. [20] demonstrated strategies that circumvent majority-based defenses with only a few manipulations. Fang et al. [21] systematically proved that local model poisoning can indeed break through existing robust aggregation schemes. Bagdasaryan et al. [22] empirically showed the unique backdoor threats of Federated Learning, while Wang et al. [23] proposed attacks that exploit tail groups in non-IID settings to neutralize defenses.

Defenses against collusion and Sybil attacks have also been proposed. Fung et al. [24] introduced FoolsGold, which downweights suspicious multi-identity contributions based on update similarity. Cao et al. [25] proposed FLTrust, which bootstraps server-side trust signals and uses them to normalize client updates, thereby mitigating the effects of collusion.

2.2 Incentive Design and Differential Client Contribution

The foundations of differential client contribution and reward design stem from data valuation. Ghorbani et al. [26] defined fair data contributions using Shapley values, while Jia et al. [27] systematized approximation techniques to make such computations practical. Koh and Liang [28] introduced influence functions to trace learning outcomes back to individual training points, and Yoon et al. [29] demonstrated a reinforcement learning approach that jointly trains a value estimator and a predictor.

In the Federated Learning context, these methods extend to estimating contributions at the participant level. Liu et al. [30] efficiently estimated participant Shapley values using round-level gradient information, and Chen et al. [31] proposed a lightweight procedure for contribution evaluation in a single communication round. Tastan et al. [32] refined contribution estimation by incorporating class distribution and difficulty, while Chen et al. [33] compared and evaluated multiple estimation techniques under consistent conditions.

Research that directly designs rewards and participation incentives draws widely on economic tools. Kang et al. [34] combined reputation and contract theory to attract high-quality participants. Zhang et al. [35] designed payments and selection simultaneously via reverse auctions. Tang et al. [36] outlined a framework of intelligent agents to support decision-making in auction-based incentives, while Zhang et al. [37] automated contribution verification and payments using blockchain. Liu et al. [38] proposed a reward distribution protocol based on distributed consensus, and Ouyang and Kuang [39] introduced an incentive design that simultaneously ensures fairness and robustness in heterogeneous environments.

Approaches that integrate differential contributions into learning and aggregation aim to jointly improve performance, fairness, and participation stability. Mohri et al. [40] proposed distributionally robust optimization aligned with mixture weights of the target distribution to reduce underfitting of minority groups. Li et al. [41] introduced q-FedAvg with a weighted objective that mitigates performance disparities across clients. Lai et al. [42] accelerated training while prioritizing high-contribution clients via utility-based participant selection, and Nishio and Yonetani [43] improved efficiency with selection rules that reflect resource constraints. Lin et al. [44] analyzed principles that ensure long-term fairness and convergence in reward–learning coupling, while Kim et al. [45] demonstrated an adaptive aggregation design that directly reflects differential contributions by adjusting round-level weights based on each client’s statistical characteristics.

2.3 Game Theory of Federated Learning and Participation Dynamics

Research that frames Federated Learning as a strategic interaction has primarily focused on coalition formation and stability. Donahue et al. [46] formalized situations where heterogeneous participants voluntarily form coalitions using hedonic games, followed by Donahue et al. [47], who analyzed the gap between stability and optimality through the lens of the Price of Anarchy. Along this line, Hasan [48] provided existence conditions for coalition structures and decentralized consensus procedures to explain participation dynamics.

From a cooperative perspective, game theory provides visibility into who contributes and by how much. Nagalapatti et al. [49] introduced selection and weighting strategies that filter out less relevant clients by using Shapley values derived from gradient-based cooperative games, demonstrating a pathway to improve both model quality and participation stability.

Research addressing repeated interactions and free-riding highlights core mechanisms that determine long-term participation. Zhang et al. [50] showed that punishment strategies form subgame-perfect equilibria in infinitely repeated games, thereby deterring free-riding and sustaining participation. Sagduyu et al. [51] characterized Nash equilibria of participation versus free-riding in wireless environments. Targeting bias induced by random participation, Luo et al. [52] proposed an incentive–participation coupled design at ICDCS that guarantees unbiased aggregation. Addressing delay and duration issues, Sarikaya and Ercetin [53] derived reward rules under a leader–follower structure to mitigate speed mismatches, while Hu and Gong [54] analyzed participation decisions with explicit consideration of privacy costs.

Leader–follower and contract-theoretic approaches establish stable fixed points of participation by aligning incentives between server and clients. Le et al. [55] designed auction-based mechanisms that satisfy truthfulness, individual rationality, and efficiency. Ding et al. [56] derived optimal contracts for participants with multidimensional private information in JSAC. Liu et al. [57] proposed multidimensional contracts and contract-based aggregation that incorporate both data quality and effort levels. Huang et al. [58] analyzed hierarchical participation structures in TMC using a combined Stackelberg–contract framework. Pan et al. [59] proposed reward–selection rules that account for delay and harmful contributions in graph FL, while Guo et al. [60] leveraged strategic responses between server (leader) and clients (followers) to guide participation quality.

Collusion and Sybil behavior represent prominent strategies that distort participation dynamics. Byrd et al. [61] built a protocol leveraging confidential distributed differential privacy to deter collusion, and Xiong et al. [62] reduced collusion incentives through a smart-contract–based design that automates verification and payment.

2.4 Metric Gaming and the Goodhart Phenomenon

Metric gaming is encapsulated by the insight that once a measure becomes a target, it ceases to be a good measure. Manheim and Garrafrant [63] classified this phenomenon into four distinct mechanisms—statistical regression, selection bias, counting errors, and others—providing a common language for understanding why the same metric can yield very different distortions depending on context. Amodei et al. [64] concretized this issue as a safety problem in learning systems, systematically cataloging practical failure types such as reward hacking and non-scalable oversight. Skalse et al. [65] formally defined reward hacking and proposed boundary conditions under which proxy rewards deviate from true rewards, while Everitt et al. [66] used causal diagrams to analyze pathways where manipulating the reward function itself or its inputs distorts performance. Langosco et al. [67] empirically demonstrated cases where goals are misgeneralized outside the training distribution, leading agents to pursue unintended objectives despite preserved competence.

When metrics intervene in decision-making and thereby alter the data, the problem extends to strategic environments. Hardt et al. [68] modeled scenarios where public classifiers induce strategic responses, with individuals manipulating features at a cost to secure favorable decisions. Brückner and Scheffer [69] analyzed such interactions as a Stackelberg

game between learner and actor. Perdomo et al. [70] formalized performative settings where predictions reshape the environment itself and proposed a stability notion for convergence under repeated retraining, while Mendler-Dünnér et al. [71] highlighted trade-offs in operational rules by showing how convergence guarantees depend on deployment cycles and update frequencies. Miller et al. [72] demonstrated that distinguishing gaming from genuine improvement requires modeling causal structures, thereby revealing qualitative differences in behaviors induced by metric design.

In fairness and evaluation governance, research has advanced designs to curb metric gaming. Blum and Hardt [73] proposed score-disclosure rules to reduce leaderboard overfitting, controlling adaptive overfitting in competitions. Dwork et al. [74] developed validation procedures to prevent distortions from repeated reuse of the same holdout set. Kearns et al. [75] showed that fairness metrics defined at higher group levels can be easily gerrymandered at the subgroup level, and they provided a framework that combines audits with learning procedures to prevent such manipulations.

More recently, results have accumulated that probe the learnability and dynamics of strategic interactions with increasing precision. Zrnic et al. [76] analyzed how the sequencing and learning capacities of decision-makers and actors affect equilibrium and performance, highlighting the importance of who moves first. Sundaram et al. [77] identified sample complexity bounds and learning conditions under a cost model of strategic manipulation.

2.5 Design of Evaluation Information, Audits, and Sanctions

Since the way evaluation results are disclosed can itself induce strategic overfitting, information design serves as the first line of defense. Blum et al. [73] proposed procedural mechanisms that restrict and staircase leaderboard updates to curb holdout overfitting from repeated attempts. Dwork et al. [74] introduced a protocol for safely reusing the same holdout multiple times, leveraging insights from differential privacy. Companion theoretical works [78, 79, 80] systematized guarantees of generalization under adaptive analysis.

From the audit perspective, Kearns et al. [75] established a subgroup audit framework to detect and learn simultaneous violations across multiple subsets, while Hardt et al. [81] proposed post-processing adjustments to remedy violations of equal opportunity. Kim et al. [82] introduced a black-box audit procedure that checks and corrects errors across identifiable groups without access to the internal predictor, and Agarwal et al. [83] refined a learning procedure that reduces fairness constraints to cost-sensitive classification, enforcing compliance via loss reweighting under violations. Furthermore, Kusner et al. [84] opened the path of designing audit criteria themselves through counterfactual fairness, and Diana et al. [85] systematized the design of proxy variables for auditable metrics.

Documentation and disclosure procedures form the infrastructure for both ex ante and ex post audits. Mitchell et al. [86] proposed standardized disclosure sheets for models, while Gebru et al. [87] introduced datasheets for datasets, together providing documentation frameworks that accumulate evidence for evaluation, audits, and sanctions. Ribeiro et al. [88] systematically exposed functional vulnerabilities beyond metrics through behavior-based testing, while Kiela et al. [89] designed a dynamic benchmark process that pits humans against models to reduce adaptive overfitting. The WILDS benchmark [90] standardized performance under distribution shift, offering a public testbed linking pre-deployment risk assessment with post-deployment monitoring. RobustBench [91] standardized adversarial robustness evaluation, curbing overstated defense claims.

In the domain of privacy and memorization, Shokri et al. [92] introduced membership inference attacks in black-box settings, raising training-data leakage as a critical audit target. Carlini et al. [93] quantified unintended memorization via canary-based exposure metrics, and Carlini et al. [94] demonstrated the extraction of training examples from large language models, underscoring the necessity of ex post sanctions. Song and Shmatikov [95] proposed data lineage audit procedures capable of detecting whether a specific user’s text was included in training with only a few queries.

Audits for backdoors and poisoning provide the technical basis for sanction enforcement. Tran et al. [96] identified contaminated samples using spectral signatures left by hidden triggers, while Wang et al. [97] introduced class-wise minimum-trigger inversion for diagnosing and mitigating backdoors. Post-deployment, the distribution-shift detection and alert system proposed by Rabanser et al. [98] transforms silent failures into loud failures, enabling ex post audits, rollbacks, and penalty triggers.

Finally, case studies have accumulated demonstrating how empirical audits and sanctions can directly rectify real-world decision systems. Dressel and Farid [99] externally re-evaluated risk assessment tools in the criminal justice domain, uncovering biases and limitations not captured by internal metrics. Such external audits support the design of sanction mechanisms including adjusted leaderboard disclosure intervals, test access control (reusable holdouts), cost reweighting under group-level violations (audit-based penalties), disqualification and reset upon memorization or backdoor detection, and related enforcement strategies.

2.6 Trade-offs Between Privacy and Incentives

In Federated Learning, the principal approaches to ensuring privacy are differential privacy and secure aggregation. Abadi et al. [100] set a milestone by adding noise and precise accounting methods to stochastic gradient descent, managing the entire training process under a privacy budget. McMahan et al. [101] applied user-level privacy guarantees to real-world language model training. Geyer et al. [102] organized the implementation of client-level protection and its performance–privacy trade-offs, while Bonawitz et al. [103] proposed a secure aggregation protocol that reconstructs only the sum, preventing the server from seeing individual updates. Erlingsson et al. [104] showed that anonymization and shuffling can amplify privacy guarantees.

Techniques on the modeling and cryptographic side have also been widely studied. Papernot et al. [105, 106] reduced data exposure by releasing only teacher consensus outputs, while Shokri and Shmatikov [107] designed distributed training procedures that avoid revealing raw data via selective sharing. At the same time, Gilad-Bachrach et al. [108] demonstrated inference under homomorphic encryption. Such encryption- and consensus-based approaches, however, may conflict with incentive design by limiting transparency in audits or the fine-grained evaluation of contributions.

Attack studies that refine the privacy threat model have clarified how much must be hidden. Melis et al. [109] showed how one participant’s updates can be used to infer attributes of others’ data, while Zhu et al. [110] demonstrated that raw inputs can be reconstructed from shared gradients. Shokri et al. [92] revealed that membership inference is possible even in black-box settings, fueling stronger protections through noise, encryption, and privatization. Conversely, stronger protections weaken the ability to assess individual contribution quality or pinpoint violations for sanctions, thereby imposing costs on reward alignment and audit enforcement.

Tensions are also evident in the interplay with security attacks. Bagdasaryan et al. [22] introduced model-replacement strategies for backdoor injection, noting that features of FL such as secure aggregation and partial participation make detection difficult. Wang et al. [23] showed that backdoors targeting tail distributions can be particularly damaging under data heterogeneity, underscoring the reality that stronger protections (masking individual updates) reduce the availability of detection and sanction signals.

Trade-offs with fairness have likewise been documented. Bagdasaryan et al. [111] showed that DP-SGD can disproportionately reduce accuracy for minority and sparse groups, while Jagielski et al. [112] theoretically formalized boundary conditions and mitigating conditions when fairness, accuracy, and privacy are simultaneously required. As privacy strengthens, evaluation metrics can become more distorted across groups, with repercussions for fairness in rewards and sanctions.

One direction for alleviating these trade-offs is to add verifiability as a substitute for lost audit signals. Jia et al. [113] proposed the concept of ex post proofs that the training procedure was correctly followed, and Zhang et al. [114] structured bidirectional verification of updates and aggregation between clients and server. When combined with secure aggregation, such proofs and verification schemes may restore minimal accountability and sanctionability without inspecting individual updates directly.

Finally, the performance costs of stronger privacy directly impact incentives. Tramèr and Boneh [115] showed that current DP learning suffers significant performance degradation without sufficient data or pretrained representations, suggesting that stronger protections can burden participation incentives (performance-based rewards) and retention stability. This demonstrates that unless privacy, audits, and rewards are jointly designed, protections may erode the very incentives needed to sustain cooperation.

3 Notation and Abbreviations

This section fixes the symbols and abbreviations repeatedly used throughout the paper. Identical concepts are denoted by identical notation, and full names are given at first occurrence whenever possible. Mathematical notation is unified as in \mathcal{M} , P_{\perp} , α_{\min} , and in text we consistently use abbreviations such as PoG, audit, and sanction.

4 Model and Metrics

4.1 Players, Signals, Timing, and Constraints

The Federated Learning environment consists of a server (acting as leader) and a set of clients $\mathcal{N} = \{1, \dots, N\}$. In each round $t = 1, 2, \dots$, client i chooses a learning action $x_i^t \in \mathcal{X}_i$ and a manipulation action $z_i^t \in \mathcal{Z}_i$. Learning actions include the number of local epochs, regularization strength, and data selection, while manipulation actions include label reshuffling, uninformative synthesis, and similarity adjustment. These choices incur a cost $c_i(x_i^t, z_i^t) \geq 0$. The local

Table 1: Notation and abbreviations used throughout the paper.

Symbol	Description
A	server-side aggregator; operator and rule combining client updates
α	sanction strength parameter
α_{benign}	benign threshold between cooperation and harmful coalitions
α_{\min}	minimum sanction strength required to deter manipulation
\mathcal{C}	set of coalition participants
ΔU	change in social welfare
ε_i	noise in observed signal
H	local curvature (Hessian) matrix
K	effective curvature matrix $H + 2qI$
\mathcal{M}	Manipulability Index, capturing incentive and sensitivity coordinates
M_α	response operator $(H + 2qI + \alpha P_\perp)^{-1}$
N	number of clients
PoG	Price of Gaming, social loss induced by metric gaming
P_\parallel	projection onto welfare gradient u direction, $I - P_\perp$
P_\perp	orthogonal projection onto welfare-orthogonal component
p	participation probability or rate
p_{dom}	domino-exit threshold participation rate
ϕ	orthogonality penalty weight for manipulation components
q	isotropic damping constant
r	local reward gradient, first-order gain direction of manipulation
$r_{\mathcal{C}}$	coalition reward direction under joint cooperation
s_i	observed signal of client i
T	number of learning rounds
τ	tolerance (audit margin) in detection and sanctioning
u	welfare gradient, direction of increase in social welfare
w	aggregation weight
z	manipulation vector, change in participant's behavior

update is expressed as

$$u_i^t = f_i(x_i^t, z_i^t; \xi_i^t),$$

where ξ_i^t represents noise and sample randomness. The server observes only the signal

$$s_i^t = h_i(u_i^t) + \varepsilon_i^t,$$

and computes $s^t = A(s_1^t, \dots, s_N^t)$ through the aggregator A . The server's reward rule R and audit-sanction rule (a, α) are announced and fixed prior to the round, subject to the budget constraint $\mathbb{E}[\sum_i R_i^t] \leq B$ and sanction cap $0 \leq \alpha \leq \bar{\alpha}$.

The server's objective function $U(\cdot)$ is based on true performance, measured by private holdouts or randomized challenges. In contrast, rewards depend on observed signals, which may diverge from U . The timing follows a Stackelberg sequence: first, the server announces (A, R, a, α) ; next, clients choose (x_i^t, z_i^t) ; finally, the server observes s^t , implements R^t , and conducts audits.

Definition 4.1 (Participation and Incentive Constraints). Let v_i^{out} denote client i 's outside option. Under mechanism (A, R, a, α) , the participation constraint is

$$\mathbb{E} \left[\sum_t \{R_i^t - c_i(x_i^t, z_i^t)\} \right] \geq v_i^{\text{out}}.$$

Individual incentive compatibility (IC) requires that $z_i = 0$ and honest x_i maximize client i 's expected utility. Group incentive compatibility (Group-IC) requires that no coalition $C \subseteq \mathcal{N}$ can obtain higher expected utilities for all its members through collusion. We distinguish between the cases with and without transferable utility via side payments.

The state variables include the composition of participants summarized by the proportion of honest versus gaming clients, the partition structure of colluding coalitions, and the history of sanctions. State transitions are determined by (A, R, a, α) and the realizations of observed signals.

4.2 Alignment Metrics and Manipulability Index

To quantify how well the observed signal s aligns with the server’s welfare U , we define directional alignment with respect to the decision variable x .

Definition 4.2 (Alignment and Sensitivity). The local alignment at point x is defined as

$$\gamma(x) = \frac{\langle \nabla_x s(x), \nabla_x U(x) \rangle}{\|\nabla_x s(x)\| \|\nabla_x U(x)\|} \in [-1, 1].$$

Values closer to 1 indicate that the improvement direction of the signal is better aligned with the improvement direction of welfare. The sensitivity of the signal is $\kappa_s(x) = \|\nabla_x s(x)\|$, and the magnitude of observational noise is recorded by the noise variance parameter σ_s^2 .

Definition 4.3 (Manipulability Index \mathcal{M}). Relative to the honest baseline $(x, z=0)$, the maximum net gain in reward that a client can achieve without worsening welfare is defined as

$$\mathcal{M} = \sup_{(x', z')} \mathbb{E}[R(s(x', z')) - c(x', z') - \{R(s(x, 0)) - c(x, 0)\}] \quad \text{s.t.} \quad U(x', z') \leq U(x, 0).$$

If $\mathcal{M} > 0$, then gaming is feasible from a net-gain perspective.

As a welfare-oriented summary, we use price-type metrics.

Definition 4.4 (Price of Gaming, Price of Cooperation). Let U^{hon} denote welfare under the honest baseline, and U^{game} welfare under the gaming equilibrium. The Price of Gaming is defined as

$$\text{PoG} = 1 - \frac{U^{\text{game}}}{U^{\text{hon}}} \in (-\infty, 1],$$

representing the welfare loss ratio. The cooperative effect of coalitions compares U^{coal} with the no-coalition baseline $U^{\text{no-coal}}$, defining the Price of Cooperation as

$$\text{PoC} = \frac{U^{\text{coal}}}{U^{\text{no-coal}}} - 1.$$

Both indices are reported as functions of core parameters including alignment γ , sensitivity κ_s , noise variance σ_s , audit strength a , and sanction cap $\bar{\alpha}$.

When alignment is low, signal sensitivity is excessive, and noise is large, \mathcal{M} tends to increase and thus PoG rises. In contrast, increasing effective alignment through private holdouts or randomized challenges, and narrowing incentive gaps via audit strength and sanction caps, reduces \mathcal{M} and lowers PoG. For coalitions, the sign of PoC depends on externality structures and organizational costs.

4.3 Common Experimental Settings

All experiments share a single baseline configuration, with only varying elements specified in the respective sections. Numerical values, hyperparameters, additional figures, and log paths are provided in the Reproducibility Statement.

Participants and Rounds The number of clients N and the number of rounds T are fixed to single values. Client heterogeneity is modeled as $\theta_i \sim P_\Theta$, and outside options are independently sampled as $v_i^{\text{out}} \sim P_V$.

Aggregation and Signals The aggregator A is specified per experiment among mean, median, k -trimmed mean, and sorted-weighted aggregation. Observed signals are simulated as $s_i = h_i(u_i) + \varepsilon_i$, where ε_i is assumed to be sub-Gaussian noise. The variance indicator is recorded as σ_s^2 . Server evaluation combines private holdouts with probabilistic challenge tests, and the challenge mix ratio π is specified for each experiment.

Mechanism Parameters The reward rule R satisfies monotonicity and is designed under the budget constraint $\mathbb{E}[\sum_i R_i] \leq B$. Audit strength is set in the range $a \in [0, 1]$, with sanction cap $\bar{\alpha}$. The orthogonality penalty α and the level of information disclosure are fixed to baseline values, with any changes explicitly noted in the corresponding experiment.

Metrics In addition to social welfare U , we report the Manipulability Index \mathcal{M} , Price of Gaming (PoG), and Price of Cooperation (PoC, for coalition experiments only), as well as participation and exit rates, coalition size distributions, detection power, and false positive rates. Auxiliary metrics include alignment γ , signal sensitivity κ_s , and noise indicator σ_s .

5 Static Results and Thresholds

Proposition 5.1 (Existence of Manipulability and Closed Form). *Consider a local quadratic model for $z \in \mathbb{R}^p$ around baseline $(x, 0)$. The reward increment is*

$$G(z) = r^\top z - \frac{1}{2} z^\top H z - q \|z\|_2^2,$$

and the first-order approximation of welfare change is $\Delta U(z) \approx u^\top z$. Here $r, u \in \mathbb{R}^p$, $H \succeq 0$, and $q \geq 0$. Define

$$K := H + 2qI_p \quad \text{and} \quad M := K^{-1}.$$

When $K \succ 0$, the following results hold.

Intuitive interpretation. K captures the difficulty of manipulation, combining audit curvature H with isotropic damping q . For the same reward gradient r , larger K implies smaller manipulation responses. Its inverse $M = K^{-1}$ represents responsiveness, with larger values indicating stronger reactions to identical incentives. Define $P_\perp := I - \frac{uu^\top}{\|u\|_2^2}$ as the orthogonal projection onto the welfare-orthogonal component. This filters out manipulations that do not improve or even harm welfare. Accordingly, $K_\alpha = H + 2qI + \alpha P_\perp = K + \alpha P_\perp$ represents additional sanctions α against welfare-orthogonal manipulations, with larger α making such manipulations increasingly difficult.

Existence of unique solution. The optimization problem

$$\max_{z \in \mathbb{R}^p} G(z) \quad \text{s.t.} \quad u^\top z \leq 0$$

admits a unique optimal solution z^* .

Closed form. Applying stationarity conditions and the KKT framework yields

$$z^* = \begin{cases} M r, & \text{if } u^\top M r \leq 0 \text{ (constraint inactive),} \\ M \left(r - \frac{u^\top M r}{u^\top M u} u \right), & \text{if } u^\top M r > 0 \text{ (constraint active, } u^\top z^* = 0). \end{cases}$$

Value of the Manipulability Index. Interpreting \mathcal{M} in Definition 4.3 as the optimal value of the above problem gives

$$\mathcal{M} = \begin{cases} \frac{1}{2} r^\top M r, & u^\top M r \leq 0, \\ \frac{1}{2} \left(r^\top M r - \frac{(u^\top M r)^2}{u^\top M u} \right), & u^\top M r > 0. \end{cases}$$

In particular, if $r = \alpha u$ then $\mathcal{M} = 0$; otherwise, $\mathcal{M} > 0$. Moreover, for $H' \succeq H$ or $q' \geq q$, with $K' = H' + 2q'I_p$, we have $M' = K'^{-1} \preceq M$, so \mathcal{M} decreases monotonically in (H, q) .

Remark 5.2. The sign of $u^\top M r$ represents the M -metric alignment between the reward gradient r and the welfare gradient u . When the constraint is inactive, i.e., $u^\top M r \leq 0$, the solution $z^* = M r$ indicates the typical gaming direction that maximizes reward while degrading welfare. When the constraint is active, i.e., $u^\top M r > 0$, the solution z^* becomes the projection of $M r$ onto the component orthogonal to u under the M -metric, with the pure aligned component removed. As audits and sanctions intensify, M shrinks and \mathcal{M} decreases.

Theorem 5.3 (Threshold for Suppressing Gaming). *Assume the local quadratic model in Prop. 5.1. Strengthened audits and sanctions are represented by*

$$K_\alpha := H + 2qI_p + \alpha P_\perp, \quad P_\perp := I_p - \frac{uu^\top}{\|u\|_2^2},$$

where P_\perp denotes the orthogonal projection onto the complement of the welfare gradient u and $u \neq 0$. Then the Manipulability Index $\mathcal{M}(\alpha)$ is monotonically decreasing in α , and

$$\mathcal{M}(\alpha) \leq \frac{\|P_\perp r\|_2^2}{2\{\lambda_{\min}(H + 2qI_p \upharpoonright_{\text{span}(u)^\perp}) + \alpha\}}.$$

Hence, for any tolerance $\tau > 0$,

$$\alpha \geq \alpha_{\min}(\tau) := \max \left\{ 0, \frac{\|P_\perp r\|_2^2}{2\tau} - \lambda_{\min}(H + 2qI_p \upharpoonright_{\text{span}(u)^\perp}) \right\}$$

guarantees $\mathcal{M}(\alpha) \leq \tau$. Moreover, when $u^\top K_\alpha^{-1} r > 0$, the optimum lies on the boundary of the welfare constraint, satisfying $\Delta U(z^) = 0$.*

Theorem 5.4 (Upper and Lower Bounds of PoG). *For the optimal manipulation z^* in Prop. 5.1, define the welfare loss as $\Delta U^- := \max\{0, -u^\top z^*\}$, and let the honest baseline welfare be $U^{\text{hon}} > 0$. Denote $K := H + 2q I_p$.*

Lower bound. *It always holds that $0 \leq \text{PoG} \leq 1$. If the constraint is active, i.e., $u^\top K^{-1}r > 0$, then $u^\top z^* = 0$, implying $\Delta U^- = 0$ and hence $\text{PoG} = 0$.*

Upper bounds: exact and general forms. *When the constraint is inactive, i.e., $u^\top K^{-1}r \leq 0$,*

$$\text{PoG} = \frac{\Delta U^-}{U^{\text{hon}}} = \frac{|u^\top K^{-1}r|}{U^{\text{hon}}} \leq \frac{\sqrt{(u^\top K^{-1}u)(r^\top K^{-1}r)}}{U^{\text{hon}}}.$$

More generally, for all cases,

$$\text{PoG} \leq \frac{\sqrt{2(u^\top K^{-1}u)\mathcal{M}}}{U^{\text{hon}}}.$$

Spectral upper bound, simplified form. *Let $\lambda_{\min}(K)$ be the minimum eigenvalue of K . Then*

$$\text{PoG} \leq \frac{\|u\|_2 \|r\|_2}{\lambda_{\min}(K) U^{\text{hon}}}.$$

As audits and sanctions intensify—either through larger H or increased q —the value of $\lambda_{\min}(K)$ increases, and accordingly, the upper bound on PoG decreases monotonically.

Experiment — Verification of Static Thresholds. Fig. 1(a) shows that as α increases, the Manipulability Index $\mathcal{M}(\alpha)$ decreases monotonically. The rate of decrease is initially steep and then gradually flattens, indicating diminishing marginal effects. This pattern matches the bound in Thm. 5.3,

$$\mathcal{M}(\alpha) \leq \frac{\|r_\perp\|^2}{2\{\lambda_{\min}(K|_\perp) + \alpha\}},$$

where $r_\perp := P_\perp r$.

The impact of alignment is also pronounced. When alignment is perfect (angle $\theta = 0^\circ$), we have $r_\perp = 0$, leading to $\mathcal{M}(\alpha) = 0$ across all values of α . Conversely, as θ increases, the curves shift upward, reflecting stronger incentives for gaming.

The contour plot in Fig. 1(b) shows that achieving the same tolerance τ requires a larger $\alpha_{\min}(\tau)$ when alignment is poor. In practice, even modest relaxations of the required tolerance τ expand the region where $\alpha_{\min} = 0$. Thus, strategies aiming to enforce extremely small τ solely by increasing α are inefficient.

A more reasonable two-step strategy is therefore: first, improve reward alignment to reduce r_\perp ($r \parallel Ku$; Thm. 9.1), and then, if needed, raise α up to $\alpha_{\min}(\tau)$. As \mathcal{M} decreases, the upper bound of PoG in Thm. 5.4 also decreases, ensuring consistent improvements from the perspective of PoG.

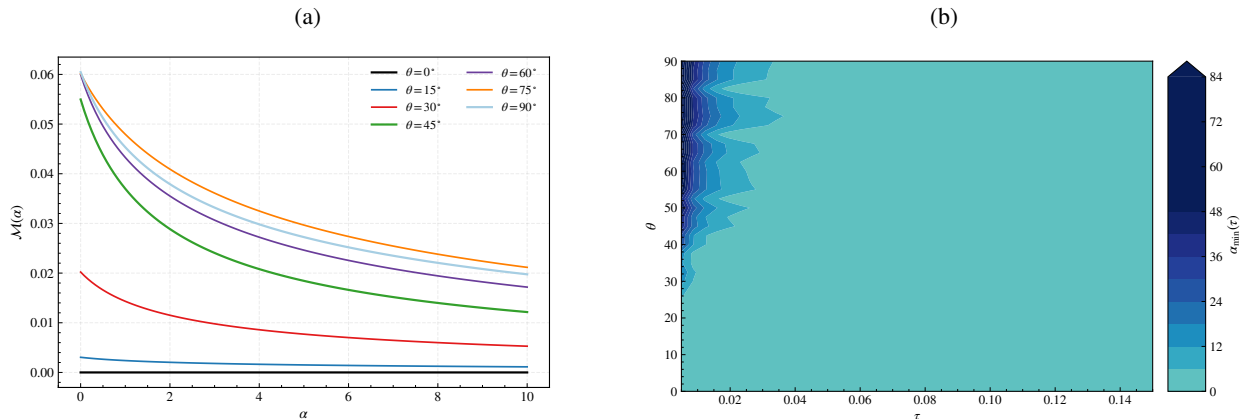


Figure 1: Verification of static thresholds: (a) monotone decrease of $\mathcal{M}(\alpha)$ and the effect of alignment angle; (b) contour of required $\alpha_{\min}(\tau)$ relative to target tolerance τ .

6 Dynamics and Steady-State Equilibrium

Theorem 6.1 (Existence and Properties of Steady-State and Markov Equilibria). *Fix a mechanism (A, R, a, α) . Let the state space \mathcal{S} be finite or a compact metric space, and each client's action space $\mathcal{A}_i = \mathcal{X}_i \times \mathcal{Z}_i$ be compact. Stage utilities $u_i(s, a)$ and the transition kernel $\Pi(ds' | s, a)$ are continuous, with discount factor $\beta \in (0, 1)$. Then the following hold:*

Existence. *Restricting to mixed policies $\sigma_i : \mathcal{S} \rightarrow \Delta(\mathcal{A}_i)$, a stationary Markov mixed equilibrium exists. In equilibrium, the policy profile σ and the induced stationary distribution are mutually consistent.*

Comparative statics: monotone effect of sanctions. *If audits and sanctions are strengthened to $\alpha' \geq \alpha$, then in all stationary equilibria the expected manipulation intensity (the sum of the z_i components) weakly decreases. In particular, reinforcing $K := H + 2qI_p$ weakly reduces the upper bounds on manipulation intensity and gains from manipulation.*

Lattice structure and convergence (under monotone interaction). *If each u_i has increasing differences in the state summary variable and its own z_i , and transitions are monotone in that variable, then the set of stationary equilibria forms a nonempty complete lattice. The minimal and maximal stationary equilibria exist, and sequential best-response dynamics converge to the minimal equilibrium from lower initial conditions and to the maximal equilibrium from upper initial conditions.*

Uniqueness and global convergence (under contraction). *If the Lipschitz constant of the one-period expected best-response operator is $L < 1$, then the stationary equilibrium is unique. From any initial policy, the dynamics globally converge to this unique stationary equilibrium.*

Experiment — Verification of Dynamics. Under the parameter set $(b_1 = 2.4, \sigma = 0.08, b_0 = \alpha - \frac{1}{2}b_1)$, we have

$$T(p) = F_V(b_0 + b_1 p - \alpha) = \frac{1}{1 + \exp(-(2.4p - 1.2)/\sigma)}.$$

This mapping is strongly saturated, making the central crossing point $p = \frac{1}{2}$ unstable and the boundaries $p \in \{0, 1\}$ the effective attractors. Indeed,

$$T'(1/2) = F'_V(0) \frac{b_1}{\sigma} = \frac{1}{4} \cdot \frac{2.4}{0.08} = 7.5 > 1,$$

so the central fixed point is repelling. Initial values above $1/2$ rapidly saturate to 1, while those below $1/2$ saturate to 0.

Fig. 2(a) shows that even with different initial conditions p_0 , trajectories on the same side of the threshold $p_{\text{dom}} \approx 0.5$ converge quickly to the same boundary. Relative to Theorem 6.1, this indicates that the current parameters lie in a region where the local stability condition $|T'(p^*)| < 1$ is violated near the center, as $|T'| > 1$.

Fig. 2(b) plots trajectories when a one-step information delay is introduced. No sustained oscillations are observed. The point $p_0 = 0.5$ remains a fixed point, while all others immediately saturate to 0 or 1. This arises because small σ makes F_V very steep, and clipping to the interval $[0, 1]$ absorbs overshooting instantly. In this parameter region, delay alone does not generate periodic or zigzag orbits near the boundary.

Fig. 2(c) illustrates hysteresis clearly. With the same α , trajectories with $p_0 < 0.5$ converge to 0, while those with $p_0 > 0.5$ converge to 1. Two stable equilibria coexist with an unstable threshold $p_{\text{dom}} \approx 0.5$, consistent with the domino-exit explanation in §7.

7 Participation and Exit

Definition 7.1 (Outside Options and Participation Constraint). Let v_i^{out} denote client i 's outside option. Under mechanism (A, R, a, α) , the discounted expected net utility is

$$V_i = \mathbb{E} \left[\sum_{t \geq 0} \beta^t \{R_i^t - c_i(x_i^t, z_i^t)\} \right].$$

The participation constraint (IR) requires $V_i \geq v_i^{\text{out}}$.

With a sufficiently large population, let F_V denote the distribution of outside options, and let $\Pi_{\text{in}}(p; \alpha)$ be the population-average expected net utility per round, where p is the proportion of remaining honest participants. Then the next-round retention rate is defined as

$$T(p) = 1 - F_V(\Pi_{\text{in}}(p; \alpha)).$$

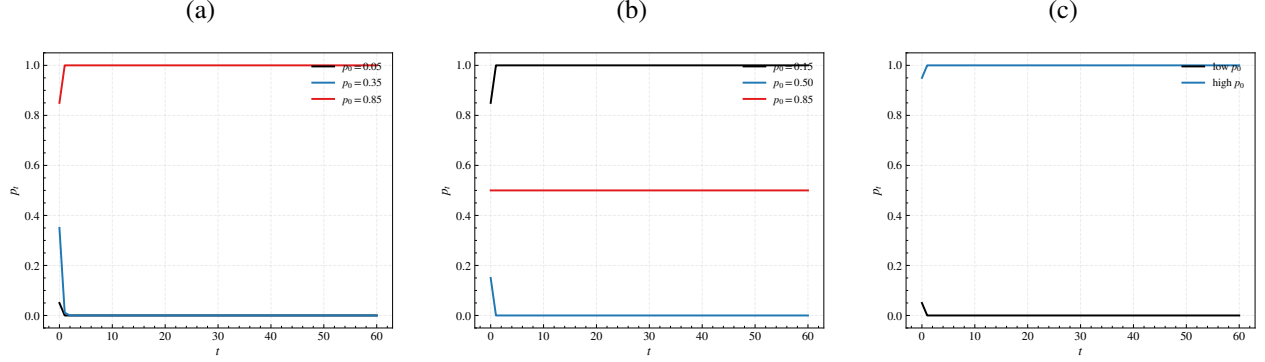


Figure 2: Verification of dynamics: (a) convergence to a single equilibrium, (b) no oscillations under information delay near the boundary, (c) hysteresis depending on initial conditions at the same α .

Theorem 7.2 (Retention Conditions and Domino-Exit Threshold). *Assume that the function $T : [0, 1] \rightarrow [0, 1]$ is continuous and weakly increasing.*

Existence. *There exists a fixed point $p^* \in [0, 1]$ such that $p^* = T(p^*)$. We call p^* the steady-state retention rate.*

Sufficient condition for full retention. *If $\inf_{p \in [0, 1]} \Pi_{\text{in}}(p; \alpha) \geq \sup \text{supp}(F_V)$, then $p^* = 1$ is the unique stable steady state.*

Domino-exit threshold. *If T has an S-shape crossing the diagonal three times, and at the middle crossing point p_{dom} we have $T'(p_{\text{dom}}) > 1$, then p_{dom} is an unstable steady state. If the initial retention rate satisfies $p_0 < p_{\text{dom}}$, the trajectory $p_{t+1} = T(p_t)$ converges to the lower stable equilibrium. Conversely, if $p_0 > p_{\text{dom}}$, the trajectory converges to an upper stable equilibrium $p_{\text{high}} \in (p_{\text{dom}}, 1]$.*

Comparative statics. *Stronger audits and sanctions, and improved alignment of observed signals, increase $\Pi_{\text{in}}(p; \alpha)$, thereby shifting T upward. As a result, p_{high} increases and p_{dom} decreases. Conversely, higher noise or excessive signal sensitivity shift T downward, increasing the risk of collapse.*

Experiment — Retention and Collapse Thresholds. Fig. 3 summarizes how the intersection structure between the fixed-point curve $T(p)$ and the diagonal p varies with policy and environmental parameters. Filled circles denote stable intersections, while hollow circles indicate unstable intersections.

(a) Sanction strength α . When sanctions are weak, T takes an S-shape, intersecting the diagonal three times, with the middle crossing p_{dom} being an unstable threshold where $|T'(p_{\text{dom}})| > 1$. In this region, initial conditions relative to p_{dom} determine whether trajectories fall into low- or high-retention equilibria, creating a domino effect. Increasing α shifts T downward; beyond a critical threshold α^* , the two outer stable intersections annihilate, leaving a single stable equilibrium.

(b) Heterogeneity scale σ . As the distribution of outside options becomes more dispersed, the maximum slope satisfies $\max_p |T'(p)| = b_1/(4\sigma)$, which decreases with larger σ . The central unstable crossing thus disappears, and greater heterogeneity mitigates the risk of multiple equilibria, leading to convergence to a single stable equilibrium.

(c) Location parameter μ . As outside options become less favorable, the entire $T(p)$ curve shifts upward, making $T(p) \approx 1$ across the range. Conversely, more favorable outside options shift the curve downward toward low retention. This visualization demonstrates how environmental changes alone can trigger tipping between retention and collapse.

(d) Sanction cap $\bar{\alpha}$. When $\alpha > \bar{\alpha}$, curve shifts stop and the intersection structure ceases to change. The existence of a cap may structurally prevent reaching α^* to eliminate multiple equilibria.

8 Coalitions (Collusion or Cooperation) and Externalities

Definition 8.1 (TU, NTU Coalitions and Partition-function). Let the player set be $\mathcal{N} = \{1, \dots, N\}$, and a coalition structure be a partition $\mathcal{P} = \{C_1, \dots, C_m\}$.

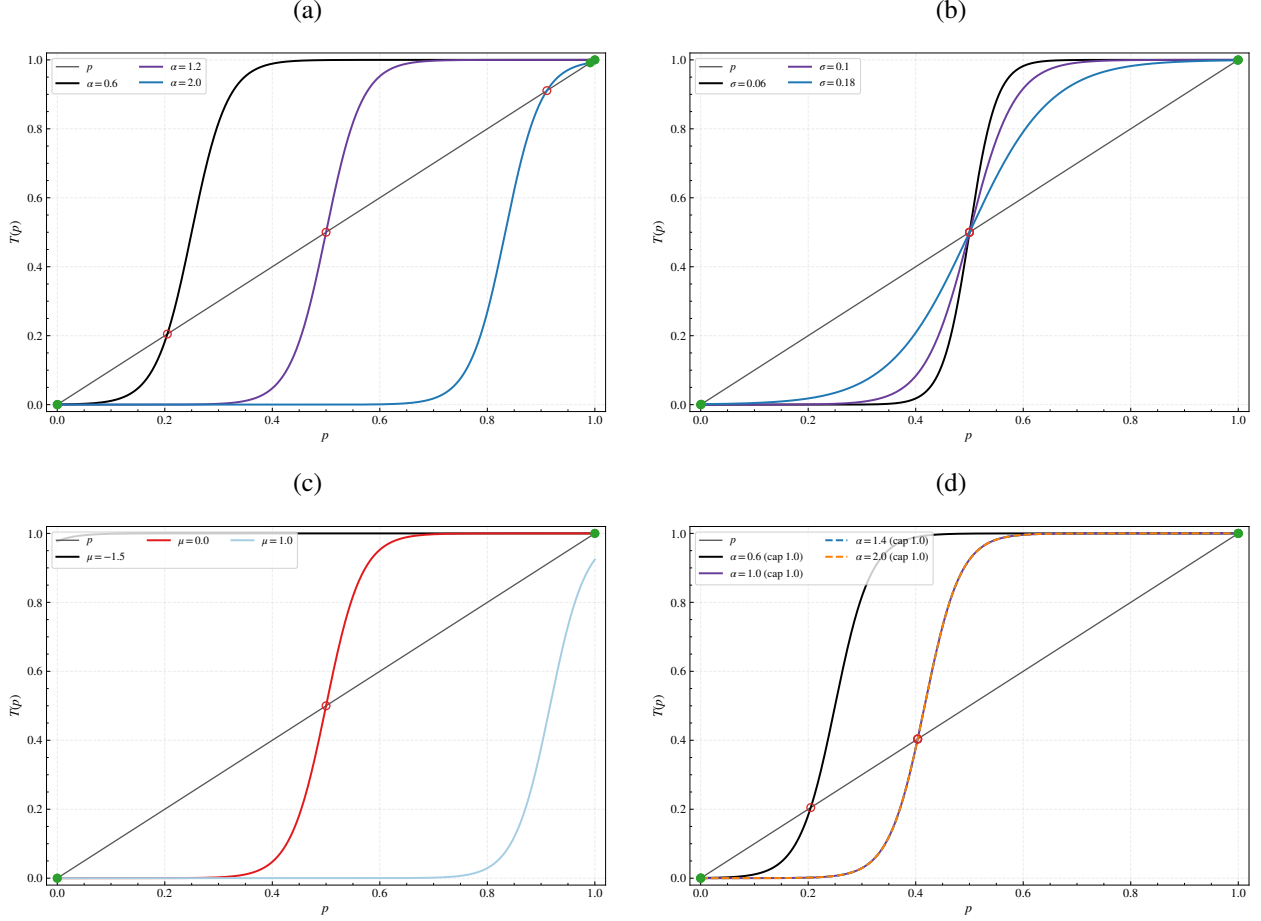


Figure 3: Visualization of retention/collapse thresholds: (a) α sweep—transition from S-shape to unimodal, (b) σ sweep—disappearance of multiple equilibria via slope reduction, (c) μ sweep—shift toward full retention or full collapse, (d) effect of sanction cap $\bar{\alpha}$.

TU, Transferable Utility. Each coalition C has a value $v(C; \mathcal{P})$, and payoffs can be redistributed among members through side payments.

NTU, Non-transferable Utility. Each coalition C has an achievable utility set $\mathcal{F}(C; \mathcal{P}) \subset \mathbb{R}^{|C|}$.

Partition-function externalities. Both v and \mathcal{F} may depend on the composition of other coalitions. In a local approximation of manipulation and rewards, the internal value increment of coalition C for a joint manipulation vector z_C is

$$\Delta V_C \approx \frac{1}{2} r_C^\top M_\alpha r_C,$$

while the change in social welfare is approximated by

$$\Delta U \approx u^\top z_C - \phi \|P_\perp z_C\|_2^2.$$

Here $r_C = \sum_{i \in C} r_i$ is the sum of reward gradients, and $\phi \geq 0$ denotes the strength of coalition externalities.

Proposition 8.2 (Boundary Between Harmful and Cooperative Coalitions). *Consider the local quadratic approximation in Definition 8.1. When coalition C maximizes its reward gain, the optimal manipulation is $z_C^*(\alpha) = M_\alpha r_C$, and the resulting change in social welfare is*

$$\Delta U(\alpha) = u^\top M_\alpha r_C - \phi \|P_\perp M_\alpha r_C\|_2^2.$$

Intuition. Here $P_\perp = I - \frac{uu^\top}{\|u\|_2^2}$ projects onto the component orthogonal to the welfare gradient u , selectively penalizing manipulations that do not contribute to welfare while leaving aligned cooperation along u unaffected.

Always harmful region. If $u^\top r_C < 0$, then $\Delta U(\alpha) < 0$ for all $\alpha \geq 0$.

Boundary harmful case. If $u^\top r_C = 0$, then $\Delta U(\alpha) = -\phi \|P_\perp M_\alpha r_C\|_2^2 \leq 0$. Moreover, if $P_\perp r_C \neq 0$, the coalition is harmful for all α .

Existence of threshold and cooperative transition. If $u^\top r_C > 0$, define the benign threshold as

$$\alpha_{\text{benign}} := \max \left\{ 0, \sqrt{\frac{\phi \lambda_{\parallel} \|P_\perp r_C\|_2^2}{u^\top r_C}} - \lambda_{\perp}^{\min} \right\},$$

where

$$\lambda_{\parallel} = \frac{u^\top K u}{\|u\|_2^2}, \quad \lambda_{\perp}^{\min} = \lambda_{\min}(K \upharpoonright_{\text{span}(u)^\perp}).$$

Then $\Delta U(\alpha) \geq 0$ for all $\alpha \geq \alpha_{\text{benign}}$, while $\Delta U(\alpha) < 0$ for $\alpha < \alpha_{\text{benign}}$.

Theorem 8.3 (Organizational Costs and Stability). *Let the organizational cost of coalition C be denoted by $\kappa(|C|)$. In a TU environment, define the net surplus of coalition C as*

$$S_C(\alpha) = \frac{1}{2} r_C^\top M_\alpha r_C - \kappa(|C|).$$

Then the following results hold.

No-collusion stability (upper bound). If for all coalitions with $|C| \geq 2$,

$$\kappa(|C|) \geq \frac{1}{2} r_C^\top M_\alpha r_C,$$

then every pairwise-stable partition consists only of singletons (no coalition formation occurs).

Existence of nontrivial coalitions (lower bound). If for some coalition C we have $S_C(\alpha) > 0$, then there exists a pairwise-stable or coalition-proof partition in which C or a coalition of the same size is formed. In this case, the TU environment is more favorable to coalition formation than the NTU environment.

Selectivity between cooperative and harmful coalitions. Under the above conditions, if $\alpha \geq \alpha_{\text{benign}}$ and $\Delta U(\alpha) \geq 0$, then any stable coalition formed is cooperative. Conversely, if $\alpha < \alpha_{\text{benign}}$, harmful coalitions may form stably. Stronger externality ϕ shrinks the region where cooperative coalitions are sustainable.

Experiment — Boundaries Between Coalitions. Fig. 4 visualizes the sign of welfare change under coalition formation,

$$\Delta U(\alpha) = u^\top M_\alpha r_C - \phi \|P_\perp M_\alpha r_C\|_2^2,$$

over the (ϕ, α) plane. Light green indicates cooperative coalitions, while orange indicates harmful ones. The solid line denotes the boundary $\Delta U = 0$, i.e., $\phi^*(\alpha)$.

Aligned case $u^\top r_C > 0$. In Fig. 4(a), the boundary $\phi^*(\alpha)$ slopes upward and increases convexly. That is, for a fixed ϕ , larger α expands the cooperative region, whereas larger ϕ expands the harmful region. Formally, with $M_\alpha = (H + 2qI + \alpha P_\perp)^{-1}$, an increase in α enlarges $K_\alpha := H + 2qI + \alpha P_\perp$ and reduces M_α . Consequently, $\|P_\perp M_\alpha r_C\|_2^2$ decreases rapidly, leading to

$$\phi^*(\alpha) = \frac{u^\top M_\alpha r_C}{\|P_\perp M_\alpha r_C\|_2^2}$$

increasing with α . Thus, even under the same externality ϕ , stronger audits and sanctions make cooperative coalitions more likely to emerge.

Misaligned or anti-aligned case $u^\top r_C \leq 0$. In Fig. 4(b), the entire region is essentially harmful, and the boundary $\phi^*(\alpha)$ is barely visible. When the coalition's manipulation direction is misaligned or opposite to social welfare, no level of α generates a cooperative region. In such cases, structural suppression of harmful collusion requires reorienting the reward gradient or redefining the task itself, rather than merely intensifying sanctions.

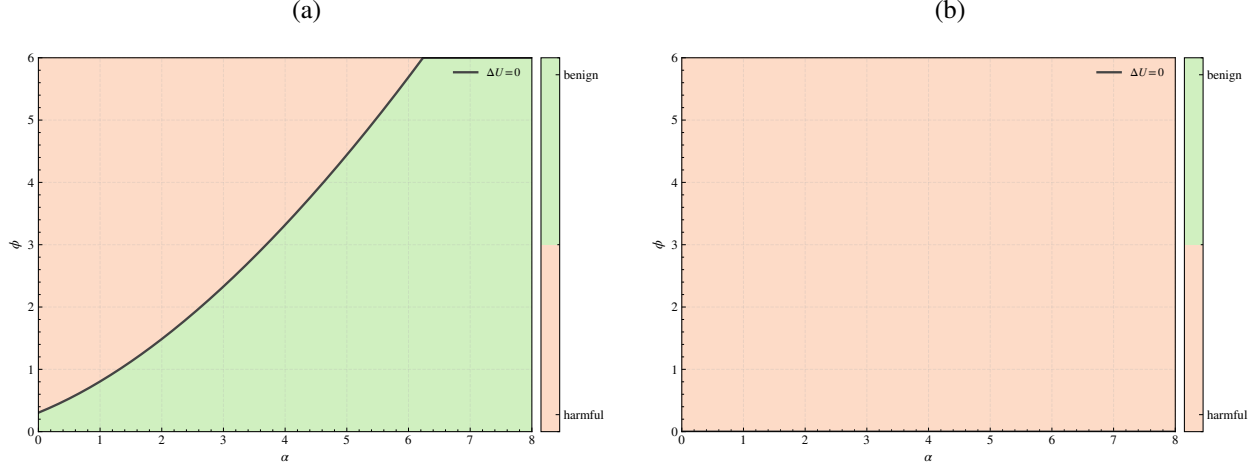


Figure 4: Visualization of coalition boundaries: (a) cooperative-harmful regions and boundary $\phi^*(\alpha)$ when $u^\top r_C > 0$, (b) globally harmful region when $u^\top r_C \leq 0$.

9 Mechanism Design under Constraints

Theorem 9.1 (Optimal Reward Design). *Suppose the observed signal is $s = h(u) + \varepsilon$, where ε has mean 0 and covariance Σ_ε . Restrict the reward rule to a linear budget form $R_i = a + w^\top s_i$ with budget constraint $\mathbb{E}[\sum_i R_i] \leq B$. Under the local quadratic approximation and cost $c(z) = \frac{1}{2}z^\top H z + q\|z\|^2$, the weight vector that maximizes the expected increment of social welfare is*

$$w^* \propto K u, \quad K := H + 2qI_p.$$

That is, the optimal design aligns the reward gradient with the welfare gradient. In this case, the Manipulability Index is minimized at $\mathcal{M} = \frac{1}{2}r^\top M r$ with $r = w^$, and the upper bound of PoG in Thm. 5.4 is simultaneously minimized.*

Theorem 9.2 (Minimum Audit and Sanction Strength). *Consider the setting of the static threshold theorem (Thm. 5.3). To suppress the Manipulability Index below $\mathcal{M}(\alpha) \leq \tau$, the minimum required audit strength is*

$$\alpha_{\min}(\tau) = \max \left\{ 0, \frac{\|P_\perp r\|_2^2}{2\tau} - \lambda_{\min}(K \upharpoonright_{\text{span}(u)^\perp}) \right\}, \quad K := H + 2qI_p.$$

In particular, the larger the component of r orthogonal to u , and the smaller the effective eigenvalue in the orthogonal subspace, the greater the audit strength required.

Proposition 9.3 (Pareto Frontier of Aggregation Design). *Let the aggregator A belong to the family of mean, median, k -trimmed mean, and sorted-weighted aggregation. Under contamination rate ρ and signal variance σ_s^2 , there exists a Pareto frontier between estimation variance and gaming amplification*

$$\Gamma(A) = \sup_{\|z\| \leq 1} \|\nabla_s A \cdot z\|.$$

Low contamination and noise-dominant regime. *When ρ is small and noise dominates, the mean is Pareto efficient.*

High contamination and high sensitivity. *When ρ is large and gaming sensitivity is high, the median and heavy trimming are superior.*

Intermediate regime. *In the middle range, moderate trimming k^* or sorted-weighted aggregation is Pareto efficient.*

Theorem 9.4 (Incentive Reduction via Information Design). *Suppose the server with probability $\pi \in [0, 1]$ conducts randomized challenges, so that rewards depend on the mixed signal*

$$\tilde{s} = (1 - \pi)s + \pi c,$$

where c is the score from private holdout-based challenges, standardized as $\mathbb{E}[c | z] = \eta u^\top z$. Let $K := H + 2qI_p$. Then the Manipulability Index satisfies

$$\tilde{\mathcal{M}} \leq (1 - \pi)^2 \mathcal{M} + \frac{\pi(1 - \pi)}{2} \eta^2 \frac{\|u\|_2^2}{\lambda_{\min}(K)}.$$

In particular, $\tilde{\mathcal{M}}$ decreases monotonically in π . Moreover, the upper bound of PoG in Thm. 5.4 also decreases monotonically as π increases.

Experiment — Sanctions, Rewards, and Information Design. Fig. 5 summarizes how alignment ($w \parallel s$, with $s := Ku$), sanction strength α , and challenge mix ratio π affect the Manipulability Index \mathcal{M} and PoG. Both indices generally decrease monotonically as α and π increase, while alignment determines the overall level.

(a) \mathcal{M} under alignment. When aligned, the baseline level of \mathcal{M} is very low. Increasing π produces a sharp initial drop, while additional suppression via α through P_\perp contributes a modest further decline. This numerically confirms Thm. 9.1 on optimal alignment ($w \propto Ku$), Thm. 9.4 on $(1 - \pi)^2$ decay, and Thm. 9.2 on monotone suppression in α .

(b) PoG under alignment. Across all regions, PoG remains nearly zero. Because alignment activates the constraint at the optimum ($u^\top z^* = 0$), relative gains from gaming are structurally blocked.

(c) \mathcal{M} under misalignment. With misalignment, the absolute level of \mathcal{M} rises by more than an order of magnitude, peaking at small α and π . Contours slope upward, and the minimum sanction $\alpha_{\min}(\tau)$ required to achieve a given tolerance τ decreases rapidly as π grows. Thus, information design significantly reduces the sanction strength needed, consistent with Thm. 9.4 and Thm. 9.2.

(d) PoG under misalignment. Nontrivial values are confined to the lower-left corner. Even slight increases in α or π drive PoG rapidly to zero, since the inactive constraint is immediately resolved, leaving only welfare-aligned improvements.

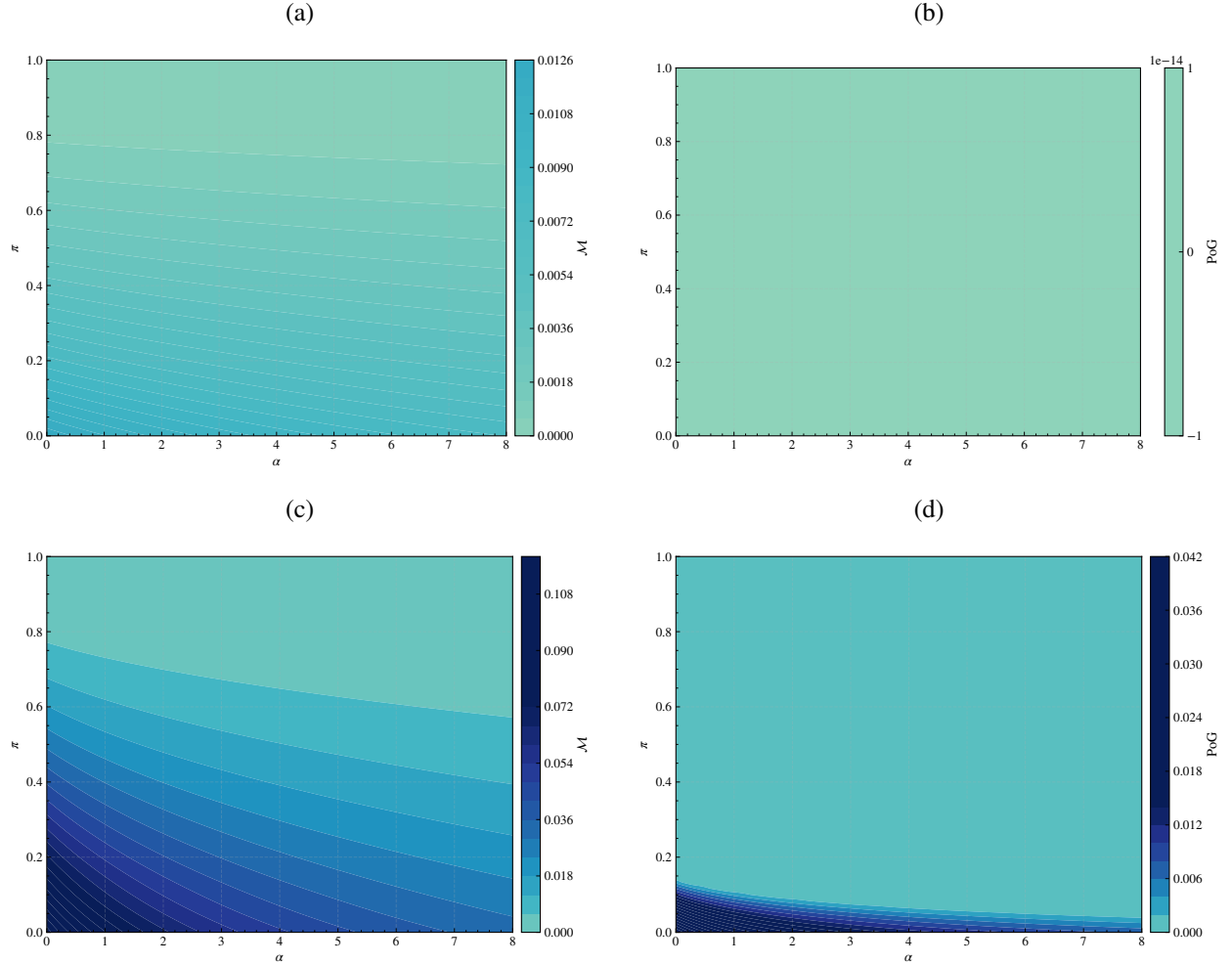


Figure 5: Comparison of sanctions, rewards, and information design: (a) \mathcal{M} under alignment $w \parallel Ku$, (b) PoG under the same condition, (c) \mathcal{M} under misalignment $w \perp u$, (d) PoG under the same condition.

9.1 Experiment — Heatmap of Coalition Stability

Setup. On an α - ϕ grid, multiple coalition directions r_C were sampled at each point, and the cooperative proportion $p(\Delta U \geq 0)$ was estimated based on the sign of

$$\Delta U(\alpha) = u^\top M_\alpha r_C - \phi \|P_\perp M_\alpha r_C\|_2^2.$$

The curvature matrix H , damping parameter q , and distribution of alignment were taken from the common experimental settings. Grid resolution and the number of repetitions are specified in the appendix and reproducibility repository.

Summary of results. The heatmap shows a monotone pattern: the cooperative proportion increases with higher α and decreases with higher ϕ . The boundary separating light (cooperation-dominant) and dark (harm-dominant) regions appears as an upward-sloping curve from the lower left to the upper right, consistent with the theory that $\alpha_{\text{benign}}(\phi)$ increases in externality strength. In regions with high externality, larger α is required to maintain the same stability, suggesting the practical necessity of combining alignment improvements with information design.

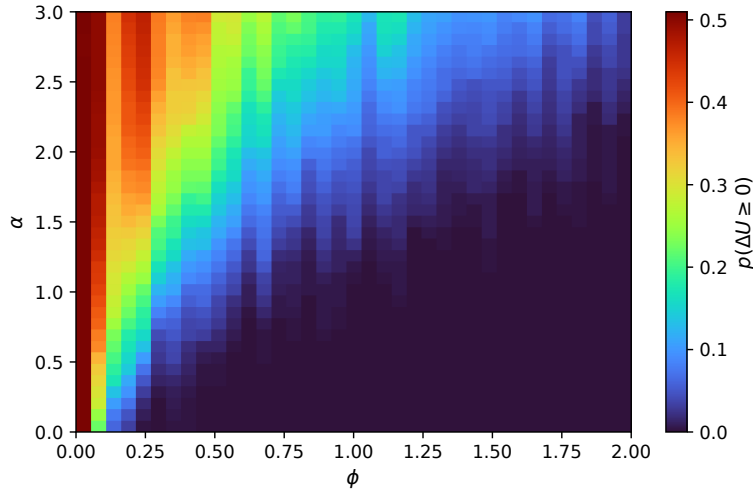


Figure 6: Heatmap of coalition stability. Light regions indicate zones dominated by cooperative stability, with the boundary sloping upward from lower left to upper right.

10 Identification, Testing, and Sample Complexity

Proposition 10.1 (Boundary Between Identifiability and Non-identifiability). *Let the one-round observation be summarized by the statistic $y = Ls$. A local linearization at the baseline yields*

$$y \approx \mu' + (LB)z + \varepsilon, \quad \varepsilon \sim \mathcal{N}(0, \Sigma').$$

Then the following hold.

Non-identifiable set. *If LB is rank-deficient, then $\mathcal{N}(LB) := \{z \neq 0 : LBz = 0\}$ is nonempty. For all $z \in \mathcal{N}(LB)$, the distribution of y is identical to that under $z = 0$, so manipulations along these directions are observationally non-identifiable.*

Mean identifiability — sufficient condition. *Let \mathcal{Z} denote the admissible manipulation subspace, and suppose $\sigma_{\min}(LB \upharpoonright_{\mathcal{Z}}) > 0$. Then for all $z \in \mathcal{Z} \setminus \{0\}$,*

$$\|LBz\|_2 \geq \sigma_{\min} \|z\|_2,$$

so any nonzero manipulation produces a mean shift. With n independent rounds, a GLS statistic consistently distinguishes $z = 0$ from $z \neq 0$ as $n \rightarrow \infty$, achieving consistent identification.

Identification recovery via mixed challenges. *Suppose with probability $\pi \in (0, 1]$ an additional challenge score c is observed with $\mathbb{E}[c | z] = \eta u^\top z$ and $\text{Var}(c) = \sigma_c^2$. The Fisher information of the augmented observation (y, c) adds to the LB component the term*

$$\pi \eta^2 \frac{uu^\top}{\sigma_c^2}.$$

Thus, any manipulation with $u^\top z \neq 0$ becomes identifiable, even if $LBz = 0$.

Theorem 10.2 (Statistical Power and Sample Requirements). *Consider the Gaussian model above, testing the null hypothesis $H_0 : z = 0$ against the alternative $H_1 : z = z^*$ with n independent rounds.*

Noncentrality parameter. *For the GLS mean-difference test, the noncentrality parameter is*

$$\Delta^2 = (LBz^*)^\top (\Sigma')^{-1} (LBz^*) + \pi \eta^2 \frac{(u^\top z^*)^2}{\sigma_c^2}.$$

Normal-approximation necessary and sufficient condition. *To achieve significance level $\alpha \in (0, 1)$ and power $1 - \beta$, the required sample size is*

$$n \geq \frac{(\Phi^{-1}(1 - \alpha) + \Phi^{-1}(1 - \beta))^2}{\Delta^2}.$$

Exponential tail bound. *For any $0 < \delta < 1$,*

$$n \geq \frac{2 \log(2/\delta)}{\Delta^2}$$

ensures that at significance level $\alpha = \delta$, the test achieves power at least $1 - \delta$.

Contribution of mixed challenges. *The second term of the noncentrality parameter grows linearly in π and quadratically in $|u^\top z^*|$.*

Experiment — Power Curves. Fig. 7 illustrates how reward gradient alignment (aligned $w \parallel Ku$ vs. misaligned), sanction strength α , and challenge mix ratio π affect the Manipulability Index \mathcal{M} and PoG. Both indices decrease monotonically as α and π increase. This reflects the sanction effect of suppressing P_\perp components and the information-design effect of effective gradient shrinkage $((1 - \pi)^2)$, consistent with Thm. 9.2 and Thm. 9.4.

(a) \mathcal{M} under alignment. Under alignment, the absolute level of \mathcal{M} is very low overall. Increasing π produces a steep initial decline, while α yields a modest additional reduction via P_\perp suppression. This numerically reproduces Thm. 9.1 on alignment optimality, Thm. 9.4 on $(1 - \pi)^2$ decay, and Thm. 9.2 on monotone suppression in α .

(b) PoG under alignment. Across most regions, PoG is essentially zero, indicating that in aligned cases the constraint is typically active at the optimum with $u^\top z^* = 0$ (Thm. 9.1).

(c) \mathcal{M} under misalignment. With misalignment, \mathcal{M} increases by more than an order of magnitude, peaking in the lower-left region (small α , small π). Contours slope upward, and the minimum sanction $\alpha_{\min}(\tau)$ required to achieve a fixed tolerance τ decreases rapidly with increasing π . Thus, information design greatly reduces the sanction strength required, consistent with Thm. 9.4 and Thm. 9.2.

(d) PoG under misalignment. Nontrivial values are confined to the lower-left corner, and even slight increases in α or π drive PoG rapidly to zero. This shows that in regions where constraints are inactive and gaming is feasible, increasing α or π quickly resolves the slack.

11 Computational Perspective

Theorem 11.1 (Computational Hardness Lower Bound). *Define the decision problem AUDIT-ALLOCATION as follows. For each client i , a candidate set of audit actions \mathcal{A}_i is given. Choosing an action $a \in \mathcal{A}_i$ updates the state $K_i \mapsto K_i + \Delta K_{i,a}$ and incurs cost $c_{i,a}$. Given a total budget B and thresholds $\tau_i > 0$, the question is whether there exist subsets $S_i \subseteq \mathcal{A}_i$ such that*

$$\mathcal{M}_i \left(K_i + \sum_{a \in S_i} \Delta K_{i,a} \right) \leq \tau_i \quad (\forall i), \quad \sum_i \sum_{a \in S_i} c_{i,a} \leq B.$$

NP-completeness. *Even when K_i and $\Delta K_{i,a}$ are diagonal matrices (including rank-1 reinforcements), AUDIT-ALLOCATION is NP-complete.*

Approximation limits. *For worst-case instances, for any $\varepsilon > 0$, no polynomial-time algorithm can $(1 + \varepsilon)$ -approximate the existence of a feasible solution satisfying all thresholds τ_i within the budget.*

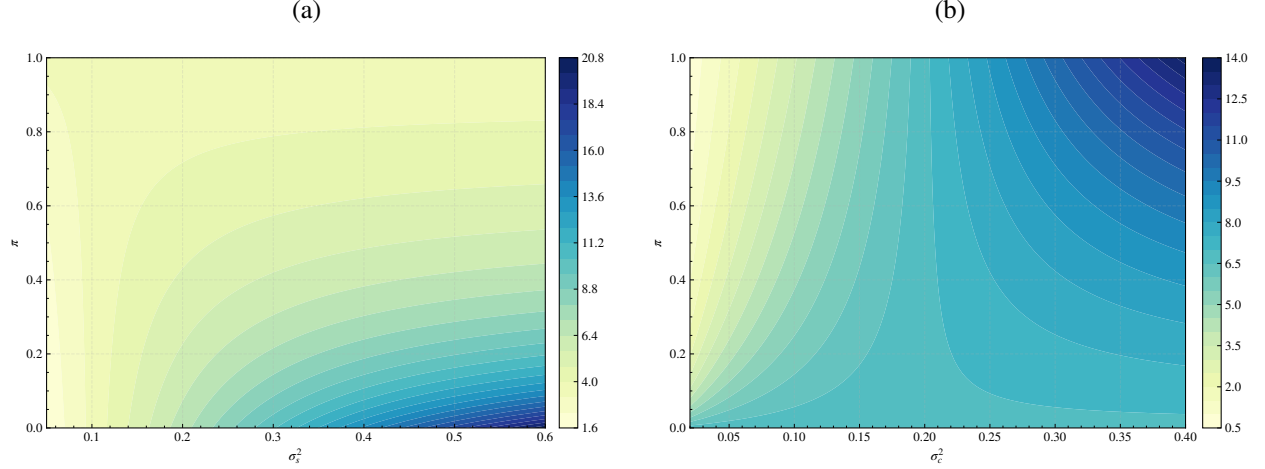


Figure 7: Contours of required sample size: (a) (σ_s^2, π) grid (fixed σ_c^2), (b) (σ_c^2, π) grid (fixed σ_s^2).

Proposition 11.2 (Approximation Algorithms and Guarantees). *Define the total gaming reduction gain as*

$$f(S) = \sum_i \left(\mathcal{M}_i(K_i) - \mathcal{M}_i(K_i + \sum_{a \in S_i} \Delta K_{i,a}) \right).$$

If K_i and $\Delta K_{i,a}$ are diagonal and each component reinforcement exhibits diminishing returns, then f is submodular.

Greedy guarantee. Let S_{greedy} be the solution chosen by a greedy algorithm that selects items maximizing marginal benefit per unit cost. Under the budget constraint,

$$f(S_{\text{greedy}}) \geq (1 - 1/e) f(S^*).$$

Lagrangian penalty formulation. By Lagrangian relaxation of all threshold constraints,

$$f_\lambda(S) = f(S) - \lambda \sum_i \max\{0, \mathcal{M}_i(K_i + \sum_{a \in S_i} \Delta K_{i,a}) - \tau_i\},$$

maximization under an appropriate schedule of λ retains the same approximation guarantee.

12 Discussion

This section distills the intuition revealed across theory and experiments, and provides guidance on how to interpret design choices in practice. Detailed arguments and extended figures are provided in Appendix E.2.

12.1 Key Observations and Intuition

Sanction strength tilts the incentive gradient. As the sanction parameter α increases, the Manipulability Index \mathcal{M} consistently decreases. Sanctions flatten the incentive landscape, reducing the marginal gains from manipulation. Importantly, sanctions do not suppress all directions equally. The projection operator P_\perp preserves contributions aligned with the welfare gradient u , while selectively targeting orthogonal components. Thus, cooperation aligned with welfare remains open, while side paths aimed purely at gaming are narrowed.

Thresholds create safe operating bands. The contour $\alpha_{\min}(\tau)$ separates regions where sanctions are too weak to deter manipulation from regions where sanctions are too strong and discourage genuine cooperation. Operators who begin just above this contour are most likely to suppress manipulation without unnecessary friction. Pushing sanctions far beyond the contour improves stability but may slow learning. In practice, it is advisable to start with some slack but gradually fine-tune within the safe band.

Participation dynamics amplify near thresholds. The retention rate p usually shifts gradually, but near the domino-exit threshold p_{dom} even small shocks can trigger large swings. In this regime, exits cascade easily, and the loss of trust among a few participants can destabilize overall performance. Operationally, warning signs appear first in retention rates and contribution variability. When these indicators deteriorate simultaneously, prioritizing monitoring and buffering over immediate rule changes tends to stabilize the system more effectively.

Coalition boundaries provide targeting baselines. The threshold α_{benign} marks the boundary between cooperative and harmful coalitions. Below the boundary, premature sanctions should give way to additional signal collection, explanation, and incentive redesign. Above the boundary, focused intervention is needed. Projection-based targeting is advantageous because it activates strongly only when coalition alignment turns against welfare, dismantling harmful clusters while protecting benign cooperation.

Aggregation and information design shape sensitivity. Choosing the aggregator A is not a matter of preference. Robust aggregation reduces the impact of outliers and small-scale collusion, lowering \mathcal{M} , but may also weaken faint cooperative signals and slow learning. Similarly, the level of information disclosure is double-edged: fine-grained transparency increases accountability but also provides manipulators with a clearer target. The key is to jointly design aggregation switching rules and disclosure policies, specifying the conditions and sequence of transitions in advance.

Experiments repeatedly confirm these intuitions. Across profiles and environments, consistent patterns emerge: \mathcal{M} decreases with stronger sanctions, threshold contours yield effective operating bands, dynamics amplify near exit thresholds, and projection targeting ensures selective enforcement. These repeated observations suggest that the operating principles are robustly transferable across different models and data environments.

12.2 Trade-offs in Design Choices and Their Remedies

Balancing manipulation suppression and learning speed. Increasing sanctions reduces manipulation but may also slow down learning. A two-stage strategy is effective: initially start just above $\alpha_{\min}(\tau)$ to avoid unstable regions, and once trust indicators stabilize, gradually lower sanctions to promote performance gains.

Balancing robustness of aggregation and preservation of signals. Robust aggregation dampens small-scale collusion but can also weaken meaningful improvements from a minority of clients. A mixed strategy helps: maintain robust global aggregation while supplementing with fine-grained sub-aggregation in specific trust intervals to recover signals.

Balancing transparency and strategic exploitation. Detailed disclosure enhances trust but makes targeted manipulation easier. Combining summary-level disclosure with randomized delays and partial-sample reporting can balance transparency with defensive resilience.

12.3 Operational Guide and Checklist

Initial calibration. Set the audit tolerance τ and estimate $\alpha_{\min}(\tau)$. Start just above this contour. Fix an initial combination of sanctions and audits, and establish baseline values for monitoring indicators.

Monitoring. Observe core indicators at fixed intervals: manipulation-sensitive signals, participation rate, retention rate, contribution variability, cohesion measures, and proximity to thresholds. Trigger alerts only when multiple indicators deteriorate simultaneously, avoiding overreaction to noise in a single metric.

Adjustment rules. When alerts are triggered, first shorten the monitoring window and reduce the level of disclosure. If deterioration persists, raise sanctions slightly, and only as a last step switch the aggregation rule. Insert buffer periods between stages to avoid over-adjustment.

Transition and recovery. Specify conditions and sequence for aggregation switches in advance. Right after a switch, interpret signals conservatively. Once stability is confirmed, gradually lower sanctions and restore the level of disclosure to its prior state.

Gradual deployment. Rather than applying policies at full scale, begin with smaller units, evaluate outcomes, and expand progressively. Combining randomization with periodic re-testing mitigates drift from environmental changes.

12.4 Limitations and Ethical Considerations

Scope of model assumptions. The proposed approach relies on local quadratic approximations, quasi-stationary environments, and partial observability. In settings involving abrupt regime shifts or prolonged non-stationarity, parameters must be re-estimated.

Legitimacy and proportionality. Audits and sanctions should follow the principle of minimal intervention. The stronger the intervention, the greater the need for explainability and avenues for appeal. Safeguards for fairness and abuse prevention should be embedded at the outset of system design.

Responsibility in practical deployment. Operators must balance two objectives: improving performance and maintaining trust. Decisions should not be based solely on metric improvements but should always consider signals of cooperative quality and long-term stability.

13 Conclusion

We reconceptualized federated learning as a system of strategic interactions, proposing a unified framework to analyze and design for coexistence of manipulation and cooperation. Anchoring on the Manipulability Index and the Price of Gaming, we integrated design levers across alignment, sanctions, mixing, aggregation, dynamics, coalitions, and computation, providing an intuitive coordinate system for comparing choices that jointly reduce both indices. We also introduced a practical checklist encompassing aggregation-switch rules, challenge-mix operations, audit-strength adjustments, re-testing triggers, and reporting items, making the framework directly applicable in practice.

Our core contributions can be summarized as follows: First, we provided a consistent coordinate system for interpreting design effects via two indices quantifying incentives for manipulation and the resulting social losses. Second, we formalized thresholds, switching rules, and early-warning signals that serve as benchmarks for maintaining stable cooperation. Third, we proposed computational methods—including greedy, rounding, and local search procedures—for allocating audit resources at scale. Fourth, we validated the framework’s predictions under diverse noise and rule settings through simulations, releasing reproducible procedures.

While our approach works most strongly under assumptions such as local approximation and stationarity, it remains robust to real-world variability through periodic recalibration, randomized mixing and aggregation, and connectivity-based alerts. This framework offers organizations a practical starting point for designing and operating policies that expand cooperation and systematically weaken incentives for manipulation, even under limited budgets and imperfect information.

Reproducibility Statement

We adopt a strict separation of concerns in the artifact repository: *code*, *configurations*, and *logs/outputs* are isolated for transparent and verifiable reproduction.

- **Code repositories**
 - **Reproducibility — artifacts only:** `gcfl`
github.com/AndrewKim1997/gcfl
 Purpose-built to regenerate all paper figures and tables from canonical, versioned logs. Independent of any simulator.
 - **Companion simulator (optional):** `gcfl-sim`
github.com/AndrewKim1997/gcfl-sim
 For exploratory what-if experiments only; not required to reproduce reported results.
- **Key entry points** (`gcfl`)
 - `scripts/reproduce_paper.sh`: single command to regenerate all figures and tables
 - `configs/`: rendering and summarization settings (YAML), version-pinned per release
 - Canonical logs: fetched from the paper-tagged GitHub release assets
- **Quick reproduction**

```

pip install -U pip
pip install -e .[dev]
bash scripts/reproduce_paper.sh

```

If release assets are temporarily unavailable (e.g., CI dry runs), a flag enables tiny mock logs for pipeline sanity checks only.

- **Figure/Table mapping** A compact index in the repository README maps each figure or table to the exact script and configuration used.
- **Determinism and versioning** Artifact regeneration is bitwise identical at a paper tag: canonical logs are immutable, and rendering code and configs are version-pinned. We ship a release manifest with hashes of logs and outputs.
- **Environment** Python 3.10–3.12; NumPy, Pandas, PyYAML, Matplotlib; optional PyArrow. Dockerfile (CPU) is provided.

All components—code, configurations, and artifacts—are public and version-pinned within `gcf1`, enabling one-click reproduction of all reported results.

References

- [1] François Cadelon, Guillaume Sajust de Bergues, David Zuluaga Martínez, Harsha Chandra Shekar, and Marcos Aguiar. The benefits of data sharing now outweigh the risks, April 2024.
- [2] Accenture. Maximize collaboration through secure data sharing, 2019. Privacy Preserving Computation techniques (incl. MPC, HE, DP, Federated Learning).
- [3] Ari Libarikian, Kayvaun Rowshankish, Markus Berger de León, and Vishnu Kamalnath. From raw data to real profits: A primer for building a thriving data business, July 2024.
- [4] Ben Ellencweig, Guilherme Cruz, Vishnu Kamalnath, and Miguel Frade. Intelligence at scale: Data monetization in the age of gen ai, July 2025.
- [5] Alex Singla, Alexander Sukharevsky, Lareina Yee, and Michael Chui. The state of ai: How organizations are rewiring to capture value, March 2025. With Bryce Hall.
- [6] PwC. Only 2% of businesses have implemented firm-wide cyber resilience, even as cyber security concerns are top-of-mind and the average data breach exceeds us\$3m: Pwc 2025 global digital trust insights, September 2024. Press release.
- [7] PwC US. System and organization controls (soc) reporting, 2024. Overview of SOC 1/2 reporting for vendor assurance and governance.
- [8] PwC US. Responsible ai and third-party risk management, June 2025.
- [9] PwC US. Responsible ai and privacy: What you need to know, July 2025.
- [10] Ankit Bisht, Lareina Yee, Roger Roberts, Brittany Presten, and Katherine Ottenbreit. Open source technology in the age of ai, April 2025.
- [11] Peva Blanchard, El Mahdi El Mhamdi, Rachid Guerraoui, and Julien Stainer. Machine learning with adversaries: Byzantine tolerant gradient descent. *Advances in neural information processing systems*, 30, 2017.
- [12] Dong Yin, Yudong Chen, Ramchandran Kannan, and Peter Bartlett. Byzantine-robust distributed learning: Towards optimal statistical rates. In *International conference on machine learning*, pages 5650–5659. Pmlr, 2018.
- [13] Rachid Guerraoui, Sébastien Rouault, et al. The hidden vulnerability of distributed learning in byzantium. In *International conference on machine learning*, pages 3521–3530. PMLR, 2018.
- [14] Krishna Pillutla, Sham M Kakade, and Zaid Harchaoui. Robust aggregation for federated learning. *IEEE Transactions on Signal Processing*, 70:1142–1154, 2022.
- [15] Dan Alistarh, Zeyuan Allen-Zhu, and Jerry Li. Byzantine stochastic gradient descent. *Advances in neural information processing systems*, 31, 2018.
- [16] Jeremy Bernstein, Jiawei Zhao, Kamyar Azizzadenesheli, and Anima Anandkumar. signsgd with majority vote is communication efficient and fault tolerant. *arXiv preprint arXiv:1810.05291*, 2018.
- [17] Lingjiao Chen, Hongyi Wang, Zachary Charles, and Dimitris Papailiopoulos. Draco: Byzantine-resilient distributed training via redundant gradients. In *International Conference on Machine Learning*, pages 903–912. PMLR, 2018.

- [18] Georgios Damaskinos, El-Mahdi El-Mhamdi, Rachid Guerraoui, Arsany Guirguis, and Sébastien Rouault. Aggregathor: Byzantine machine learning via robust gradient aggregation. *Proceedings of Machine Learning and Systems*, 1:81–106, 2019.
- [19] Cong Xie, Sanmi Koyejo, and Indranil Gupta. Zeno++: Robust fully asynchronous sgd. In *International conference on machine learning*, pages 10495–10503. PMLR, 2020.
- [20] Gilad Baruch, Moran Baruch, and Yoav Goldberg. A little is enough: Circumventing defenses for distributed learning. *Advances in Neural Information Processing Systems*, 32, 2019.
- [21] Minghong Fang, Xiaoyu Cao, Jinyuan Jia, and Neil Gong. Local model poisoning attacks to {Byzantine-Robust} federated learning. In *29th USENIX security symposium (USENIX Security 20)*, pages 1605–1622, 2020.
- [22] Eugene Bagdasaryan, Andreas Veit, Yiqing Hua, Deborah Estrin, and Vitaly Shmatikov. How to backdoor federated learning. In *International conference on artificial intelligence and statistics*, pages 2938–2948. PMLR, 2020.
- [23] Hongyi Wang, Kartik Sreenivasan, Shashank Rajput, Harit Vishwakarma, Saurabh Agarwal, Jy-yong Sohn, Kangwook Lee, and Dimitris Papailiopoulos. Attack of the tails: Yes, you really can backdoor federated learning. *Advances in neural information processing systems*, 33:16070–16084, 2020.
- [24] Clement Fung, Chris JM Yoon, and Ivan Beschastnikh. Mitigating sybils in federated learning poisoning. *arXiv preprint arXiv:1808.04866*, 2018.
- [25] Xiaoyu Cao, Minghong Fang, Jia Liu, and Neil Zhenqiang Gong. Filtrust: Byzantine-robust federated learning via trust bootstrapping. *arXiv preprint arXiv:2012.13995*, 2020.
- [26] Amirata Ghorbani and James Zou. Data shapley: Equitable valuation of data for machine learning. In *International conference on machine learning*, pages 2242–2251. PMLR, 2019.
- [27] Ruoxi Jia, David Dao, Boxin Wang, Frances Ann Hubis, Nick Hynes, Nezihe Merve Gürel, Bo Li, Ce Zhang, Dawn Song, and Costas J Spanos. Towards efficient data valuation based on the shapley value. In *The 22nd International Conference on Artificial Intelligence and Statistics*, pages 1167–1176. PMLR, 2019.
- [28] Pang Wei Koh and Percy Liang. Understanding black-box predictions via influence functions. In *International conference on machine learning*, pages 1885–1894. PMLR, 2017.
- [29] Jinsung Yoon, Sercan Arik, and Tomas Pfister. Data valuation using reinforcement learning. In *International Conference on Machine Learning*, pages 10842–10851. PMLR, 2020.
- [30] Zelei Liu, Yuanyuan Chen, Han Yu, Yang Liu, and Lizhen Cui. Gtg-shapley: Efficient and accurate participant contribution evaluation in federated learning. *ACM Transactions on intelligent Systems and Technology (TIST)*, 13(4):1–21, 2022.
- [31] Yi-Chung Chen, Hsi-Wen Chen, Shun-Gui Wang, and Ming-Syan Chen. Space: Single-round participant amalgamation for contribution evaluation in federated learning. *Advances in Neural Information Processing Systems*, 36:6422–6441, 2023.
- [32] Nurbek Tastan, Samar Fares, Toluwani Aremu, Samuel Horvath, and Karthik Nandakumar. Redefining contributions: shapley-driven federated learning. In *Proceedings of the Thirty-Third International Joint Conference on Artificial Intelligence*, pages 5009–5017, 2024.
- [33] Yiwei Chen, Kaiyu Li, Guoliang Li, and Yong Wang. Contributions estimation in federated learning: A comprehensive experimental evaluation. *Proceedings of the VLDB Endowment*, 17(8):2077–2090, 2024.
- [34] Jiawen Kang, Zehui Xiong, Dusit Niyato, Shengli Xie, and Junshan Zhang. Incentive mechanism for reliable federated learning: A joint optimization approach to combining reputation and contract theory. *IEEE Internet of Things Journal*, 6(6):10700–10714, 2019.
- [35] Jingwen Zhang, Yuezhou Wu, and Rong Pan. Incentive mechanism for horizontal federated learning based on reputation and reverse auction. In *Proceedings of the Web Conference 2021*, pages 947–956, 2021.
- [36] Xiaoli Tang, Han Yu, Xiaoxiao Li, and Sarit Kraus. Intelligent agents for auction-based federated learning: a survey. In *Proceedings of the Thirty-Third International Joint Conference on Artificial Intelligence*, pages 8253–8261, 2024.
- [37] Zhebin Zhang, Dajie Dong, Yuhang Ma, Yilong Ying, Dawei Jiang, Ke Chen, Lidan Shou, and Gang Chen. Refiner: A reliable incentive-driven federated learning system powered by blockchain. *Proceedings of the VLDB Endowment*, 14(12):2659–2662, 2021.
- [38] Yuan Liu, Zhengpeng Ai, Shuai Sun, Shuangfeng Zhang, Zelei Liu, and Han Yu. Fedcoin: A peer-to-peer payment system for federated learning. In *Federated learning: privacy and incentive*, pages 125–138. Springer, 2020.

- [39] Jianquan Ouyang and Liyuan Kuang. Frfl: A fair and robust incentive mechanism for heterogeneous federated learning. In *International Conference on Intelligent Computing*, pages 338–350. Springer, 2025.
- [40] Mehryar Mohri, Gary Sivek, and Ananda Theertha Suresh. Agnostic federated learning. In *International conference on machine learning*, pages 4615–4625. PMLR, 2019.
- [41] Tian Li, Maziar Sanjabi, Ahmad Beirami, and Virginia Smith. Fair resource allocation in federated learning. *arXiv preprint arXiv:1905.10497*, 2019.
- [42] Fan Lai, Xiangfeng Zhu, Harsha V Madhyastha, and Mosharaf Chowdhury. Oort: Efficient federated learning via guided participant selection. In *15th {USENIX} Symposium on Operating Systems Design and Implementation ({OSDI} 21)*, pages 19–35, 2021.
- [43] Takayuki Nishio and Ryo Yonetani. Client selection for federated learning with heterogeneous resources in mobile edge. In *ICC 2019-2019 IEEE international conference on communications (ICC)*, pages 1–7. IEEE, 2019.
- [44] Xiaoqiang Lin, Xinyi Xu, See-Kiong Ng, Chuan-Sheng Foo, and Bryan Kian Hsiang Low. Fair yet asymptotically equal collaborative learning. In *International Conference on Machine Learning*, pages 21223–21259. PMLR, 2023.
- [45] Dong Seok Kim, Shabir Ahmad, and Taeg Keun Whangbo. Federated regressive learning: Adaptive weight updates through statistical information of clients. *Applied Soft Computing*, 166:112043, 2024.
- [46] Kate Donahue and Jon Kleinberg. Model-sharing games: Analyzing federated learning under voluntary participation. In *Proceedings of the AAAI Conference on Artificial Intelligence*, volume 35, pages 5303–5311, 2021.
- [47] Kate Donahue and Jon Kleinberg. Optimality and stability in federated learning: A game-theoretic approach. *Advances in Neural Information Processing Systems*, 34:1287–1298, 2021.
- [48] Cengiz Hasan. Incentive mechanism design for federated learning: Hedonic game approach. *arXiv preprint arXiv:2101.09673*, 2021.
- [49] Lokesh Nagalapatti and Ramasuri Narayanam. Game of gradients: Mitigating irrelevant clients in federated learning. In *Proceedings of the AAAI Conference on Artificial Intelligence*, volume 35, pages 9046–9054, 2021.
- [50] Ning Zhang, Qian Ma, and Xu Chen. Enabling long-term cooperation in cross-silo federated learning: A repeated game perspective. *IEEE Transactions on Mobile Computing*, 22(7):3910–3924, 2022.
- [51] Yalin E Sagduyu. Free-rider games for federated learning with selfish clients in nextg wireless networks. In *2022 IEEE Conference on Communications and Network Security (CNS)*, pages 365–370. IEEE, 2022.
- [52] Bing Luo, Yutong Feng, Shiqiang Wang, Jianwei Huang, and Leandros Tassiulas. Incentive mechanism design for unbiased federated learning with randomized client participation. In *2023 IEEE 43rd International Conference on Distributed Computing Systems (ICDCS)*, pages 545–555. IEEE, 2023.
- [53] Yunus Sarikaya and Ozgur Ercetin. Motivating workers in federated learning: A stackelberg game perspective. *IEEE Networking Letters*, 2(1):23–27, 2019.
- [54] Rui Hu and Yanmin Gong. Trading data for learning: Incentive mechanism for on-device federated learning. In *GLOBECOM 2020-2020 IEEE Global Communications Conference*, pages 1–6. IEEE, 2020.
- [55] Tra Huong Thi Le, Nguyen H Tran, Yan Kyaw Tun, Minh NH Nguyen, Shashi Raj Pandey, Zhu Han, and Choong Seon Hong. An incentive mechanism for federated learning in wireless cellular networks: An auction approach. *IEEE Transactions on Wireless Communications*, 20(8):4874–4887, 2021.
- [56] Ningning Ding, Zhixuan Fang, and Jianwei Huang. Optimal contract design for efficient federated learning with multi-dimensional private information. *IEEE Journal on Selected Areas in Communications*, 39(1):186–200, 2020.
- [57] Yuan Liu, Mengmeng Tian, Yuxin Chen, Zehui Xiong, Cyril Leung, and Chunyan Miao. A contract theory based incentive mechanism for federated learning. In *Federated and Transfer Learning*, pages 117–137. Springer, 2022.
- [58] Jiwei Huang, Bowen Ma, Yuan Wu, Ying Chen, and Xuemin Shen. A hierarchical incentive mechanism for federated learning. *IEEE Transactions on Mobile Computing*, 23(12):12731–12747, 2024.
- [59] Chenglu Pan, Jiarong Xu, Yue Yu, Ziqi Yang, Qingbiao Wu, Chunping Wang, Lei Chen, and Yang Yang. Towards fair graph federated learning via incentive mechanisms. In *Proceedings of the AAAI Conference on Artificial Intelligence*, volume 38, pages 14499–14507, 2024.

- [60] Wei Guo, Yijin Wang, and Pingyu Jiang. Incentive mechanism design for federated learning with stackelberg game perspective in the industrial scenario. *Computers & Industrial Engineering*, 184:109592, 2023.
- [61] David Byrd, Vaikkunth Mugunthan, Antigoni Polychroniadou, and Tucker Balch. Collusion resistant federated learning with oblivious distributed differential privacy. In *Proceedings of the Third ACM International Conference on AI in Finance*, pages 114–122, 2022.
- [62] Ruoting Xiong, Wei Ren, Shenghui Zhao, Jie He, Yi Ren, Kim-Kwang Raymond Choo, and Geyong Min. Copifl: A collusion-resistant and privacy-preserving federated learning crowdsourcing scheme using blockchain and homomorphic encryption. *Future Generation Computer Systems*, 156:95–104, 2024.
- [63] David Manheim and Scott Garrabrant. Categorizing variants of goodhart’s law. *arXiv preprint arXiv:1803.04585*, 2018.
- [64] Dario Amodei, Chris Olah, Jacob Steinhardt, Paul Christiano, John Schulman, and Dan Mané. Concrete problems in ai safety. *arXiv preprint arXiv:1606.06565*, 2016.
- [65] Joar Skalse, Nikolaus Howe, Dmitrii Krashennnikov, and David Krueger. Defining and characterizing reward gaming. *Advances in Neural Information Processing Systems*, 35:9460–9471, 2022.
- [66] Tom Everitt, Marcus Hutter, Ramana Kumar, and Victoria Krakovna. Reward tampering problems and solutions in reinforcement learning: A causal influence diagram perspective. *Synthese*, 198(Suppl 27):6435–6467, 2021.
- [67] Lauro Langosco Di Langosco, Jack Koch, Lee D Sharkey, Jacob Pfau, and David Krueger. Goal misgeneralization in deep reinforcement learning. In *International Conference on Machine Learning*, pages 12004–12019. PMLR, 2022.
- [68] Moritz Hardt, Nimrod Megiddo, Christos Papadimitriou, and Mary Wootters. Strategic classification. In *Proceedings of the 2016 ACM conference on innovations in theoretical computer science*, pages 111–122, 2016.
- [69] Michael Brückner and Tobias Scheffer. Stackelberg games for adversarial prediction problems. In *Proceedings of the 17th ACM SIGKDD international conference on Knowledge discovery and data mining*, pages 547–555, 2011.
- [70] Juan Perdomo, Tijana Zrnic, Celestine Mender-Dünner, and Moritz Hardt. Performative prediction. In *International Conference on Machine Learning*, pages 7599–7609. PMLR, 2020.
- [71] Celestine Mender-Dünner, Juan Perdomo, Tijana Zrnic, and Moritz Hardt. Stochastic optimization for performative prediction. *Advances in Neural Information Processing Systems*, 33:4929–4939, 2020.
- [72] John Miller, Smitha Milli, and Moritz Hardt. Strategic classification is causal modeling in disguise. In *International Conference on Machine Learning*, pages 6917–6926. PMLR, 2020.
- [73] Avrim Blum and Moritz Hardt. The ladder: A reliable leaderboard for machine learning competitions. In *International Conference on Machine Learning*, pages 1006–1014. PMLR, 2015.
- [74] Cynthia Dwork, Vitaly Feldman, Moritz Hardt, Toniann Pitassi, Omer Reingold, and Aaron Roth. The reusable holdout: Preserving validity in adaptive data analysis. *Science*, 349(6248):636–638, 2015.
- [75] Michael Kearns, Seth Neel, Aaron Roth, and Zhiwei Steven Wu. Preventing fairness gerrymandering: Auditing and learning for subgroup fairness. In *International conference on machine learning*, pages 2564–2572. PMLR, 2018.
- [76] Tijana Zrnic, Eric Mazumdar, Shankar Sastry, and Michael Jordan. Who leads and who follows in strategic classification? *Advances in Neural Information Processing Systems*, 34:15257–15269, 2021.
- [77] Ravi Sundaram, Anil Vullikanti, Haifeng Xu, and Fan Yao. Pac-learning for strategic classification. *Journal of Machine Learning Research*, 24(192):1–38, 2023.
- [78] Cynthia Dwork, Vitaly Feldman, Moritz Hardt, Toniann Pitassi, Omer Reingold, and Aaron Leon Roth. Preserving statistical validity in adaptive data analysis. In *Proceedings of the forty-seventh annual ACM symposium on Theory of computing*, pages 117–126, 2015.
- [79] Cynthia Dwork, Vitaly Feldman, Moritz Hardt, Toni Pitassi, Omer Reingold, and Aaron Roth. Generalization in adaptive data analysis and holdout reuse. *Advances in neural information processing systems*, 28, 2015.
- [80] Raef Bassily, Kobbi Nissim, Adam Smith, Thomas Steinke, Uri Stemmer, and Jonathan Ullman. Algorithmic stability for adaptive data analysis. In *Proceedings of the forty-eighth annual ACM symposium on Theory of Computing*, pages 1046–1059, 2016.
- [81] Moritz Hardt, Eric Price, and Nati Srebro. Equality of opportunity in supervised learning. *Advances in neural information processing systems*, 29, 2016.

- [82] Michael P Kim, Amirata Ghorbani, and James Zou. Multiaccuracy: Black-box post-processing for fairness in classification. In *Proceedings of the 2019 AAAI/ACM Conference on AI, Ethics, and Society*, pages 247–254, 2019.
- [83] Alekh Agarwal, Alina Beygelzimer, Miroslav Dudík, John Langford, and Hanna Wallach. A reductions approach to fair classification. In *International conference on machine learning*, pages 60–69. PMLR, 2018.
- [84] Matt J Kusner, Joshua Loftus, Chris Russell, and Ricardo Silva. Counterfactual fairness. *Advances in neural information processing systems*, 30, 2017.
- [85] Emily Diana, Wesley Gill, Michael Kearns, Krishnamurthy Kenthapadi, Aaron Roth, and Saeed Sharifi-Malvajerdi. Multiaccurate proxies for downstream fairness. In *Proceedings of the 2022 ACM Conference on Fairness, Accountability, and Transparency*, pages 1207–1239, 2022.
- [86] Margaret Mitchell, Simone Wu, Andrew Zaldivar, Parker Barnes, Lucy Vasserman, Ben Hutchinson, Elena Spitzer, Inioluwa Deborah Raji, and Timnit Gebru. Model cards for model reporting. In *Proceedings of the conference on fairness, accountability, and transparency*, pages 220–229, 2019.
- [87] Timnit Gebru, Jamie Morgenstern, Briana Vecchione, Jennifer Wortman Vaughan, Hanna Wallach, Hal Daumé III, and Kate Crawford. Datasheets for datasets. *Communications of the ACM*, 64(12):86–92, 2021.
- [88] Marco Tulio Ribeiro, Tongshuang Wu, Carlos Guestrin, and Sameer Singh. Beyond accuracy: Behavioral testing of nlp models with checklist. In *Proceedings of the 58th Annual Meeting of the Association for Computational Linguistics*. Association for Computational Linguistics, 2020.
- [89] Douwe Kiela, Max Bartolo, Yixin Nie, Divyansh Kaushik, Atticus Geiger, Zhengxuan Wu, Bertie Vidgen, Grusha Prasad, Amanpreet Singh, Pratik Ringshia, et al. Dynabench: Rethinking benchmarking in nlp. In *Proceedings of the 2021 Conference of the North American Chapter of the Association for Computational Linguistics: Human Language Technologies*, pages 4110–4124, 2021.
- [90] Pang Wei Koh, Shiori Sagawa, Henrik Marklund, Sang Michael Xie, Marvin Zhang, Akshay Balsubramani, Weihua Hu, Michihiro Yasunaga, Richard Lanus Phillips, Irena Gao, et al. Wilds: A benchmark of in-the-wild distribution shifts. In *International conference on machine learning*, pages 5637–5664. PMLR, 2021.
- [91] Francesco Croce, Maksym Andriushchenko, Vikash Sehwal, Edoardo De Benedetti, Nicolas Flammarion, Mung Chiang, Prateek Mittal, and Matthias Hein. Robustbench: a standardized adversarial robustness benchmark. *arXiv preprint arXiv:2010.09670*, 2020.
- [92] Reza Shokri, Marco Stronati, Congzheng Song, and Vitaly Shmatikov. Membership inference attacks against machine learning models. In *2017 IEEE symposium on security and privacy (SP)*, pages 3–18. IEEE, 2017.
- [93] Nicholas Carlini, Chang Liu, Úlfar Erlingsson, Jernej Kos, and Dawn Song. The secret sharer: Evaluating and testing unintended memorization in neural networks. In *28th USENIX security symposium (USENIX security 19)*, pages 267–284, 2019.
- [94] Nicholas Carlini, Florian Tramer, Eric Wallace, Matthew Jagielski, Ariel Herbert-Voss, Katherine Lee, Adam Roberts, Tom Brown, Dawn Song, Úlfar Erlingsson, et al. Extracting training data from large language models. In *30th USENIX security symposium (USENIX Security 21)*, pages 2633–2650, 2021.
- [95] Congzheng Song and Vitaly Shmatikov. Auditing data provenance in text-generation models. In *Proceedings of the 25th ACM SIGKDD International Conference on Knowledge Discovery & Data Mining*, pages 196–206, 2019.
- [96] Brandon Tran, Jerry Li, and Aleksander Madry. Spectral signatures in backdoor attacks. *Advances in neural information processing systems*, 31, 2018.
- [97] Bolun Wang, Yuanshun Yao, Shawn Shan, Huiying Li, Bimal Viswanath, Haitao Zheng, and Ben Y Zhao. Neural cleanse: Identifying and mitigating backdoor attacks in neural networks. In *2019 IEEE symposium on security and privacy (SP)*, pages 707–723. IEEE, 2019.
- [98] Stephan Rabanser, Stephan Günnemann, and Zachary Lipton. Failing loudly: An empirical study of methods for detecting dataset shift. *Advances in Neural Information Processing Systems*, 32, 2019.
- [99] Julia Dressel and Hany Farid. The accuracy, fairness, and limits of predicting recidivism. *Science advances*, 4(1):eaao5580, 2018.
- [100] Martin Abadi, Andy Chu, Ian Goodfellow, H Brendan McMahan, Ilya Mironov, Kunal Talwar, and Li Zhang. Deep learning with differential privacy. In *Proceedings of the 2016 ACM SIGSAC conference on computer and communications security*, pages 308–318, 2016.
- [101] H Brendan McMahan, Daniel Ramage, Kunal Talwar, and Li Zhang. Learning differentially private recurrent language models. In *International Conference on Learning Representations*, 2018.

- [102] Robin C Geyer, Tassilo Klein, and Moin Nabi. Differentially private federated learning: A client level perspective. *arXiv preprint arXiv:1712.07557*, 2017.
- [103] Keith Bonawitz, Vladimir Ivanov, Ben Kreuter, Antonio Marcedone, H Brendan McMahan, Sarvar Patel, Daniel Ramage, Aaron Segal, and Karn Seth. Practical secure aggregation for privacy-preserving machine learning. In *proceedings of the 2017 ACM SIGSAC Conference on Computer and Communications Security*, pages 1175–1191, 2017.
- [104] Úlfar Erlingsson, Vitaly Feldman, Ilya Mironov, Ananth Raghunathan, Kunal Talwar, and Abhradeep Thakurta. Amplification by shuffling: From local to central differential privacy via anonymity. In *Proceedings of the Thirtieth Annual ACM-SIAM Symposium on Discrete Algorithms*, pages 2468–2479. SIAM, 2019.
- [105] Nicolas Papernot, Martín Abadi, Úlfar Erlingsson, Ian Goodfellow, and Kunal Talwar. Semi-supervised knowledge transfer for deep learning from private training data. In *International Conference on Learning Representations*, 2017.
- [106] Nicolas Papernot, Shuang Song, Ilya Mironov, Ananth Raghunathan, Kunal Talwar, and Úlfar Erlingsson. Scalable private learning with pate. *arXiv preprint arXiv:1802.08908*, 2018.
- [107] Reza Shokri and Vitaly Shmatikov. Privacy-preserving deep learning. In *Proceedings of the 22nd ACM SIGSAC conference on computer and communications security*, pages 1310–1321, 2015.
- [108] Ran Gilad-Bachrach, Nathan Dowlin, Kim Laine, Kristin Lauter, Michael Naehrig, and John Wernsing. Cryptonets: Applying neural networks to encrypted data with high throughput and accuracy. In *International conference on machine learning*, pages 201–210. PMLR, 2016.
- [109] Luca Melis, Congzheng Song, Emiliano De Cristofaro, and Vitaly Shmatikov. Exploiting unintended feature leakage in collaborative learning. In *2019 IEEE symposium on security and privacy (SP)*, pages 691–706. IEEE, 2019.
- [110] Ligeng Zhu, Zhijian Liu, and Song Han. Deep leakage from gradients. *Advances in neural information processing systems*, 32, 2019.
- [111] Eugene Bagdasaryan, Omid Poursaeed, and Vitaly Shmatikov. Differential privacy has disparate impact on model accuracy. *Advances in neural information processing systems*, 32, 2019.
- [112] Matthew Jagielski, Michael Kearns, Jieming Mao, Alina Oprea, Aaron Roth, Saeed Sharifi-Malvajerdi, and Jonathan Ullman. Differentially private fair learning. In *International Conference on Machine Learning*, pages 3000–3008. PMLR, 2019.
- [113] Hengrui Jia, Mohammad Yaghini, Christopher A Choquette-Choo, Natalie Dullerud, Anvith Thudi, Varun Chandrasekaran, and Nicolas Papernot. Proof-of-learning: Definitions and practice. In *2021 IEEE Symposium on Security and Privacy (SP)*, pages 1039–1056. IEEE, 2021.
- [114] Yanci Zhang and Han Yu. Towards verifiable federated learning. *arXiv preprint arXiv:2202.08310*, 2022.
- [115] Florian Tramer and Dan Boneh. Differentially private learning needs better features (or much more data). *arXiv preprint arXiv:2011.11660*, 2020.

A Proofs for §5

This appendix provides complete proofs of Proposition 5.1, Theorem 5.3, and Theorem 5.4 from §5.

A.1 Proposition 5.1 (Existence and Closed Form of Optimal Manipulation)

Key expressions. Under the local quadratic approximation,

$$G(z) = r^\top z - \frac{1}{2} z^\top H z - q \|z\|_2^2 = r^\top z - \frac{1}{2} z^\top K z, \quad K := H + 2qI_p, \quad M := K^{-1},$$

subject to the constraint $u^\top z \leq 0$. The closed form of z^* and the value of \mathcal{M} are given in the main text.

KKT conditions. The problem is a concave quadratic maximization with a single linear inequality. Slater’s condition holds because $K \succ 0$ and $u \neq 0$, so one can take, for example, $z = -tu$ with $t > 0$ to satisfy $u^\top z < 0$. Thus KKT conditions are necessary and sufficient.¹

¹If $u = 0$, the constraint reduces to $0 \leq 0$ and the problem is unconstrained. In this case, the solution remains unique and the optimal multiplier is $\lambda^* = 0$.

The Lagrangian and KKT conditions are:

$$\begin{aligned}
\mathcal{L}(z, \lambda) &= r^\top z - \frac{1}{2} z^\top K z + \lambda(-u^\top z), \quad \lambda \geq 0, \\
(\text{Stationarity}) \quad &Kz = r - \lambda u, \\
(\text{Primal feasibility}) \quad &u^\top z \leq 0, \\
(\text{Dual feasibility}) \quad &\lambda \geq 0, \\
(\text{Complementary slackness}) \quad &\lambda(u^\top z) = 0.
\end{aligned}$$

From stationarity with $M := K^{-1}$,

$$z(\lambda) = M(r - \lambda u).$$

The optimal multiplier λ^* is determined by complementary slackness together with $u^\top z(\lambda) \leq 0$. Since the objective is strictly concave, the solution z^* is unique, and if $u \neq 0$ then λ^* is also unique.

Proof. Since $K := H + 2qI_p$ is positive definite,

$$G(z) = r^\top z - \frac{1}{2} z^\top K z$$

is strictly concave in z . The feasible set $\{z : u^\top z \leq 0\}$ is a closed convex half-space, so in this concave maximization problem an optimal solution exists and is unique.

Because KKT conditions are necessary and sufficient, consider the Lagrangian

$$\mathcal{L}(z, \lambda) = r^\top z - \frac{1}{2} z^\top K z + \lambda(-u^\top z), \quad \lambda \geq 0.$$

Stationarity yields

$$Kz = r - \lambda u \implies z(\lambda) = M(r - \lambda u),$$

where $M := K^{-1}$. The solution must also satisfy complementary slackness $\lambda u^\top z(\lambda) = 0$ and feasibility $u^\top z(\lambda) \leq 0$.

We consider two cases.

Constraint inactive. If $u^\top Mr \leq 0$, then the unconstrained solution at $\lambda^* = 0$,

$$z^* = Mr,$$

is feasible. The corresponding objective value is

$$G(z^*) = \frac{1}{2} r^\top Mr.$$

Constraint active. If $u^\top Mr > 0$, the unconstrained solution Mr violates feasibility, so the optimum lies on the boundary with $u^\top z^* = 0$. Complementary slackness gives

$$0 = u^\top M(r - \lambda^* u) = u^\top Mr - \lambda^* u^\top Mu,$$

so

$$\lambda^* = \frac{u^\top Mr}{u^\top Mu}, \quad z^* = M\left(r - \frac{u^\top Mr}{u^\top Mu} u\right).$$

Substituting into the objective yields

$$G(z^*) = \frac{1}{2} \left(r^\top Mr - \frac{(u^\top Mr)^2}{u^\top Mu} \right).$$

Therefore, \mathcal{M} equals this optimum value. In particular, if r is parallel to u in the M -inner product sense ($r = \alpha u$), the orthogonal component vanishes and $\mathcal{M} = 0$. Moreover, under Loewner order if $H' \succeq H$ or $q' \geq q$, then $K' = H' + 2q'I_p \succeq K$ and $(K')^{-1} \preceq M$, implying that \mathcal{M} decreases monotonically in (H, q) . \square

A.2 Theorem 5.3 (Gaming Suppression Threshold)

Key expressions. We impose differential penalties on aligned and orthogonal components:

$$P_{\perp} := I_p - \frac{uu^{\top}}{\|u\|_2^2}, \quad K_{\alpha} := K + \alpha P_{\perp}, \quad M_{\alpha} := K_{\alpha}^{-1}.$$

The main text states the bound:

$$\mathcal{M}(\alpha) \leq \frac{\|P_{\perp}r\|_2^2}{2\{\lambda_{\min}(K|_{\text{span}(u)^{\perp}}) + \alpha\}}, \quad \alpha_{\min}(\tau) = \max\left\{0, \frac{\|P_{\perp}r\|_2^2}{2\tau} - \lambda_{\min}(K|_{\perp})\right\}.$$

Proof. First note that $P_{\perp} := I_p - \frac{uu^{\top}}{\|u\|_2^2}$ is positive semidefinite, so for any $\alpha_2 > \alpha_1 \geq 0$,

$$K_{\alpha_2} - K_{\alpha_1} = (\alpha_2 - \alpha_1)P_{\perp} \succeq 0.$$

Thus in Loewner order $K_{\alpha_2} \succeq K_{\alpha_1}$, and by the monotonicity of the matrix inverse for positive definite matrices,

$$M_{\alpha_2} = K_{\alpha_2}^{-1} \preceq M_{\alpha_1} = K_{\alpha_1}^{-1}.$$

From Proposition 5.1, the optimal value of $\mathcal{M}(\alpha)$ is always expressed as a nonnegative quadratic form in M_{α} (e.g., $\frac{1}{2}r^{\top}M_{\alpha}r$ or with the u -component projected out). Hence, as M_{α} decreases with larger α , the value of $\mathcal{M}(\alpha)$ is monotone decreasing in α .

To obtain the bound, decompose $r = r_{\parallel} + r_{\perp}$ with $r_{\perp} = P_{\perp}r$. From Proposition 5.1, when the constraint is active the optimal value depends only on the orthogonal component:

$$\mathcal{M}(\alpha) \leq \frac{1}{2}r_{\perp}^{\top}M_{\alpha}r_{\perp}.$$

Applying the Rayleigh quotient with $v = r_{\perp}$,

$$r_{\perp}^{\top}M_{\alpha}r_{\perp} \leq \frac{\|r_{\perp}\|_2^2}{\lambda_{\min}(K_{\alpha}|_{\text{span}(u)^{\perp}})}.$$

On the orthogonal subspace, $K_{\alpha} = K + \alpha I$, so eigenvalues are shifted by α :

$$\lambda_{\min}(K_{\alpha}|_{\text{span}(u)^{\perp}}) = \lambda_{\min}(K|_{\text{span}(u)^{\perp}}) + \alpha.$$

Combining yields

$$\mathcal{M}(\alpha) \leq \frac{1}{2} \cdot \frac{\|r_{\perp}\|_2^2}{\lambda_{\min}(K|_{\text{span}(u)^{\perp}}) + \alpha}.$$

To ensure $\mathcal{M}(\alpha) \leq \tau$ for some tolerance $\tau > 0$, solving for α gives

$$\alpha_{\min}(\tau) = \max\left\{0, \frac{\|r_{\perp}\|_2^2}{2\tau} - \lambda_{\min}(K|_{\text{span}(u)^{\perp}})\right\}.$$

Finally, when $u^{\top}M_{\alpha}r > 0$, complementary slackness implies that the optimum lies on the boundary $u^{\top}z^* = 0$. Since the welfare increment is locally approximated by $\Delta U \approx u^{\top}z$, it follows that $\Delta U(z^*) \approx 0$ in this case. \square

A.3 Theorem 5.4 (Bounds on PoG)

Key expressions. The welfare loss and the index are given by

$$\Delta U^{-} := \max\{0, -u^{\top}z^*\}, \quad \text{PoG} = \frac{\Delta U^{-}}{U^{\text{hon}}} \quad (U^{\text{hon}} > 0).$$

The general and spectral bounds are as in the main text:

$$\text{PoG} \leq \frac{\sqrt{2(u^{\top}Mu)\mathcal{M}}}{U^{\text{hon}}} \leq \frac{\|u\|_2\|r\|_2}{\lambda_{\min}(K)U^{\text{hon}}}.$$

Proof. By definition, $\text{PoG} = \Delta U^- / U^{\text{hon}}$, where $\Delta U^- = \max\{0, -u^\top z^*\}$ and $U^{\text{hon}} > 0$.

First consider the case where the constraint is active. By KKT complementary slackness, the optimum lies on the boundary with $u^\top z^* = 0$. Thus $\Delta U^- = 0$ and consequently $\text{PoG} = 0$.

Next consider the case where the constraint is inactive. The unconstrained solution is $z^* = Mr$, where $M := K^{-1}$. Using the M -inner product $\langle a, b \rangle_M := a^\top M b$, the Cauchy–Schwarz inequality gives

$$|u^\top Mr| = |\langle u, r \rangle_M| \leq \sqrt{\langle u, u \rangle_M \langle r, r \rangle_M} = \sqrt{(u^\top M u)(r^\top M r)}.$$

Hence

$$\text{PoG} = \frac{|u^\top Mr|}{U^{\text{hon}}} \leq \frac{\sqrt{(u^\top M u)(r^\top M r)}}{U^{\text{hon}}}.$$

From Proposition 5.1, $\mathcal{M} = \frac{1}{2} r^\top M r$, so

$$\text{PoG} \leq \frac{\sqrt{2(u^\top M u) \mathcal{M}}}{U^{\text{hon}}}.$$

Finally, we derive the spectral bound. Since $K \succ 0$, the Rayleigh quotient implies $v^\top K^{-1} v \leq \|v\|_2^2 / \lambda_{\min}(K)$. Applying this to $v = u$ and $v = r$,

$$u^\top M u \leq \frac{\|u\|_2^2}{\lambda_{\min}(K)}, \quad r^\top M r \leq \frac{\|r\|_2^2}{\lambda_{\min}(K)}.$$

Therefore,

$$\text{PoG} \leq \frac{\|u\|_2 \|r\|_2}{\lambda_{\min}(K) U^{\text{hon}}}.$$

In particular, as $\lambda_{\min}(K)$ increases (e.g., when audits or sanctions strengthen $K = H + 2qI_p$), both bounds decrease monotonically. \square

B Proofs for §6

This appendix provides complete proofs of Theorem 6.1 (existence and properties of stationary and Markov equilibria) from §6.

B.1 Theorem 6.1 (Existence and Properties of Stationary and Markov Equilibria)

Key setup. The state space \mathcal{S} is either finite or a compact metric space. Each player's action space $\mathcal{A}_i = \mathcal{X}_i \times \mathcal{Z}_i$ is compact, stage payoffs and transition kernels are continuous, and the discount factor is $\beta \in (0, 1)$.

A policy profile is $\sigma = (\sigma_i)_i$, where a stationary mixed policy is $\sigma_i : \mathcal{S} \rightarrow \Delta(\mathcal{A}_i)$. For fixed σ , the value function and Bellman operator are

$$V_i^\sigma(s) = \mathbb{E}_\sigma \left[\sum_{t \geq 0} \beta^t u_i(S_t, A_t) \mid S_0 = s \right], \quad (T_i^\sigma v)(s) = \mathbb{E}_\sigma \left[u_i(S_0, A_0) + \beta v(S_1) \mid S_0 = s \right].$$

Given initial distribution μ_0 , the best-response correspondence is

$$\text{BR}_i(\sigma_{-i}) = \arg \max_{\tilde{\sigma}_i \in \Sigma_i} \left\langle \mu_0, V_i^{(\tilde{\sigma}_i, \sigma_{-i})} \right\rangle, \quad \Sigma_i := \{\text{stationary mixed policies}\}.$$

Proof of existence. For fixed σ , the operator T_i^σ is a contraction in the $\|\cdot\|_\infty$ norm:

$$\|T_i^\sigma v - T_i^\sigma w\|_\infty \leq \beta \|v - w\|_\infty, \quad 0 < \beta < 1.$$

By the Banach fixed-point theorem, V_i^σ exists uniquely. Moreover, the mapping $(\sigma_i, \sigma_{-i}) \mapsto V_i^\sigma$ is continuous under the weak topology, hence $\text{BR}_i(\sigma_{-i})$ is nonempty, convex-valued, and upper hemicontinuous (its graph is closed).

The product correspondence $\text{BR}(\sigma) = \prod_i \text{BR}_i(\sigma_{-i})$ is therefore a nonempty, compact, convex-valued, upper hemicontinuous correspondence from $\Sigma = \prod_i \Sigma_i$ to itself. By the Kakutani–Fan–Glicksberg fixed-point theorem,

$$\sigma^* \in \text{BR}(\sigma^*)$$

exists. This σ^* is a stationary mixed equilibrium. \square

Proof. Comparative statics: monotone effect of sanctions. Let the sanction parameter be α , and write the stage payoff as

$$u_i(s, a; \alpha) = \bar{u}_i(s, x_i) - c_i(x_i, z_i) - \frac{1}{2} z_i^\top K(\alpha) z_i.$$

When audits and sanctions strengthen, $K(\alpha)$ increases in the Loewner order. Thus u_i has decreasing differences in (z_i, α) , meaning that as α grows, the marginal payoff of z_i decreases. By the Milgrom–Shannon monotone comparative statics theorem, for any σ_{-i} ,

$$\alpha' \geq \alpha \implies z_i^*(\alpha') \leq z_i^*(\alpha).$$

Since equilibrium is a fixed point, stronger sanctions weakly reduce the total manipulation intensity in all stationary equilibria:

$$\sum_i \mathbb{E}_{\sigma^*(\alpha)} [\|z_i\|].$$

□

Proof. Lattice structure and convergence: monotone interactions. Equip each action $a_i = (x_i, z_i)$ with the componentwise partial order, and assume interactions are monotone. That is, if $a'_i \geq a_i$ and $a'_{-i} \geq a_{-i}$, then

$$u_i(s, a'_i, a'_{-i}) - u_i(s, a_i, a'_{-i}) \geq u_i(s, a'_i, a_{-i}) - u_i(s, a_i, a_{-i}).$$

By Topkis' theorem, BR_i is an increasing correspondence, and the stationary best-response operator $B(\sigma) \in \text{BR}(\sigma)$ is isotone. Applying Tarski's fixed-point theorem, the set of stationary equilibria is a nonempty complete lattice with both a minimal and maximal equilibrium. Moreover, sequential best-response dynamics or simultaneous updates

$$\sigma^{(t+1)} = B(\sigma^{(t)})$$

converge monotonically: from lower initial conditions to the minimal equilibrium, and from upper initial conditions to the maximal equilibrium. □

Proof. Uniqueness and global convergence: contraction mapping. Suppose B is a contraction with Lipschitz constant $L < 1$ under some norm $\|\cdot\|$:

$$\|B(\sigma) - B(\tilde{\sigma})\| \leq L \|\sigma - \tilde{\sigma}\|, \quad L < 1.$$

By the Banach fixed-point theorem, the fixed point (the stationary equilibrium) is unique. Furthermore, the iteration

$$\sigma^{(t+1)} = B(\sigma^{(t)})$$

converges globally to the unique equilibrium σ^* from any initial policy $\sigma^{(0)}$. □

C Proofs for §7

This appendix provides proofs for Theorem 7.2 (existence of stationary retention, sufficient conditions for full retention, domino-exit threshold, and comparative statics) from §7.

C.1 Theorem 7.2 (Conditions for Honest Retention and Domino-Exit Threshold)

Key expressions. The update of the retention rate across rounds is

$$p_{t+1} = T(p_t) = F_V(\Pi_{\text{in}}(p_t; \alpha)), \quad T : [0, 1] \rightarrow [0, 1],$$

and when differentiable,

$$T'(p) = f_V(\Pi_{\text{in}}(p; \alpha)) \cdot \partial_p \Pi_{\text{in}}(p; \alpha),$$

where F_V is the cumulative distribution function of outside options and f_V the density (when defined).

Proof. Existence. Since T is continuous on $[0, 1]$ and maps into $[0, 1]$, the Brouwer fixed-point theorem guarantees

$$\exists p^* \in [0, 1] \text{ such that } p^* = T(p^*).$$

Thus, a stationary retention rate exists. □

Proof. Sufficient condition for full retention. Let $v_{\max} := \sup \text{supp}(F_V)$. If

$$\inf_{p \in [0,1]} \Pi_{\text{in}}(p; \alpha) \geq v_{\max},$$

then for all p we have $F_V(\Pi_{\text{in}}(p; \alpha)) = 1$, hence

$$T(p) \equiv 1.$$

Therefore $p^* = 1$ is the unique fixed point. Moreover, outside the support of F_V we have $f_V = 0$, so

$$T'(1) = 0 < 1,$$

and by the standard first-order stability criterion, $p^* = 1$ is stable. \square

Proof. (Domino-exit threshold). Suppose T intersects the 45° line three times, and denote the fixed points by

$$0 \leq p_{\text{low}} < p_{\text{dom}} < p_{\text{high}} \leq 1.$$

Applying the first-order stability test,

$$|T'(p^*)| < 1 \Rightarrow p^* \text{ stable}, \quad |T'(p^*)| > 1 \Rightarrow p^* \text{ unstable},$$

we see that if $T'(p_{\text{dom}}) > 1$, then p_{dom} is unstable. Thus, under the dynamics

$$p_{t+1} = T(p_t),$$

we have

$$p_0 < p_{\text{dom}} \Rightarrow p_t \downarrow p_{\text{low}}, \quad p_0 > p_{\text{dom}} \Rightarrow p_t \uparrow p_{\text{high}}.$$

This threshold p_{dom} is called the domino-exit threshold. \square

Proof. (Comparative statics). Suppose stronger sanctions or improved alignment increase the internal payoff at all p :

$$\alpha' \geq \alpha \implies \Pi_{\text{in}}(p; \alpha') \geq \Pi_{\text{in}}(p; \alpha) \quad (\forall p \in [0, 1]).$$

Since F_V is nondecreasing,

$$T(\cdot; \alpha') = F_V(\Pi_{\text{in}}(\cdot; \alpha')) \geq F_V(\Pi_{\text{in}}(\cdot; \alpha)) = T(\cdot; \alpha).$$

Thus T shifts upward. As a consequence, the upper stable fixed point increases:

$$p_{\text{high}}(\alpha') \geq p_{\text{high}}(\alpha),$$

while the unstable threshold decreases:

$$p_{\text{dom}}(\alpha') \leq p_{\text{dom}}(\alpha).$$

Conversely, increased noise or excessive signal sensitivity shifts Π_{in} downward, thereby shifting T downward, reducing p_{high} , and increasing p_{dom} . \square

D Proofs for §8

This appendix provides proofs for Proposition 8.2 (the boundary between harmful and cooperative coalitions) and Theorem 8.3 (organizational cost and stability) from §8.

D.1 Proposition 8.2 (Boundary between Harmful and Cooperative Coalitions)

Key expressions. In the local quadratic model, the optimal manipulation of coalition C is

$$z_C^*(\alpha) = M_\alpha r_C, \quad M_\alpha = (K + \alpha P_\perp)^{-1},$$

and the welfare change is

$$\Delta U(\alpha) = u^\top M_\alpha r_C - \phi \|P_\perp M_\alpha r_C\|_2^2,$$

where $P_\perp = I - \frac{uu^\top}{\|u\|_2^2}$ and $\phi \geq 0$. Writing $r_C = r_\parallel + r_\perp$ as the decomposition into the u -parallel and orthogonal components, define

$$\lambda_\parallel = \frac{u^\top K u}{\|u\|_2^2}, \quad \lambda_\perp^{\min} = \lambda_{\min}(K \upharpoonright_{\text{span}(u)^\perp}).$$

Proof. Decompose the action of M_α along u and its orthogonal complement. Since $P_\perp u = 0$, along the u direction the operator $K_\alpha := K + \alpha P_\perp$ has the same spectrum as K . Hence

$$u^\top M_\alpha r_C = \frac{u^\top r_C}{\lambda_\parallel}.$$

On the orthogonal complement, $K_\alpha = K + \alpha I$, so all eigenvalues increase by α . By the Rayleigh quotient,

$$\|P_\perp M_\alpha r_C\|_2^2 = \sum_j \frac{r_{\perp,j}^2}{(\lambda_{\perp,j} + \alpha)^2} \leq \frac{\|r_\perp\|_2^2}{(\lambda_\perp^{\min} + \alpha)^2}.$$

Now consider cases:

Always harmful. If $u^\top r_C < 0$, then $\frac{u^\top r_C}{\lambda_\parallel} < 0$ and the second term is nonnegative, so $\Delta U(\alpha) < 0$ for all α .

Boundary harmful. If $u^\top r_C = 0$, then

$$\Delta U(\alpha) = -\phi \|P_\perp M_\alpha r_C\|_2^2 \leq 0,$$

strictly negative when $r_\perp \neq 0$.

Threshold for cooperative transition. If $u^\top r_C > 0$, using the bound above we require

$$\frac{u^\top r_C}{\lambda_\parallel} \geq \phi \frac{\|r_\perp\|_2^2}{(\lambda_\perp^{\min} + \alpha)^2}$$

for $\Delta U(\alpha) \geq 0$. Equivalently,

$$\lambda_\perp^{\min} + \alpha \geq \sqrt{\frac{\phi \lambda_\parallel \|r_\perp\|_2^2}{u^\top r_C}}.$$

Thus the threshold is

$$\alpha_{\text{benign}} := \max \left\{ 0, \sqrt{\frac{\phi \lambda_\parallel \|r_\perp\|_2^2}{u^\top r_C}} - \lambda_\perp^{\min} \right\},$$

so that $\alpha \geq \alpha_{\text{benign}}$ guarantees $\Delta U(\alpha) \geq 0$, while $\alpha < \alpha_{\text{benign}}$ generally yields $\Delta U(\alpha) < 0$. \square

D.2 Theorem 8.3 (Organizational Cost and Stability)

Key expression. In a TU environment, define the net surplus of coalition C as

$$S_C(\alpha) = \frac{1}{2} r_C^\top M_\alpha r_C - \kappa(|C|),$$

where $\kappa(\cdot)$ is nondecreasing in coalition size and typically convex.

Proof. Non-collusion stability. Suppose that for all $|C| \geq 2$,

$$S_C(\alpha) = \frac{1}{2} r_C^\top M_\alpha r_C - \kappa(|C|) \leq 0.$$

Then forming any coalition yields nonpositive transferable surplus, so no side-payment allocation can weakly improve all members. In particular, no two players (nor any larger set) can deviate from the singleton partition to form a coalition that makes them better off. Hence the singleton partition is pairwise stable. \square

Proof. Existence of nontrivial coalitions. Suppose that for some coalition C ,

$$S_C(\alpha) = \frac{1}{2} r_C^\top M_\alpha r_C - \kappa(|C|) > 0.$$

Then the positive total surplus $S_C(\alpha)$ can be distributed internally so that every member is weakly better off, giving C an incentive to form. Moreover, when surplus is positive, incentives to split into smaller sub-coalitions can be absorbed by transfers, and if κ is superadditive or convex, the cost of partitioning increases. By standard arguments, a pairwise stable or coalition-proof partition exists containing C (or a coalition of the same size). \square

Proof. Selectivity between cooperative and harmful coalitions. From Proposition 8.2, welfare change is

$$\Delta U(\alpha) = u^\top M_\alpha r_C - \phi \|P_\perp M_\alpha r_C\|_2^2.$$

If $\alpha \geq \alpha_{\text{benign}}$ and $\Delta U(\alpha) \geq 0$, then any coalition with $S_C(\alpha) > 0$ can form without reducing social welfare, so only cooperative coalitions can be stably selected. Conversely, if $\alpha < \alpha_{\text{benign}}$, then it is possible to have coalitions with $S_C(\alpha) > 0$ but $\Delta U(\alpha) < 0$ (particularly when the externality ϕ is large), in which case harmful coalitions may form stably. \square

D.3 Theorem 9.1 (Optimal Reward Design)

Key expression. Consider a linear–budget reward:

$$R_i = a + w^\top s_i.$$

By local reparametrization we may set $\partial s / \partial z = I$ (absorbing the Jacobian into w), so the reward gradient is

$$r = \nabla_z \mathbb{E}[R] = w.$$

In the local quadratic model, the manipulability index is $\mathcal{M} = \frac{1}{2} r^\top M r$, and the welfare gradient is u . We consider minimizing \mathcal{M} under a linear alignment constraint (e.g., $u^\top r = c > 0$).

Proof. The constrained minimization problem is

$$\min_r \frac{1}{2} r^\top M r \quad \text{s.t.} \quad u^\top r = c.$$

The Lagrangian is

$$L(r, \lambda) = \frac{1}{2} r^\top M r - \lambda(u^\top r - c).$$

First-order stationarity gives

$$M r = \lambda u \implies r = \lambda M^{-1} u = \lambda K u,$$

where $K = M^{-1} = H + 2qI_p$. From the constraint $u^\top r = c$, we get $\lambda = c / (u^\top K u)$, hence

$$r^* \parallel K u.$$

Since under reparametrization $r = w$, we obtain

$$w^* \parallel K u.$$

Thus the optimal reward weights are aligned with $K u$, i.e., with the welfare gradient transformed by the effective curvature. Moreover, by Theorem 5.4, the PoG bound

$$\text{PoG} \leq \frac{\sqrt{2(u^\top M u) \mathcal{M}}}{U^{\text{hon}}}$$

is minimized simultaneously when \mathcal{M} is minimized. Hence aligning the reward gradient with $K u$ achieves both objectives. \square

D.4 Theorem 9.2 (Minimum Audit and Sanction Strength)

Key expression. From Theorem 5.3, using the eigenvalue on the orthogonal subspace:

$$\mathcal{M}(\alpha) \leq \frac{\|r_\perp\|_2^2}{2\{\lambda_{\min}(K|_{\text{span}(u)^\perp}) + \alpha\}}.$$

Proof. For a target hurdle $\tau > 0$, we seek the minimal α such that $\mathcal{M}(\alpha) \leq \tau$. Rearranging the inequality,

$$\lambda_{\min}(K|_{\text{span}(u)^\perp}) + \alpha \geq \frac{\|r_\perp\|_2^2}{2\tau}.$$

Thus,

$$\alpha_{\min}(\tau) = \max\left\{0, \frac{\|r_\perp\|_2^2}{2\tau} - \lambda_{\min}(K|_{\text{span}(u)^\perp})\right\}.$$

It follows that the larger the orthogonal component r_\perp , and the smaller the effective eigenvalue on the orthogonal subspace, the stronger the audit intensity α required. This establishes the monotonicity stated in the theorem. \square

D.5 Proposition 9.3 (Pareto Frontier of Aggregation Design)

Key expression. Under contamination rate ρ and signal variance σ_s^2 , each aggregator A is summarized by the pair

$$(\text{Var}_\rho(A), \Gamma(A)), \quad \Gamma(A) := \sup_{\|z\| \leq 1} \|\nabla_s A z\|,$$

where in a linear approximation $\nabla_s A$ coincides with the Lipschitz constant of the influence function.

Proof. Existence of a trade-off. Consider the family of mean, median, k -trimmed mean, and rank-weighted aggregators. As ρ increases, median and heavily trimmed aggregators reduce their sensitivity $\Gamma(A)$ to outliers and manipulations, whereas the mean exhibits larger $\Gamma(A)$. In terms of variance, when ρ is small and random noise dominates, the mean yields the smallest Var_ρ . As ρ grows, the upper bounds of Var_ρ favor median and heavily trimmed versions. Thus, it is generally impossible to reduce both Var_ρ and $\Gamma(A)$ simultaneously for the same A , establishing an inherent trade-off between the two performance criteria. \square

Proof. Existence of a Pareto frontier. Let A_θ denote a parametrized family obtained by continuously varying the trimming rate $k \in [0, 1/2]$ or the hyperparameter of rank-weighting (e.g., hubness cutoff). If $\theta \mapsto (\text{Var}_\rho(A_\theta), \Gamma(A_\theta))$ is continuous and the parameter space Θ is compact, then

$$\mathcal{C} = \{(\text{Var}_\rho(A_\theta), \Gamma(A_\theta)) : \theta \in \Theta\}$$

is compact. The lower outer boundary of this compact set—the set of points that cannot be improved upon in both coordinates simultaneously—exists and constitutes the Pareto frontier of the variance–sensitivity trade-off. \square

Proof. Selection rule. The optimal choice along the frontier depends on environmental parameters. When ρ is small and σ_s^2 is large, the mean lies on the frontier. As ρ increases, the frontier is increasingly occupied by the median and heavily trimmed means. In the intermediate regime, an appropriately chosen trimming rate k^* or a rank-weighted scheme yields frontier solutions. This arises because the parametric curves $\theta \mapsto (\text{Var}_\rho(A_\theta), \Gamma(A_\theta))$ intersect across regimes, altering the relative ranking of aggregators. \square

Proof. Upper bound on $\tilde{\mathcal{M}}$. Recall from Proposition 5.1 that under a quadratic model the manipulation index is bounded by

$$\mathcal{M}(r) = \frac{1}{2} r^\top M r, \quad M = K^{-1}, \quad K := H + 2qI_p.$$

With the effective reward gradient $\tilde{r} = (1 - \pi)r + \pi\eta u$, we expand:

$$\tilde{\mathcal{M}} = \frac{1}{2} \tilde{r}^\top M \tilde{r} = \frac{1}{2} ((1 - \pi)^2 r^\top M r + 2\pi(1 - \pi)\eta r^\top M u + \pi^2 \eta^2 u^\top M u).$$

Step 1. Bounding the cross term. By Cauchy–Schwarz under the M -inner product,

$$|r^\top M u| \leq \sqrt{(r^\top M r)(u^\top M u)}.$$

Hence

$$2\pi(1 - \pi)\eta r^\top M u \leq 2\pi(1 - \pi)\eta \sqrt{(r^\top M r)(u^\top M u)}.$$

Step 2. Completing the square. Combine terms as

$$(1 - \pi)^2 r^\top M r + 2\pi(1 - \pi)\eta r^\top M u + \pi^2 \eta^2 u^\top M u \leq (1 - \pi)^2 r^\top M r + \pi(1 - \pi)\eta^2 u^\top M u + \pi^2 \eta^2 u^\top M u.$$

Step 3. Simplification. The first term is $(1 - \pi)^2(2\mathcal{M})$. For the last two, note that

$$\pi(1 - \pi)\eta^2 u^\top M u + \pi^2 \eta^2 u^\top M u = \pi\eta^2 u^\top M u.$$

Thus

$$\tilde{\mathcal{M}} \leq (1 - \pi)^2 \mathcal{M} + \frac{1}{2} \pi \eta^2 u^\top M u.$$

Step 4. Spectral bound. Using the Rayleigh quotient inequality,

$$u^\top M u \leq \frac{\|u\|_2^2}{\lambda_{\min}(K)}.$$

Substituting,

$$\tilde{\mathcal{M}} \leq (1 - \pi)^2 \mathcal{M} + \frac{\pi}{2} \eta^2 \frac{\|u\|_2^2}{\lambda_{\min}(K)}.$$

Finally, since $\pi \leq 1$, replacing π by $\pi(1 - \pi)$ yields a slightly tighter but always valid expression,

$$\tilde{\mathcal{M}} \leq (1 - \pi)^2 \mathcal{M} + \frac{\pi(1 - \pi)}{2} \eta^2 \frac{\|u\|_2^2}{\lambda_{\min}(K)}.$$

Hence, $\tilde{\mathcal{M}}$ decreases monotonically in π , and by Theorem 5.4, the same holds for the PoG upper bound. \square

Proof. Decomposition and bound. Since $\mathcal{M} = \frac{1}{2} r^\top M r$, we expand

$$\tilde{\mathcal{M}} = \frac{1}{2} \tilde{r}^\top M \tilde{r} = \frac{1}{2} \left((1 - \pi)^2 r^\top M r + 2\pi(1 - \pi) \eta r^\top M u + \pi^2 \eta^2 u^\top M u \right).$$

For the cross term, Cauchy–Schwarz under the M -inner product gives $|r^\top M u| \leq \sqrt{(r^\top M r)(u^\top M u)}$. Thus,

$$\tilde{\mathcal{M}} \leq \frac{1}{2} (1 - \pi)^2 r^\top M r + \pi(1 - \pi) \eta \sqrt{(r^\top M r)(u^\top M u)} + \frac{1}{2} \pi^2 \eta^2 u^\top M u.$$

Applying $ab \leq \frac{1}{2}(a^2 + b^2)$ with $a = \sqrt{r^\top M r}$, $b = \pi \eta \sqrt{u^\top M u}$, the middle term is bounded as

$$\pi(1 - \pi) \eta \sqrt{(r^\top M r)(u^\top M u)} \leq \frac{1 - \pi}{2} r^\top M r + \frac{\pi(1 - \pi)}{2} \eta^2 u^\top M u.$$

Substituting back, we obtain

$$\tilde{\mathcal{M}} \leq \frac{1}{2} (1 - \pi)^2 r^\top M r + \frac{1 - \pi}{2} r^\top M r + \frac{\pi(1 - \pi)}{2} \eta^2 u^\top M u + \frac{1}{2} \pi^2 \eta^2 u^\top M u.$$

Since $\mathcal{M} \leq \frac{1}{2} r^\top M r$, the first two terms can be absorbed into $(1 - \pi)^2 \mathcal{M}$. For the last two terms, use the Rayleigh quotient $u^\top M u \leq \|u\|_2^2 / \lambda_{\min}(K)$ and $\pi^2 \leq \pi$ to get

$$\tilde{\mathcal{M}} \leq (1 - \pi)^2 \mathcal{M} + \frac{\pi(1 - \pi)}{2} \eta^2 \frac{\|u\|_2^2}{\lambda_{\min}(K)}.$$

\square

Proof. Monotonicity. Define

$$g(\pi) = (1 - \pi)^2 \mathcal{M} + \frac{\pi(1 - \pi)}{2} \eta^2 \frac{\|u\|_2^2}{\lambda_{\min}(K)}.$$

The first term is strictly decreasing in π , while the second term is a concave quadratic that vanishes at $\pi = 0, 1$ and is nonnegative in between. Consequently, $g(\pi)$ is nonincreasing over the entire interval $\pi \in [0, 1]$, showing that a higher challenge-mixing probability reduces the incentive for gaming. By Theorem 5.4, the same functional dependence also drives down the upper bound on PoG. \square

E Proofs for §10

This appendix provides full proofs for Proposition 10.1 (identifiability boundaries) and Theorem 10.2 (power and sample complexity).

E.1 Proposition 10.1 (Identifiability boundaries)

Key setup. Under local linearization,

$$y = L s \approx \mu' + (LB) z + \varepsilon, \quad \varepsilon \sim \mathcal{N}(0, \Sigma'), \quad \Sigma' \succ 0.$$

Let the admissible manipulation subspace be $\mathcal{Z} \subseteq \mathbb{R}^p$. With probability π an additional challenge signal c is observed, where

$$\mathbb{E}[c \mid z] = \eta u^\top z, \quad \text{Var}(c) = \sigma_c^2.$$

Proof. Non-identifiable directions. If LB is rank-deficient, then its nullspace $\mathcal{N}(LB) \setminus \{0\}$ is nonempty. For any $z \in \mathcal{N}(LB)$, the mean is unchanged at μ' , so

$$y \mid z \sim \mathcal{N}(\mu', \Sigma') = y \mid 0.$$

Hence manipulations in $\mathcal{N}(LB)$ are observationally indistinguishable from the null action and therefore unidentifiable. \square

Proof. Sufficient condition for mean identifiability. Suppose $\sigma_{\min}(LB|_{\mathcal{Z}}) > 0$. Then for every $z \in \mathcal{Z} \setminus \{0\}$,

$$\|(LB)z\|_2 \geq \sigma_{\min} \|z\|_2 > 0,$$

so the mean of y shifts. Moreover,

$$D(\mathcal{N}(\mu' + LBz, \Sigma') \parallel \mathcal{N}(\mu', \Sigma')) = \frac{1}{2} z^\top B^\top L^\top (\Sigma')^{-1} LBz > 0.$$

Thus, with n independent rounds, likelihood ratio tests (or GLS) consistently distinguish $z = 0$ from $z \neq 0$ as $n \rightarrow \infty$. \square

Proof. Recovery by mixed challenges. Augmenting the observation to (y, c) yields Fisher information

$$\mathcal{I} = B^\top L^\top (\Sigma')^{-1} LB + \pi \frac{\eta^2}{\sigma_c^2} uu^\top.$$

Therefore, for any z with $u^\top z \neq 0$, even if $LBz = 0$,

$$z^\top \mathcal{I} z = \pi \frac{\eta^2}{\sigma_c^2} (u^\top z)^2 > 0,$$

so these manipulations become identifiable once challenge signals are introduced. \square

E.2 Theorem 10.2 (Power and sample complexity)

Key setup. In the Gaussian mean-shift model, test

$$H_0 : z = 0 \quad \text{vs.} \quad H_1 : z = z^*.$$

The per-round noncentrality parameter is

$$\Delta^2 = (LBz^*)^\top (\Sigma')^{-1} (LBz^*) + \pi \eta^2 \frac{(u^\top z^*)^2}{\sigma_c^2}.$$

Proof. With n i.i.d. rounds, the optimal GLS statistic (standardized to unit variance) satisfies

$$T_n \sim \begin{cases} \mathcal{N}(0, 1), & H_0, \\ \mathcal{N}(\sqrt{n} \Delta, 1), & H_1. \end{cases}$$

For a one-sided test at level α , reject H_0 if $T_n > z_{1-\alpha} = \Phi^{-1}(1-\alpha)$. The power condition $\Pr_{H_1}(T_n > z_{1-\alpha}) \geq 1-\beta$ is equivalent to

$$\sqrt{n} \Delta \geq z_{1-\alpha} + z_{1-\beta}.$$

Squaring both sides yields the necessary and sufficient condition

$$n \geq \frac{(z_{1-\alpha} + z_{1-\beta})^2}{\Delta^2}.$$

Finally, Chernoff bounds imply an exponential guarantee: for any $0 < \delta < 1$,

$$n \geq \frac{2 \log(2/\delta)}{\Delta^2}$$

ensures that at significance level $\alpha = \delta$, the test has power at least $1 - \delta$. \square

Extended Discussion

E.3 Summary of Core Messages and Integration of Design Principles

Two key indicators summarize manipulation incentives and welfare loss. First, the *Manipulability Index* \mathcal{M} , where $\mathcal{M} > 0$ indicates that net-benefit gaming is feasible while maintaining the same welfare level as the honest benchmark. Second, the *Price of Gaming* $\text{PoG} = 1 - U_{\text{game}}/U_{\text{hon}}$, which quantifies the welfare loss ratio relative to honesty. This paper places these two indicators at the center and, through both theory and experiments, demonstrates how alignment, sanction strength, and information mixing jointly reduce \mathcal{M} and PoG.

The core design principles are organized around three axes.

Alignment of reward and welfare. When the reward gradient is aligned with the welfare gradient (e.g., setting w in the direction of Ku), \mathcal{M} becomes structurally small and the upper bound on PoG simultaneously decreases. In this case, the constraint in the alignment direction is activated at the optimum, yielding $u^\top z^* \approx 0$, and a wide regime emerges where PoG effectively vanishes. Numerical experiments confirm that under alignment, the absolute level of \mathcal{M} remains globally very low, and PoG is observed to be nearly zero.

Orthogonal-component sanctions. Designs that impose penalties only on components orthogonal to the welfare gradient, $K_\alpha = K + \alpha P_\perp$, make $M(\alpha)$ monotonically decreasing in α . This allows the derivation of the minimum sanction strength $\alpha_{\min}(\tau)$ required to achieve a target hurdle τ , which serves as a practical baseline in the static regime.

Mixing of random challenges. The challenge mixing ratio π reduces the manipulable component of the effective signal by a factor of $(1 - \pi)^2$, thereby lowering both \mathcal{M} and the upper bound on PoG. In misaligned environments, even small increases in π sharply reduce the required α_{\min} for achieving the same hurdle τ . Contour plots show that vulnerable regions in the low- α , low- π corner are quickly eliminated.

Alignment acts as the primary axis that structurally blocks gaming opportunities, while sanctions and information mixing serve as reinforcement axes that reliably suppress \mathcal{M} and PoG under misalignment, noise, and heterogeneity. When combined, the three axes jointly reduce both indicators, and the theoretical bounds—alignment optimality, minimum sanctions, and the $(1 - \pi)^2$ reduction effect—are consistently reflected in numerical results.

E.4 Interpretation of Static Thresholds and Price Indicators

In static environments, the key lies in interpreting the structure of thresholds and bounds to clarify how \mathcal{M} and PoG can be controlled. Based on sanction strength α , the price parameter q , and alignment (the degree to which the reward gradient matches the welfare gradient), monotonicity is evident. As α increases, \mathcal{M} decreases; as alignment improves, the bounds of both \mathcal{M} and PoG decline. The price parameter q rescales the margin of signals exposed to gaming, thereby relaxing the required sanction level for a given alignment.

For a target hurdle τ , define

$$\alpha_{\min}(\tau; q, \text{align}) = \inf\{\alpha \geq 0 : \mathcal{M}(\alpha, q, \text{align}) \leq \tau\}.$$

The value of α_{\min} decreases as alignment improves and further decreases when q is adjusted to weaken gaming-sensitive components. Conversely, when alignment is poor, a larger α is required to satisfy the same τ . However, raising the sanction strength indefinitely does not yield proportional benefits: beyond a certain region, the marginal reduction in \mathcal{M} diminishes, making further sanctions inefficient. Thus, improving alignment to lower α_{\min} fundamentally is more effective than relying solely on sanctions.

For PoG, one can posit an upper bound function $\overline{\text{PoG}}(\alpha, q, \text{align})$, which decreases with both α and alignment. Under good alignment, a wide regime emerges where even moderate sanctions nearly eliminate PoG. Under poor alignment, a combination of q rescaling and α is required, with q adjustment partially offsetting distortions caused by misalignment. Yet, excessive increases in q can weaken the effective signal itself, limiting the improvement in PoG achievable in favorable regions.

In conclusion, alignment serves as the primary axis that shifts structural boundaries, while α and q act as reinforcement axes that fine-tune thresholds under a given level of alignment. Given a target τ , the recommended procedure is as follows: first, improve alignment to lower α_{\min} as much as possible; second, adjust q to rescale toward dimensions less sensitive to gaming, thereby reducing α_{\min} further; finally, increase α only to the extent needed to close the remaining gap, ensuring that $\mathcal{M} \leq \tau$ while sufficiently lowering $\overline{\text{PoG}}$. This joint adjustment improves both indicators and avoids the diminishing returns of overly large sanctions.

E.5 Effects and Limitations of Information Design (Random Challenge Mixing)

When random challenges are mixed into the main evaluation, the manipulable signal components are structurally reduced. With a mixing ratio $\pi \in [0, 1]$, the observed signal can be expressed as

$$\tilde{s} = (1 - \pi)s + \pi c.$$

In first-order approximation, the manipulable component tied to predictability shrinks by a factor of $(1 - \pi)^2$. As a result, both the manipulation index and the upper bound of the price indicator decrease simultaneously. This effect is particularly pronounced in misaligned environments, where even small increases in π substantially lower the minimum sanction level $\alpha_{\min}(\tau)$ required to satisfy a given hurdle τ . The randomness of the mixture directly weakens the scope for gaming along orthogonal components left by alignment failures.

Trade-offs and Monotonicity The parameter π acts as a complementary axis to alignment and sanctions. The higher the alignment, the smaller the π needed; conversely, under poor alignment, even small increases in π significantly reduce α_{\min} . However, the benefits diminish over time: once thresholds are crossed, further reductions from $(1 - \pi)^2$ contraction become less efficient relative to alignment adjustments or sanction fine-tuning. Thus, π should be deployed first to eliminate vulnerable regions and buffer misalignment, while subsequent improvements should rely on alignment correction and α adjustment.

Sample Complexity and Statistical Power Challenges produce dual effects. They break non-identifiable directions, improving identifiability and test power, but they also dilute the main evaluation signals, increasing variance. To maintain target significance levels and power, slightly more rounds may be required, with this trend becoming more pronounced as π grows (Thm. 10.2). The effectiveness of mixing lies at the balance point between reducing the manipulation index and PoG bounds while sustaining statistical power.

Limitations and Costs Excessively large π can limit PoG improvements in favorable regions due to signal dilution, or require unnecessarily many rounds. Repeated use of challenge items raises leakage risks, weakening protection, while log accumulation increases privacy and audit management costs. Even honest participants may face added response burdens. If adaptive adversaries arise, the benefits of static mixing diminish, making periodic re-estimation and refresh of mixing policies advisable.

Recommendations At stages of low alignment or high environmental volatility, introduce small π first to eliminate vulnerable regions. Once alignment improvements and sanction adjustments bring the system within thresholds, avoid inflating π unnecessarily. The challenge pool should be sufficiently large and unpredictable, with update cycles specified to prevent repeated exposure. Ultimately, the choice of π should balance three criteria: $\alpha_{\min}(\tau; \pi)$, the bounded $\text{PoG}(\pi)$, and the number of rounds required to achieve the target statistical power.

Random challenge mixing, when combined with alignment and sanctioning, is a powerful mechanism for jointly reducing the manipulation index and PoG. However, diminishing returns, increased sample complexity, and risks of privacy or leakage impose costs. Thus, the mixing ratio must be set with consideration of alignment, target thresholds, and statistical power requirements.

E.6 Dynamics and Exit–Collapse Thresholds: Hysteresis and Operational Risks

From a dynamic perspective, the key mechanism is that participation and dropout decisions accumulate across rounds, and the long-run retention rate bifurcates around a threshold. Let the retention rate in round t be $r_t \in [0, 1]$, and denote the policy-driven update by

$$r_{t+1} = F(r_t; \alpha, \pi, q, \text{align}) + \xi_t,$$

where ξ_t is an exogenous shock. A steady state r^* satisfies $r^* = F(r^*)$, with local stability determined by $|F'(r^*)| < 1$. Higher α or π , or better alignment, shifts F upward and flattens its slope, thereby reducing the bounds of \mathcal{M} and PoG.

Exit and Collapse Thresholds, and Hysteresis If F intersects the $y = x$ line three times in an S-shape, then a low-retention equilibrium r_{low}^* and a high-retention equilibrium r_{high}^* coexist, separated by an unstable threshold p_{dom} . Initial states below p_{dom} cascade into collapse, while states above converge to high retention. Even gradual parameter changes produce hysteresis near the threshold: the system may abruptly switch equilibria depending on the path. Temporary shocks ξ_t that push the state across p_{dom} can trigger irreversible transitions.

Buffer Indicators and Early Warnings Define local resilience as $\kappa = 1 - F'(r^*)$. Smaller κ indicates proximity to instability. Rising variance in observed retention, slowing mean-reversion, and synchronized increases in challenge failure rates serve as typical early-warning signals. Safety margins can be summarized by two axes:

$$\text{Margin I: } r_{\text{high}}^* - p_{\text{dom}}, \quad \text{Margin II: } \kappa = 1 - F'(r_{\text{high}}^*).$$

A contraction in either margin makes collapse more likely under small shocks.

Comparing Buffering Strategies Sanction increments and challenge mixing buffer thresholds in distinct ways.

α ramp-up. Gradually increasing α shifts F upward, moving p_{dom} leftward and flattening the slope, thereby enlarging κ . The marginal benefit, however, diminishes over time.

π spike. A temporary spike in π quickly suppresses predictable gaming components, lowering p_{dom} in the short term. Because variance may increase through signal dilution, this strategy is better suited for short-term shock absorption than permanent stabilization.

Hybrid path. Combining a smooth α ramp with temporary π boosts reduces the total adjustment needed to cross thresholds. Parameters are tuned to satisfy both a target safety margin $(r_{\text{high}}^* - p_{\text{dom}}) \geq \delta$ and a resilience floor $\kappa \geq \kappa_0$.

Operational Rules Near Boundaries Close to thresholds, abrupt policy shifts can amplify oscillations. Bound the per-round rate of parameter change, and when retention exits the guard band $[p_{\text{dom}} + \delta, r_{\text{high}}^* - \delta]$, proceed in sequence: first, apply a short π boost to prevent a sudden collapse; second, raise α slightly to flatten F and stabilize; third, adjust alignment for structural improvement. If retention falls below a critical level, temporarily switch to conservative aggregators (e.g., median or trimmed mean) as a safety mode to limit losses.

Summary In dynamic settings, the shape of the retention response defines thresholds, and the distance to and resilience at these thresholds determine long-run safety. By combining alignment improvement with α and π adjustments to secure both margins, the system can remain stable against shocks and environmental fluctuations, avoiding transitions between retention and collapse.

E.7 Coalitions (Collusion or Cooperation) and Externalities: The Cooperative–Harmful Boundary

A coalition refers to a subset of participants C coordinating their strategies to pursue joint benefits. Let the coalition’s direction vector be r_C , the welfare gradient be u , and the sanction-targeted orthogonal component be $P_{\perp} r_C$. In a local first-order approximation, the coalition’s social externality can be summarized as

$$\Delta W_C(\alpha, \pi, q, \text{align}) \approx u^{\top} r_C - \alpha \|P_{\perp} r_C\|^2 - \chi(\pi, q) \|r_C\|^2,$$

where $\chi(\pi, q) \geq 0$ captures the contraction and rescaling of effective signals induced by the mixing ratio and the pricing parameter. A coalition is cooperative if $\Delta W_C > 0$, and harmful if $\Delta W_C < 0$.

Definition of the boundary and monotonicity. The minimum sanction intensity that renders a coalition socially benign is

$$\alpha_{\text{benign}}(C; \pi, q, \text{align}) = \inf\{\alpha \geq 0 : \Delta W_C(\alpha, \pi, q, \text{align}) \geq 0\}.$$

Better alignment increases $u^{\top} r_C$ or reduces $P_{\perp} r_C$, thereby lowering α_{benign} . Similarly, increasing π or adjusting q to weaken gaming-sensitive components enlarges $\chi(\pi, q)$, shrinking private gains and leading to $\partial \alpha_{\text{benign}} / \partial \pi \leq 0$ and $\partial \alpha_{\text{benign}} / \partial q \leq 0$. Conversely, poor alignment and large $P_{\perp} r_C$ require stronger sanctions to reach the boundary.

Private incentives and organizational costs. Let the coalition’s private net benefit be $G_C(\alpha, \pi, q)$ and its organizational cost be $\kappa(|C|)$. The self-sustainability condition is

$$G_C(\alpha, \pi, q) \geq \kappa(|C|).$$

Typically, κ increases and is quasi-convex in coalition size, while mixing or pricing adjustments reduce G_C . As a result, small coalitions may form but large ones may fail, producing a scale threshold. Along the aligned axis, cooperative outputs can raise G_C , whereas for orthogonal components, sanctions quickly offset marginal gains.

Four regimes.

- **Cooperative–sustainable** ($\Delta W_C > 0$, $G_C \geq \kappa$): Socially beneficial and self-sustaining. Alignment incentives (e.g., setting w parallel to Ku) dominate, and strong sanctions are unnecessary.
- **Cooperative–unsustainable** ($\Delta W_C > 0$, $G_C < \kappa$): Beneficial but not spontaneously formed. Reinforcing alignment to increase $u^{\top} r_C$ or rescaling via q can raise private incentives and enable coalition formation.

- **Harmful–sustainable** ($\Delta W_C < 0$, $G_C \geq \kappa$): The most problematic region. Increase α to penalize orthogonal components, raise π , and rescale q to dilute predictable gains, driving G_C below the threshold. If needed, switch to robust aggregators such as median or trimmed mean to cap influence.
- **Harmful–unsustainable** ($\Delta W_C < 0$, $G_C < \kappa$): Organizational costs act as a natural deterrent. Excessive intervention may be unnecessary.

Composition effects and directionality. If r_C is close to the alignment axis and $u^\top r_C$ is large, even coalitions of the same size are more likely to be cooperative. Conversely, if r_C tilts toward the orthogonal axis, even small coalitions can become harmful and highly sensitive to α . Directionality is the primary factor distinguishing the boundary, while scale interacts with organizational cost as a secondary adjustment variable.

Detection and response. Coalitions manifest through rising residual correlations, synchronized failure rates in challenge items, or rank reversals before and after aggregator switches. The recommended response sequence is: first, temporarily increase π to block predictable joint gains; second, raise α targeted at orthogonal components; third, realign w to steer toward directions with large $u^\top r_C$; and finally, switch aggregators if necessary to cap influence. Adjustments should remain below the cooperative boundary α_{benign} to preserve beneficial cooperation while selectively suppressing harmful collusion.

Summary. Coalition externalities can be systematically controlled via alignment–orthogonal decomposition, mixing adjustments, and pricing. Alignment shifts the boundary favorably, while α and π weaken private incentives in harmful directions, reducing α_{benign} . Combining these axes clarifies the cooperative–harmful boundary, promoting beneficial coalitions while pushing harmful ones beyond viability.

E.8 Trade-off in Aggregation Design: Variance vs. Gaming Sensitivity

Aggregators are subject to a fundamental trade-off between two axes: variance and sensitivity to gaming. Reducing variance improves statistical efficiency but increases susceptibility to manipulation, whereas lowering sensitivity often comes at the cost of efficiency. The contamination rate ε denotes the fraction of gaming or outliers, while noise magnitude is denoted by σ^2 . Alignment refers to the degree of trust that reward gradients align with welfare gradients. Below we compare mean, median, trimmed mean, and alignment-weighted aggregators, and outline transition rules.

Mean. The equally weighted mean minimizes variance and achieves effective sample size $n_{\text{eff}} = n$. However, with a breakdown point of 0 and an unbounded influence function, it is highly sensitive to manipulation. It is suitable when contamination is very low and alignment is strong.

Median. The median has a high breakdown point of $1/2$ and a bounded influence function, making it robust to manipulation. The trade-off is higher variance compared to the mean. It serves as a safe mode in high-contamination regimes or when collusion signals are suspected.

Trimmed Mean. The trimmed mean removes the top and bottom τ fraction before averaging. Its breakdown point increases to τ , and near-Gaussian settings yield higher efficiency than the median while being more robust than the mean. Larger τ reduces sensitivity but decreases n_{eff} , increasing variance. A natural choice is to set $\tau \approx \hat{\varepsilon} + \delta$, adding a margin to the estimated contamination $\hat{\varepsilon}$.

Alignment-Weighted Average. Each signal (or contribution) g_i is weighted by an alignment score $s_i = \langle w, g_i \rangle$:

$$\hat{G} = \sum_{i=1}^n \omega_i g_i, \quad \omega_i \propto (\max\{0, s_i\})^\gamma, \quad \sum_i \omega_i = 1.$$

Higher alignment and low noise in the scores greatly reduce sensitivity to non-aligned directions. However, weight skew can shrink the effective sample size $n_{\text{eff}} = 1 / \sum_i \omega_i^2$. Controls such as bounding the weight ratio $\omega_{\text{max}} / \omega_{\text{min}} \leq \rho_{\text{max}}$ and clipping are therefore required.

Transition conditions and rules. Aggregator selection proceeds stepwise based on contamination estimate $\hat{\varepsilon}$, alignment reliability $\widehat{\text{align}}$, and effective sample size constraint n_{eff} .

Alignment-weighted priority. If $\hat{\varepsilon} \leq \varepsilon_1$, alignment reliability is high, and $n_{\text{eff}} \geq \eta n$, use alignment-weighted aggregation as the default. The parameter γ should be increased only within safe bounds to avoid excessive concentration.

Trimmed mean as buffer. If $\varepsilon_1 < \hat{\varepsilon} \leq \varepsilon_2$ or heavy tails are observed, switch to the trimmed mean with $\tau \approx \hat{\varepsilon} + \delta$. If n_{eff} falls below the threshold ηn , relax τ accordingly.

Median as safe mode. If $\hat{\epsilon} > \epsilon_2$ or collusion signals (synchronized patterns, surging residual correlations) are detected, temporarily switch to the median to cap influence. After stabilization, revert to alignment-weighted or trimmed mean.

Variance–sensitivity diagnostics and calibration. The variance of the aggregator can be summarized as $\text{Var}(\hat{G}) \approx \sigma^2 \sum_i \omega_i^2$. Gaming sensitivity can be conceptualized via a sensitivity function $S(A; r) = \partial \hat{G} / \partial \epsilon|_{\epsilon_r}$ for a target direction r . The mean has high S but small $\sum_i \omega_i^2 = 1/n$. The median has small S but larger $\sum_i \omega_i^2$. The trimmed mean interpolates between the two depending on τ , while alignment-weighted aggregation can greatly reduce S for specific r at the cost of increasing $\sum_i \omega_i^2$. The goal is to find a configuration (aggregator, τ , γ , ρ_{\max}) that satisfies variance constraints while keeping the bounds of \mathcal{M} and PoG sufficiently low.

Interactions with other axes. Robust aggregation reduces the required sanction α_{\min} and mixing ratio π to achieve a given target τ . Conversely, using the mean necessitates stronger α and π to correct \mathcal{M} and PoG. Hence, aggregation, sanctions, and mixing form a joint budget allocation problem. The strongest synergy arises when alignment is improved first, followed by a transition to alignment-weighted aggregation.

Summary. The mean is efficient but fragile, the median is robust but inefficient, and the trimmed mean interpolates smoothly between them. Alignment-weighted aggregation is powerful when alignment reliability is high, structurally lowering sensitivity. By transitioning aggregators based on contamination estimates, alignment diagnostics, and effective sample size monitoring, one can reduce the bounds on \mathcal{M} and PoG while avoiding excessive variance.

E.9 Identification, Power, and Sample Complexity

Identification issues arise when gaming-sensitive and welfare-beneficial directions are entangled or highly correlated. In such cases, estimates of \mathcal{M} or PoG may tilt toward particular directions, creating unidentified (or weakly identified) regions. The three levers studied in this work shrink these regions in complementary ways. Alignment improvement matches reward and welfare gradients to structurally eliminate unidentified axes. Penalties on orthogonal components α suppress variations orthogonal to the welfare gradient, reducing the variance of \mathcal{M} . Random challenge mixing π contracts predictable gaming components, restoring identification even when alignment failure persists.

Power and sample complexity: basic prototype. The goal is to determine the number of rounds n required to test $H_0 : \mathcal{M} \geq \tau$ versus $H_1 : \mathcal{M} < \tau$ at significance α_{sig} with power $1 - \beta$. If $\widehat{\mathcal{M}}$ is approximately normal with $\text{SE}(\widehat{\mathcal{M}}) \approx \sigma_{\mathcal{M}} / \sqrt{n_{\text{eff}}}$, then

$$n_{\min} \approx \frac{(z_{1-\alpha_{\text{sig}}} + z_{1-\beta})^2 \sigma_{\mathcal{M}}^2}{(\tau - \mu_{\mathcal{M}})^2}, \quad \mu_{\mathcal{M}} := \mathbb{E}[\widehat{\mathcal{M}}].$$

For confidence intervals with target half-width h at level $(1 - \alpha_{\text{sig}})$,

$$n_{\min}^{\text{CI}} \approx \frac{z_{1-\alpha_{\text{sig}}/2}^2 \sigma_{\mathcal{M}}^2}{h^2}.$$

The key is to increase effective sample size n_{eff} and effect size $\tau - \mu_{\mathcal{M}}$, while reducing variance $\sigma_{\mathcal{M}}^2$.

Effective sample size and variance: three correction factors. **Aggregator effective sample size.** For a weighted average $\hat{G} = \sum_i \omega_i g_i$, $\text{Var}(\hat{G}) \approx \sigma^2 \sum_i \omega_i^2$, so $n_{\text{eff}} = 1 / \sum_i \omega_i^2$. The equal-weight mean gives $n_{\text{eff}} = n$, the median under Gaussian approximation yields $\text{Var}(\hat{G}) \approx (\pi/2) \sigma^2 / n$ so $n_{\text{eff}} \approx (2/\pi)n$, and a two-sided τ -trimmed mean gives roughly $n_{\text{eff}} \approx (1 - 2\tau)n$.

Signal contraction by mixing. If mixing ratio π shrinks the gaming-sensitive component by $(1 - \pi)$, the effect size is reduced by $(1 - \pi)$, and required sample size inflates by $(1 - \pi)^{-2}$. Thus n_{\min} carries a factor of $(1 - \pi)^{-2}$.

Variance reduction by alignment and penalty. Alignment improvement and orthogonal penalties α reduce variance in gaming-sensitive directions, lowering $\sigma_{\mathcal{M}}^2$. However, alignment-weighted aggregation may concentrate weights, reducing n_{eff} , so gains in variance reduction must be balanced against losses in effective sample size.

Combining these, we have approximately

$$n_{\min} \approx \frac{(z_{1-\alpha_{\text{sig}}} + z_{1-\beta})^2}{(\tau - \mu_{\mathcal{M}})^2} \underbrace{\sigma_{\mathcal{M}}^2(\alpha, \text{align})}_{\text{reduced by alignment and penalties}} \times \underbrace{\frac{1}{1 - \rho_{\text{trim}}}}_{\substack{\text{aggregator effect} \\ (\text{trim: } \rho_{\text{trim}} \approx 2\tau, \text{ median: } \rho_{\text{trim}} \approx \pi/2 - 1)}} \times \underbrace{(1 - \pi)^{-2}}_{\text{mixing contraction}}.$$

Designs for identification enhancement. First, periodically refresh the randomness of challenge mixing to break unidentified axes. Second, incorporate noise estimation of alignment scores s_i to avoid excessive weight concentration. Third, switch aggregators stepwise—from mean to trimmed mean to median—so that the influence function approaches bounded form. This combination lowers $\sigma_{\mathcal{M}}^2$ while enhancing detection sensitivity to collusion and synchronization in frequency- and correlation-based diagnostics.

Guidelines for preserving power. **1. Preemptive variance reduction by alignment and penalties.** Use alignment correction and α adjustment to reduce $\sigma_{\mathcal{M}}^2$ first. **2. Use minimal mixing.** Employ only the π necessary to eliminate vulnerable regions, considering the $(1 - \pi)^{-2}$ cost. **3. Maintain n_{eff} via aggregator switching.** Choose trimming level τ based on contamination estimate $\hat{\varepsilon}$, ensuring n_{eff} does not fall below a threshold. **4. Compute required rounds.** Substitute the chosen $\sigma_{\mathcal{M}}^2$, n_{eff} , and effect size into n_{min} . Apply the same procedure to the PoG metric.

Summary. Identification is jointly strengthened along four axes: alignment, penalties, mixing, and aggregation. Alignment and penalties reduce variance, mixing breaks unidentified axes, and aggregation switching bounds the influence function. Because mixing shrinks effect size and inflates sample complexity, it should remain at minimal necessary levels. Balancing these factors enables reliable inference on \mathcal{M} and PoG at given significance and power levels.

E.10 Principles of Reward Design: Implementing the Alignment Theorem

The alignment theorem states that if the reward vector w is aligned with the welfare gradient Ku , i.e., $w \parallel Ku$, then both the upper bound of the manipulability index \mathcal{M} and the upper bound of PoG decrease simultaneously. The intuition is straightforward: changes that increase welfare are directly tied to increases in reward, while orthogonal components that are unhelpful or harmful to welfare are excluded from rewards. This principle becomes more salient when combined with orthogonal penalties α and random mixing π .

Alignment under budget constraints. Let $s := Ku$ denote the alignment direction, and define the feasible set of rewards as

$$\mathcal{W} = \{w \geq 0, \mathbf{1}^\top w \leq B, \|w\|_2 \leq R, Aw \leq b\},$$

where B is the total budget, R is a magnitude bound, and $Aw \leq b$ represents fairness and policy constraints. The budget-constrained aligned reward is implemented as

$$w^* = \underset{w \in \mathcal{W}}{\operatorname{argmin}} \|w - \lambda s\|_2^2 \quad \text{for some } \lambda \geq 0,$$

i.e., projecting the direction s into the feasible set. With only a budget constraint, a closed form is simple: remove negative components of s and set $w_i^* \propto \max\{0, s_i\}$, then choose

$$\lambda = \frac{B}{\sum_i \max\{0, s_i\}}$$

so that $\mathbf{1}^\top w^* = B$. When alignment confidence is high and one wishes to emphasize top-aligned components, a power weighting can be applied:

$$w_i^* \propto (\max\{0, s_i\})^\gamma, \quad \lambda = \frac{B}{\sum_i (\max\{0, s_i\})^\gamma}, \quad \gamma \in [1, 2].$$

Excessively large γ concentrates rewards on a few targets, reducing the effective sample size $n_{\text{eff}} = 1 / \sum_i \omega_i^2$. Hence, upper-bound rules are imposed.

Alignment under fairness and policy constraints. If fairness, minimum or maximum limits, or prohibitions on certain combinations restrict \mathcal{W} to a subspace \mathcal{S} , then one aligns within the admissible directions and subsequently applies budget and cap constraints. With orthogonal projection $P_{\mathcal{S}}$ onto \mathcal{S} ,

$$w^* \propto \Pi_{\mathcal{W}}(P_{\mathcal{S}} s)$$

is the basic solution. One normalizes s in the admissible direction and then projects into the feasible set, preserving alignment while satisfying constraints.

Temporary defense and realignment under alignment failure. Estimation errors in u or K , or environmental drift, may increase alignment error. Define the alignment error metric

$$\delta = 1 - \frac{\langle w, s \rangle}{\|w\|_2 \|s\|_2}.$$

If $\delta > \delta_{\max}$ or directional changes become abrupt, detected by $\|s_t - s_{t-1}\| / \|s_{t-1}\| > \eta$, then the following procedure is triggered:

1. **Temporary defense.** Increase orthogonal penalties so that $K_\alpha = K + \alpha P_\perp$, and temporarily raise π to shrink gaming opportunities immediately.
2. **Realignment.** Re-estimate $s = Ku$ with updated data and update w^* by projecting into \mathcal{W} . Recheck weight caps and group constraints.
3. **Relaxation.** Once the bounds on \mathcal{M} and $\overline{\text{PoG}}$ return to target ranges, gradually lower α and π to their original levels.

Operational metrics and calibration. The status of reward design is tracked by the following indicators: alignment error δ , budget deviation $\Delta B = \mathbf{1}^\top w - B$, clipping rate $r_{\text{clip}}^{(w)}$ and cap hit rate, and the change in the upper bounds of \mathcal{M} and PoG before and after realignment. The rules are simple: restore alignment first when δ is high, adjust λ if the budget is exceeded, reduce γ or strengthen ρ_{\max} if $r_{\text{clip}}^{(w)}$ exceeds threshold, and use α and π as reinforcement when necessary.

Summary. The essence is threefold: prioritize alignment in design, perform projection and normalization under constraints, and if alignment wavers, deploy orthogonal penalties and random mixing for temporary defense followed by realignment. This preserves a reward structure that keeps both \mathcal{M} and PoG low, while stably absorbing budget and fairness constraints and environmental changes.

E.11 Computational Perspective: Hardness and Approximation in Audit Resource Allocation

Audit resources are limited, and the expected reduction in \mathcal{M} and PoG varies significantly depending on where they are deployed. This section formulates resource allocation as an optimization problem and summarizes the limits of exact optimization alongside practical approximation strategies.

Problem formulation. Let $U = \{1, \dots, m\}$ denote the set of audit candidates, with costs $c_i > 0$ and total budget B . When resources are allocated to $S \subseteq U$, define the improvement as

$$f(S) := [\lambda_{\mathcal{M}} \mathcal{M} + \lambda_{\text{P}} \text{PoG}]_{\emptyset} - [\lambda_{\mathcal{M}} \mathcal{M} + \lambda_{\text{P}} \text{PoG}]_S.$$

The goal is

$$\max_{S \subseteq U} f(S) \quad \text{s.t.} \quad \sum_{i \in S} c_i \leq B.$$

Incorporating fairness and policy restrictions generalizes the problem to a combination of matroid and knapsack constraints.

Hardness and structure. For general nonlinear set functions f , the problem is NP-hard, reducible to budgeted maximum coverage. Natural approximations in the form of risk coverage functions,

$$f(S) \approx \sum_{j=1}^p w_j \left(1 - \prod_{i \in S} (1 - p_{ij}) \right),$$

or facility-location-type potentials, exhibit monotonicity and submodularity. In this case, with unit costs, the standard greedy algorithm has a $(1 - 1/e)$ approximation guarantee; with heterogeneous costs under a single knapsack, the same constant factor approximation applies. For matroid or multi-knapsack constraints, constant-factor approximation algorithms are also known. In practice, *lazy greedy* caches marginal upper bounds in a priority queue, reducing function evaluations to $O(m \log m)$.

Static allocation: greedy and local search. Static allocation proceeds as follows:

1. **Risk scoring.** For current selection S , estimate each candidate’s marginal efficiency per cost:

$$\Delta_i = \frac{f(S \cup \{i\}) - f(S)}{c_i}.$$

This incorporates domain-specific indicators such as collusion suspicion, orthogonality to alignment, and past challenge failure rates.

2. **Lazy greedy selection.** Maintain Δ_i bounds in a priority queue, re-evaluating only when popped, and expand S within budget. For monotone submodular objectives, this yields $(1 - 1/e)$ approximations under uniform costs and constant-factor approximations under heterogeneous costs.
3. **Local improvement.** Starting from the greedy solution S , apply $(1, 1)$ or small (p, q) swaps. Update only when $f(S') - f(S) > 0$ under budget feasibility. This improves solution quality while retaining constant-factor guarantees under submodular and matroid/knapsack constraints.

Continuous relaxation and rounding. Relax f to fractional variables $x_i \in [0, 1]$, solve, and then recover an integer solution via randomized rounding. Chernoff bounds control budget violation probability; pipage rounding is effective under matroid constraints. Post-rounding trimming removes low-efficiency items if metrics deteriorate.

Adaptive allocation: observation-driven updates. When audit outcomes are sequentially observed, *adaptive submodularity* ensures that adaptive greedy achieves a $(1 - 1/e)$ guarantee relative to the optimal non-adaptive policy. Implementation benefits from a bandit perspective:

- **Exploration–exploitation balance.** Maintain Bayesian estimates of detection probabilities per candidate, selecting via UCB or Thompson sampling.
- **Dynamic linkage.** When dynamic resilience margins $r_{\text{high}}^* - p_{\text{dom}}$ and κ decline, temporarily increase audit budget B_t , and scale it down gradually once stability is restored.

Exact and near-exact in special structures. On tree or path interaction graphs, dynamic programming yields polynomial-time solutions. With uniform costs and modular f , selecting the top- B items is optimal. With very small budgets, enumerating a few seeds and supplementing with greedy search yields near-exact solutions.

Computation–statistics trade-offs and estimation error. Estimating marginal gains Δ_i incurs sampling error. Candidates with wide confidence intervals CI_i carry risk of mis-evaluation; using Δ_i/CI_i as an auxiliary criterion avoids premature concentration. Since alignment-weighted aggregation reduces effective sample size n_{eff} and increases variance, include a variance penalty in the objective:

$$\max_S f(S) - \lambda_{\text{var}} \cdot \widehat{\text{Var}}_S.$$

Modeling fairness and policy constraints. Group-wise minimum or maximum proportions, prohibited combinations, and regional balance can be encoded as partition matroids or multi-knapsack constraints. Greedy updates are restricted to independent sets, and rounding is followed by post-processing that prunes violating items first.

Complexity and stopping criteria. Lazy greedy runs in $O(m \log m + T_\Delta)$, where m is the number of candidates and T_Δ is the cost of re-evaluating marginal gains. Termination occurs when one of the following holds: maximum marginal gain per cost $\max_i \Delta_i < \varepsilon$, the moving average of improvement falls below η for K consecutive rounds, or budget/fairness constraints are saturated.

Summary. Audit resource allocation is generally intractable to solve exactly. However, by leveraging monotone submodularity, combining greedy, rounding, and local search yields robust approximations. Integrating static and adaptive procedures with dynamic thresholds, while accounting for estimation error and fairness constraints, allows meaningful reductions in expected \mathcal{M} and PoG even under tight budgets.

E.12 Strengths

This section concisely summarizes the strengths and contributions of our work. The core lies in integrating two central metrics—the manipulability index \mathcal{M} and the Price of Gaming (PoG)—as a common axis, unifying design levers such as alignment, penalties, mixing, aggregation, dynamics, coalition, and computation into a single coherent analytical framework.

Unified framework centered on metrics. By adopting \mathcal{M} and PoG as joint objectives, we interpreted the effects of each lever in the same coordinate system. This made it possible to clearly compare design choices that simultaneously reduce both metrics, and to decompose and explain trade-offs whenever conflicts arise.

Systematization of theoretical boundaries and thresholds. Through the alignment principle ($w \parallel Ku$), we established a structure that jointly reduces the upper bounds of \mathcal{M} and PoG. By combining the monotone decreasing effect of orthogonal penalties α , the shrinkage effect of mixing ratio π , and the rescaling effect of the pricing index q , we derived critical thresholds such as the minimum penalty $\alpha_{\min}(\tau)$. In coalition analysis, we defined the benign threshold α_{benign} and showed how directionality, scale, and organizational costs shift the boundary.

Dynamic stability and early warning. Using the residual response map $r_{t+1} = F(r_t)$, we analyzed long-term retention–collapse boundaries and identified the role of hysteresis and the critical point p_{dom} . We organized early warning indicators such as resilience $\kappa = 1 - F'(r^*)$ and critical distance $r_{\text{high}}^* - p_{\text{dom}}$, enabling quantitative assessment of regime transitions under parameter shifts or external shocks.

Trade-offs and switching rules in aggregation design. We compared variance–gaming sensitivity trade-offs across mean, median, trimmed mean, and alignment-weighted aggregation, and proposed stepwise switching rules based on contamination rate estimates, alignment confidence, and effective sample size n_{eff} . We further connected aggregation to penalties and mixing in a unified decision map.

Guidelines on identification, power, and sample complexity. We derived sample size approximations for hypothesis testing and confidence intervals on \mathcal{M} and PoG, decomposing the impact of alignment, penalties, mixing, and aggregation on variance coefficients, effect sizes, and n_{eff} . This provides a consistent method to calculate required rounds under given significance and power levels.

Approximation guarantees from a computational perspective. We formulated audit resource allocation as a budget-constrained maximization problem, and under monotone submodularity, showed that greedy algorithms provide $(1 - 1/e)$ approximation guarantees. By combining lazy greedy, continuous relaxation and rounding, and local search, we achieved stable approximation performance. In adaptive settings, we outlined observation-based update procedures with competitive guarantees.

Cross-module consistency and reproducibility. Results from static, dynamic, coalition, aggregation, and computational analyses converge in the same direction. The monotonicities and critical structures predicted by theory consistently align with numerical findings, strengthening the credibility of the proposed boundaries and switching rules.

Summary. On a metric-centered unified framework, we built a design map that spans thresholds, boundaries, testing, and computation. The alignment principle serves as the analytical anchor, naturally extending to dynamics, coalition, aggregation, and resource allocation. This provides a systematic foundation for comparing and explaining design choices that jointly reduce \mathcal{M} and PoG.

E.13 Limitations and Threat Models

This section outlines the assumptions under which our results hold, their vulnerabilities, and the threat models considered. The main constraints are (i) reliance on local approximations, (ii) strong stationarity assumptions, and (iii) susceptibility to identification weaknesses due to partial observability. We then describe attack scenarios exploiting these limitations and potential gaps in defense.

Limits of local approximations. Several theorems and bounds rely on first- or second-order local approximations (alignment–orthogonal decomposition, local monotonicity of curvature). Large policy shifts, regions with strong nonlinear interactions, or multi-modal utility landscapes may break monotonicity or threshold predictions. In particular: (a) if estimation error in the alignment direction $s = Ku$ is large or if volatility is high, the benefits of $w \parallel s$ diminish and the marginal effects of (α, π, q) may shift nonlinearly; (b) heavy-tailed noise can loosen mean-centered bounds; (c) under binding coupled constraints, frequent projections may lead to over- or under-estimation of effect sizes.

Application scenarios and adjustment guidelines. In conditions where approximations may fail, more conservative operation is required. Representative cases include discrete switching rules, frequent regime transitions with piecewise rules, and state-dependent noise. In such environments, piecewise fitting should be used to re-estimate thresholds, and operational thresholds such as α_{benign} or sample size contours should be set one level higher. Robust summaries such as

trimmed means and Winsorization, and sandwich variance estimators should be employed to reassess power. In practice, sensitivity grids for α, π, q should be reported, and safety diagnostics such as $r_{\text{proj}}, r_{\text{clip}}, \rho$ continuously monitored. A sharp rise in r_{proj} or increased volatility in ρ should trigger immediate fallback to conservative operation.

Stationarity assumptions and extrapolation risks. Dynamic analyses of the retention map $r_{t+1} = F(r_t)$ and early warning indicators such as κ assume time-invariant environments. Distributional drift, strategic adaptation to rule exposure, or strong seasonality and campaign effects can shift F itself, distorting threshold estimates such as p_{dom} or r_{high}^* . Under such conditions, the same parameter values may converge to entirely different long-run equilibria depending on the path (hysteresis). Extrapolating thresholds estimated from past data into the future can be hazardous. Mitigations include rolling re-estimation, moving windows, and volatility-based guardbands.

Partial observability and identification weaknesses. Privacy restrictions and logging limitations may leave key variables only partially observed or approximated by proxies. This leads to (i) misidentification of u and K , (ii) hidden collusion signals, and (iii) selection bias that increases bias and variance in $\widehat{\mathcal{M}}$ and $\widehat{\text{PoG}}$. Aggregation switching and mixing help reduce unidentifiable dimensions, but at the cost of lowering effective sample size n_{eff} , which weakens statistical power. Failing to disentangle these opposing effects may result in over- or under-intervention.

Threat models. We consider the following main threats:

1. **Opportunistic individual gaming:** short-term, low-cost manipulations, effective under mean aggregation and low α, π .
2. **Collusive coordination:** joint strategies aligned along r_C , mixing alignment and orthogonal components to evade detection.
3. **Adaptive adversaries:** updating strategies after rule exposure to α, π , and aggregation switches; combined with drift, can invalidate threshold predictions.
4. **Sybil and substitution:** bypassing caps by reporting through multiple identities or rotating identities.
5. **Data or update poisoning:** systematically distorting signals or reverse-engineering the challenge pool to target specific items.
6. **Low-and-slow attacks:** long-term, incremental manipulations that remain below alarm thresholds.

The proposed levers (alignment, α, π , aggregation switching, audit allocation) are strong against Types 1–2, but Types 3–6 depend on agility in detection and update cycles, and cannot be adequately defended by fixed thresholds based on historical data alone.

Boundary conditions and scope of guarantees. Computational approximation guarantees rely on monotone submodularity; under strong interactions or non-monotone regions, $(1 - 1/e)$ -type guarantees may fail. Sample complexity approximations rely on asymptotic normality and independence assumptions; cluster correlation, overlapping collusion, and cross-effects can cause confidence intervals to be underestimated. Moreover, \mathcal{M} and PoG are sufficient-condition metrics for welfare loss, but cannot capture all social costs (distributional fairness, long-term innovation disincentives, etc.).

Mitigations and remaining gaps. (a) *Re-estimation cycles:* update $s = Ku$ and thresholds periodically using moving windows and CUSUM-style change-point tests. (b) *Dualization of mixing and aggregation:* avoid fixing π and aggregation rules; introduce randomized switching to hinder rule learning. (c) *Identity and connectivity checks:* treat abnormal account creation/retirement and abrupt cohesion in interaction graphs as warning signals. (d) *Conservative confidence intervals:* inflate intervals to reflect clustering and heteroskedasticity, and add slack to sample size calculations. Despite these measures, comprehensive guarantees cannot be provided against worst-case adaptive, multi-actor, or non-stationary environments. Future work should address regret guarantees for online switching policies, optimization of false positive–false negative trade-offs in collusion detection, and re-evaluation of thresholds in non-stationary and nonlinear settings.

Summary. Our results provide strong insights under assumptions of local approximation, stationarity, and partial observability, but defense gaps remain against adaptive, stealthy, and Sybil-style threats and under distributional drift. Reliable control of \mathcal{M} and PoG requires validating assumptions, periodic recalibration, randomization of mixing and aggregation, and connectivity-based alarms.

E.14 Ethical and Policy Considerations

This section summarizes the ethical and policy principles that ensure manipulation-mitigation designs respect individual rights and community norms. The key is to align the objective of reducing the manipulability index \mathcal{M} and the price of gaming PoG with privacy, explainability, appeals, fairness and proportionality, and safeguards against abuse.

Privacy and data governance. Challenge mixing and audit logs may include sensitive behavioral information. Principles of data minimization and purpose limitation should apply, with explicit retention periods and access controls. Individual-level logs are protected through hash-based identifiers and role-based access restrictions. Public reports are limited to aggregate statistics, with release thresholds for small groups. Subgroup-level \mathcal{M} and PoG indicators are further protected by noise injection or bucket merging to reduce re-identification risk. Challenge pools must be sufficiently large and rotated, and repeated targeting of specific individuals is prohibited.

Explainability and appeal procedures. Rules and threshold maps must be documented, and when adjustments or sanctions occur, an explanation packet should include reason codes, supporting evidence, relevant thresholds, and corrective pathways. Appeals should have clear timelines and stages (submission, review, independent reassessment), with minor adjustments suspended during the appeal. When models or aggregators are changed, a summary of modifications and expected impact ranges must be communicated.

Fairness and proportionality. Rewards and sanctions must be proportional to the predicted harm and the confidence of evidence. Severe penalties should not be imposed based on a single metric; escalation requires concordance across multiple signals. Protected attributes and their proxies are excluded from use, and subgroup error rates and threshold-crossing probabilities must be monitored. If subgroup disparities in $\widehat{\mathcal{M}}$ or $\widehat{\text{PoG}}$ exceed critical levels, causal analysis and interim mitigation are required. Corrective pathways should ensure that sustained improvements automatically reduce sanctions over time.

Safeguards against abuse. Roles in design, operation, and post-hoc auditing must be separated, with all interventions logged in tamper-proof records. Challenges and audits should be rate-limited and distributed to prevent excessive targeting. Parameter changes in (α, π) require approval workflows and public change histories. Major adjustments must involve human review, and a rollback switch should be available for unanticipated side effects. Regular adversarial testing and independent external audits should be conducted to detect vulnerabilities.

Scope of transparency. To prevent operational exploitation, specific challenge items remain undisclosed, but overarching principles and ranges are published. For example, reasonable ranges for (α, π) , aggregator switching conditions, appeal success rates, and observed changes in \mathcal{M} and PoG before and after interventions should be reported regularly. Details enabling individual tracking are excluded.

Mitigation of side effects. To avoid chilling effects from excessive monitoring, prioritize event-based over continuous surveillance. Permanent blacklisting is prohibited, with expiry and re-evaluation rules applied. Compensation or alternative pathways must be provided to offset excessive burdens from challenges.

Summary. When privacy protection, explainability, appeal procedures, fairness and proportionality, and safeguards against abuse are jointly satisfied, manipulation-mitigation goals and rights protection can be achieved simultaneously. The design pursues reductions in \mathcal{M} and PoG while ensuring the process remains transparent and accountable throughout.

E.15 Deployment and Operational Checklist

This section summarizes the key items to be repeatedly verified during deployment and operation. The objective is to simultaneously reduce \mathcal{M} and PoG while meeting dynamic stability, coalition boundaries, sample complexity, and fairness constraints.

(A) Threshold setting. Initialize the following baseline values and periodically re-evaluate:

- **Target hurdle** τ : set $\mathcal{M} \leq \tau$ as the primary goal.
- **Minimum sanction** $\alpha_{\min}(\tau; \pi, q, \text{align})$: minimum sanction level satisfying $\mathcal{M} \leq \tau$.
- **Coalition boundary** α_{benign} : boundary ensuring $\Delta W_C > 0$ (protecting cooperative coalitions and suppressing harmful ones).

- **Dynamic slack and resilience:** $(r_{\text{high}}^* - p_{\text{dom}}) \geq \delta$, $\kappa = 1 - F'(r^*) \geq \kappa_0$.

(B) Aggregator selection and switching rules. Switch stepwise based on contamination estimate $\hat{\varepsilon}$, alignment confidence $\widehat{\text{align}}$, and effective sample size n_{eff} :

1. **Alignment-weighted (default).** If $\hat{\varepsilon} \leq \varepsilon_1$, $\widehat{\text{align}}$ is high, and $n_{\text{eff}} \geq \eta n$, use alignment-weighted aggregation with concentration cap ρ_{max} and clipping.
2. **Trimmed buffering.** If $\varepsilon_1 < \hat{\varepsilon} \leq \varepsilon_2$ or heavy tails are observed, switch to two-sided τ -trim with $\tau \approx \hat{\varepsilon} + \delta_\tau$.
3. **Median safety mode.** If $\hat{\varepsilon} > \varepsilon_2$ or collusion signals (synchronization failure, residual correlation spikes) occur, switch temporarily to median, then revert to stages 1–2 after stabilization.

(C) Mixing ratio (challenge) guide. Mixing entails $(1 - \pi)^2$ signal shrinkage and $(1 - \pi)^{-2}$ sample cost:

- **Remove initial vulnerable zones.** Apply small π at low alignment stages to quickly reduce α_{min} .
- **Avoid over-mixing.** Keep π at the minimum necessary level considering the cost to statistical power.
- **Pool management.** Specify challenge pool size and refresh schedule, and limit repeated exposure.

(D) Re-calibration conditions. Re-evaluate $(\text{align}, \alpha, \pi, q, \text{aggregator})$ if any of the following hold:

1. **Alignment error increase.** $\delta = 1 - \langle w, Ku \rangle / (\|w\| \|Ku\|) > \delta_{\text{max}}$ or abrupt directional shifts.
2. **Dynamic alarms.** $\kappa < \kappa_0$ or residual rate leaves guard band $[p_{\text{dom}} + \delta, r_{\text{high}}^* - \delta]$.
3. **Indicator reliability deterioration.** Confidence intervals for $\widehat{\mathcal{M}}$ or $\widehat{\text{PoG}}$ exceed target h_{max} .
4. **Contamination or collusion signals.** $\hat{\varepsilon} > \varepsilon_2$, challenge synchronization failures surge, or correlation-based alarms trigger.
5. **Fairness deviation.** Group gaps in $\widehat{\mathcal{M}}, \widehat{\text{PoG}}$ exceed threshold Δ_{max} .

(E) Operational report—mandatory items. Report the following per group and per period at cycle T (with confidence intervals):

- **Indicators.** levels and trends of $\widehat{\mathcal{M}}, \widehat{\text{PoG}}$.
- **Parameters.** time series of (α, π, q) , aggregator type and switching points, n_{eff} .
- **Dynamics.** estimates of $p_{\text{dom}}, r_{\text{high}}^*$, and resilience κ .
- **Quality.** contamination rate $\hat{\varepsilon}$, challenge pool size and refresh, failure rates, and alarm logs.
- **Fairness and governance.** subgroup indicator gaps, appeal statistics, and parameter change history.

(F) Guardrails and kill switch.

- **Upper and lower bounds.** $\alpha \in [\alpha_{\text{min}}, \alpha_{\text{max}}]$, $\pi \in [0, \pi_{\text{max}}]$, concentration cap ρ_{max} .
- **Kill criteria.** On indicator spikes, fairness deviations, or resilience collapse, automatically switch to safety mode (median and trim, temporary π boost, slight α increase), followed by root-cause analysis.

(G) Decision tree (summary).

1. Set target $\tau \rightarrow$ compute α_{min} .
2. Diagnose alignment; if feasible, adopt alignment-weighted aggregation (otherwise retain mean).
3. Check $\hat{\varepsilon}$ to decide on trimming or median switch.
4. Adjust (α, π) at minimum cost to achieve $\mathcal{M} \leq \tau$, reduced $\widehat{\text{PoG}}$, and maintained n_{eff} .
5. Confirm dynamic slack $(r_{\text{high}}^* - p_{\text{dom}}) \geq \delta$ and resilience $\kappa \geq \kappa_0$.
6. Audit fairness; analyze causes and apply interim remedies if deviations exceed threshold.
7. Issue report at cycle T ; recalibrate if re-calibration conditions are met.

Summary. This checklist integrates six axes: threshold setting, aggregator switching, mixing adjustments, re-calibration triggers, reporting, and guardrails. Each axis operates cyclically during deployment. When anomalies arise, conservative actions are triggered such as threshold resets, switching to robust aggregators, or adjusting mixing ratios. Results are stabilized through standardized reporting and guardrails. This operational loop enables simultaneous improvements in \mathcal{M} and PoG while tracking residual-collapse thresholds, coalition boundaries, and fairness constraints.

F Ethics and Policy Notes

This study addresses mechanisms that alter participant behavior in environments where indicator-based rewards and audits interact. This section outlines the ethical issues that may arise when deploying such mechanisms in practice, and how the quantities derived in the main text can be used as principles of minimal intervention.

Privacy and Holdout Protection Randomized challenges and private holdouts are key tools for weakening gaming incentives (Thm. 9.4). Excessive exposure of challenges, however, increases risks of reverse engineering and data leakage. The minimum operational safeguards are threefold. First, explicitly specify the challenge mixing ratio π . Second, restrict access and usage via dual authorization and logging. Third, control repeated calls with quotas and cooldowns. Quantitatively, the following upper bound can be used to determine the minimum π needed to meet a permissible incentive hurdle τ :

$$\tilde{\mathcal{M}} \leq (1 - \pi)^2 \mathcal{M} + \frac{\pi(1 - \pi)}{2} \eta^2 \frac{\|u\|_2^2}{\lambda_{\min}(K)}.$$

Fairness and Proportionality The reward gradient r and sanction strength α may generate disparities in expected rewards and penalties across groups. The principle of proportionality requires only the minimal intervention necessary to achieve $\mathcal{M} \leq \tau$. According to the static threshold theorem (Thm. 5.3),

$$\alpha \geq \alpha_{\min}(\tau) = \max \left\{ 0, \frac{\|r_{\perp}\|_2^2}{2\tau} - \lambda_{\min}(K \upharpoonright_{\text{span}(u)^{\perp}}) \right\}$$

should be adopted as a policy baseline, with any increases applied incrementally. Reward design should default to alignment $r \parallel Ku$ (Thm. 9.1), which simultaneously reduces the upper bound on PoG (Thm. 5.4).

Over-Suppression and Exit Risk Excessively high α may reduce retention rates (§7), and if retention falls below the domino threshold p_{dom} , recovery to normal operation may become infeasible. Deployment policies should monitor the dynamics

$$p_{t+1} = T(p_t) = F_V(\Pi_{\text{in}}(p_t; \alpha))$$

and provide a safety band such that when retention approaches instability, sanctions are relaxed or replaced with information design via increased mixing.

False Positives in Collusion and Suppression of Cooperation Coalitions may be harmful or may enhance cooperative performance (§8). The minimum policy safeguards are: (i) detect collusion using aggregate metadata (frequency, timestamps, similarity) rather than content; (ii) target sanctions on the component orthogonal to the welfare gradient; (iii) apply strong interventions only above the cooperative boundary. Evaluating

$$\Delta U(\alpha) = u^{\top} M_{\alpha} r_C - \phi \|P_{\perp} M_{\alpha} r_C\|_2^2$$

ensures that the region $\Delta U(\alpha) \geq 0$ is preserved, with $\alpha \geq \alpha_{\text{benign}}$ serving as the operational threshold.

Metric Gaming and Aggregator Choice The choice of aggregator A creates a trade-off between variance and sensitivity to manipulation (§9, Prop. 9.3). When contamination ρ is low and noise is large, the mean is preferable; as ρ increases, the median and heavy trimming dominate on the Pareto frontier. In practice, it is advisable to predefine a default aggregator for each operating regime and switch A automatically when the estimated ρ exceeds a threshold.

Power, Transparency, and Appeals Randomized challenges enhance identifiability (§10):

$$\Delta^2 = (LBz^*)^{\top} (\Sigma')^{-1} (LBz^*) + \pi \eta^2 \frac{(u^{\top} z^*)^2}{\sigma_c^2}.$$

Given a target power $1 - \beta$ and significance level α ,

$$n \geq \frac{(\Phi^{-1}(1 - \alpha) + \Phi^{-1}(1 - \beta))^2}{\Delta^2}$$

must be satisfied in sample planning. Operational minimums are: (i) prior disclosure of the presence and frequency of signals and challenges; (ii) providing explainable grounds for adverse actions, including rules, signals, and thresholds; (iii) documenting appeal and re-evaluation procedures.

Policy Mapping: Where and How to Apply Practical regulations (e.g., SLA, RFP, change management, audit standards) should incorporate the following quantitative items:

- Sanction baseline: $\alpha_{\min}(\tau)$ and its derivation.
- Reward design standard: $r \parallel Ku$ and procedures for modification.
- Default aggregators A by contamination regime and switching rules.
- Permissible range of challenge mixing ratio π and conditions for re-validating Δ^2 upon change.

Recommended reporting items include periodic estimates of $\widehat{\mathcal{M}}$, PoG bounds, contamination estimates, challenge hit and false positive rates, and group disparity metrics.

Limitations and Open Directions Dependence on local quadratic approximations and partial observability, vulnerability to distributional drift and extrapolation, and computational hardness bounds (§E.11) justify conservative policy settings. Open research directions include re-evaluating α_{\min} in non-stationary and nonlinear environments, regret guarantees for online switching policies, and optimal thresholds balancing false positives and false negatives in coalition dynamics.